JAERI-Research
96-036

DEVELOPMENT OF A NEW LOWER HYBRID ANTENNA MODULE USING A POLOIDAL POWER DIVIDER

July 1996

Sunao MAEBARA, Masami SEKI, Kazuaki SUGANUMA
Tsuyoshi IMAI, Marc GONICHE*, Philippe BIBET*, Stephane BERIO*
Jean BROSSAUD*, Guy REY* and Gianfranco TONON*

日本原子力研究所
Japan Atomic Energy Research Institute

本レポートは，日本原子力研究所が不定期に公刊している研究報告書です。
入手の問合わせは，日本原子力研究所研究情報部研究情報課（〒319-11 茨城県那珂郡東海村）あて，お申し越しください。なお，このほかに財団法人原子力弘済会資料センター（〒319-11 茨城県那珂郡東海村日本原子力研究所内）で複写による実費頒布をおこなっております。

This report is issued irregularly.
Inquiries about availability of the reports should be addressed to Research Information Division, Department of Intellectual Resources, Japan Atomic Energy Research Institute, Tokai-mura, Naka-gun, Ibaraki-ken 319-11, Japan.

編集兼発行　日本原子力研究所
印　　刷　㈱原子力資料サービス

Development of a New Lower Hybrid Antenna Module Using a Poloidal Power Divider

Sunao MAEBARA, Masami SEKI+, Kazuaki SUGANUMA+
Tsuyoshi IMAI, Marc GONICHE*, Philippe BIBET*
Stephane BERIO*, Jean BROSSAUD*, Guy REY*
and Gianfranco TONON*

Department of Fusion Engineering Research
Naka Fusion Research Establishment
Japan Atomic Energy Research Institute
Naka-machi, Naka-gun, Ibaraki-ken

(Received June 3, 1996)

The antenna using poloidal power divider is an effective method for simplification of Lower Hybrid Current Drive (LHCD) antenna system. This method should allow to reduce the power density in the antenna while maintaining a good flexibility of $N_{/\!/}$ spectrum of waves. For this purpose, three types of poloidal power divider which split the power in three, and the 3×6 multi-junction module were developed. r.f. properties and outgassing of these components were evaluated using the CEA Cadarache RF Test Facility.

A good power dividing ratio of $33 \pm 4\,\%$ was obtained for each of these poloidal dividers, and the reflection coefficient was lower value than 1.5 %. For the 3×6 multi-junction, reflection coefficient was less than 1.3 % and r.f. losses lower than 1.0 % were measured. On the other hand, it was found in the scattering matrix analysis that reflection coefficient at plasma has to be less than a few % in order to operate these components under available conditions. In combination with two poloidal power dividers connected to the 3×6 multi-junction module, quasi stationary operation for r.f. injection time of 1000 sec at 300 kW was demonstrated under water cooling. In this case, it was found that the outgassing rate is in the lower range of 10^{-7} Pa m^3 s^{-1} m^{-2} within the maximum module temperature of ~100 ℃.

+Department of Fusion Facility
*Centre d'Etudes de Cadarache, Association EURATOM-CEA

This report describes the experimental and analytical results of a new lower hybrid (LH) antenna module using the poloidal power divider.

Keywords: LHCD, Antenna, Poloidal Power Divider, R.f. Property, Outgassing

ポロイダル電力分配を用いた新型LHアンテナモジュールの開発

日本原子力研究所那珂研究所核融合工学部
前原　直・関　正美[+]・菅沼　和明[+]
今井　剛・Marc Goniche[*]・Philippe Bibet[*]
Stephane Bério[*]・Jean Brossaud[*]・Guy Rey[*]
Gianfranco Tonon[*]

（1996年6月3日受理）

ポロイダル方向へ電力分配するアンテナ設計は，LHCDアンテナシステムの簡素化に有効な手段である。この手法は，$N_{/\!/}$パラメターを広くとることが可能であるとともにアンテナの電力密度を軽減することが期待できる。このためにポロイダル方向へ3分配する3種類の電力分配器と，3×6分割マルチジャンクションモジュールを開発し，これらの高周波特性とコンポーネントからのガス放出量について，フランス原子力庁・カダラッシュ研究所の高周波出力試験装置を用いて評価した。

3種類のポロイダル電力分配器は，33±4％の良好な電力分配比が得られ，反射係数は，1.5％以下の低い値であった。また3×6分割マルチジャンクションモジュールでは，1.3％以下の反射係数と1％以下の高周波損失が測定された。しかしながら，これらの満足する値を維持するためには，プラズマからの反射係数を数%以下にしなければならないことが，解析結果から明らかになった。3×6分割マルチジャンクションモジュールに2つのポロイダル電力分配器を取付けた系では，コンポーネントを水冷した時に，高周波電力300kWで1000秒の準定常運転を実証することができた。この時のガス放出率は，最大モジュール温度100℃において，10^{-7} Pa m^3 s^{-1} m^{-2}の低いレンジであった。

この報告書は，ポロイダル電力分配器を用いた新しい低域混成波（LH）アンテナモジュールの実験と解析結果について，記述したものである。

那珂研究所：〒319－01　茨城県那珂郡那珂町向山801－1
+ 核融合装置試験部
* フランス原子力庁，カダラッシュ研究所

Contents

1. Introduction ····· 1
2. R.F. Components ····· 3
2.1 Background ····· 3
2.2 CEA E/H Plane Multi-junction and Mode Converter ····· 3
2.3 JAERI Poloidal Power Divider and 3 × 6 Multi-junction Module ····· 4
3. R.F. Properties in Low Power Test ····· 5
3.1 CEA Components ····· 5
3.2 JAERI Components ····· 8
3.3 Combination System ····· 12
4. Analysis of Low Power Test ····· 13
4.1 Measurement of the Scattering Matrix ····· 13
4.2 Analysis of Stability with Respect of the Reflected Power ····· 15
5. High Power Test ····· 18
5.1 Experimental set-up ····· 18
5.2 CEA E/H Plane Multi-junction on Short Circuit ····· 19
5.3 JAERI Components with Short Circuit ····· 20
5.4 JAERI Components + CEA E/H Plane Multi-junction ····· 21
5.5 CEA Mode Converter + CEA E/H Plane Multi-junction ····· 22
5.6 JAERI Components + CEA Mode Converter ····· 23
6. Analysis of High Power Test ····· 26
7. Conclusion ····· 28
Acknowledgments ····· 29
Reference ····· 29
Appendix 1 CEA Cadarache RF Test Facility ····· 79
Appendix 2 General Data for JAERI and CEA Components ····· 81

目　　次

1. はじめに …… 1
2. コンポーネント …… 3
2.1 バックグランド …… 3
2.2 CEA モード変換器と E／H マルチジャンクション …… 3
2.3 JAERI ポロイダル電力分配器と３×６分割マルチジャンクションモジュール …… 4
3. 低電力試験による高周波特性 …… 5
3.1 CEA コンポーネント …… 5
3.2 JAERI コンポーネント …… 8
3.3 組合わせた系 …… 12
4. 低電力試験による解析 …… 13
4.1 散乱行列の測定 …… 13
4.2 反射電力による安定性の解析 …… 15
5. 大電力試験 …… 18
5.1 実験構成 …… 18
5.2 CEA E／H マルチジャンクションのショートロード …… 19
5.3 JAERI コンポーネントのショートロード …… 20
5.4 JAERI コンポーネント＋CEA E／H マルチジャンクション …… 21
5.5 CEA モード変換器＋CEA E／H マルチジャンクション …… 22
5.6 JAERI コンポーネント＋CEA モード変換器 …… 23
6. 大電力試験の解析 …… 26
7. 結　　論 …… 28
謝　　辞 …… 29
参考文献 …… 29
付録１　CEA カダラッシュの高周波出力試験装置 …… 79
付録２　JAERI と CEA コンポーネントの一般データ …… 81

1. INTRODUCTION

In order to provide a steady-state current drive in a tokamak plasma, non-inductive current drive is indispensable for a steady-state tokamak reactor. Lower Hybrid Current Drive (LHCD) using the Lower Hybrid Range of Frequencies (LHRF) is one of the promising method and LHCD experiments for the physical and the technical study have been performed on JT-60U, Tore Supra, JET, TdeV tokamaks and others[1-4]. For a launcher design in future LHCD system, evaluation of outgassing from a waveguide during a high power and a long pulse r.f. operation, is essential issue, because the increase in outgassing due to the temperature rise of the waveguides, may cause r.f. breakdowns.

On International Thermonuclear Experimental Reactor (ITER) Conceptual Design Activities (CDA), it was reported that difference in outgassing rates of more than two orders of magnitude between JAERI and CEA. Namely, the outgassing rate of an antenna module on JT-60U was evaluated to be 10^{-6} Pa m^3 s^{-1} m^{-2} at the waveguide temperature of 250 °C [5], while the outgassing rate on a Tore Supra antenna module was measured to be 10^{-4} Pa m^3 $s^{-1}m^{-2}$ at 300 °C [6]. This difference has not been known whether it was caused by a low pre-baking temperature, pulse length, r.f. conditioning or antenna material. Cooperative activities between JAERI and CEA, therefore, started to obtain a detailed outgassing database. r.f. test were performed at the CEA Cadarache RF Test Facility which allowed high power injection up to 500 kW, under quasi-continuous operation at a frequency of 3.7 GHz.

The cooperative activities have been planned in two steps at the CEA Cadarache RF Test Facility. For the first step, outgassing experiment was carried out with the test module I in 1993 [7~8]. This test module I was an E-plane multi-junction with 4 secondary waveguides in the same row. This module was made of Dispersion Strengthened Copper (DSC) by JAERI. The DSC combines high mechanical property, up to 500 °C, even under neutron irradiation, with high thermal conductivity. The module was assembled by diffusion bonding method.

Test module I was successfully tested at the maximum r.f. power of 450 kW during 120 sec and very long operation up to 6,000 sec was achieved at a density power level of a 50 MW m^{-2} and a temperature up to 500 °C. Outgassing rats under high power and long pulse operation after good pre-baking and r.f. conditioning were evaluated to be of the order of 10^{-6} Pa m^3 s^{-1} m^{-2} at 300 °C, which were almost the same as one from stainless steel. It was deduced from the database that the outgassing rate is strongly dependent on pre-baking temperature and waveguide temperature during r.f. operation but is quasi independent on r.f. power after r.f. conditioning. This outgassing result agreed with measurements done on a JT-60U antenna module within one order of magnitude. On Tore Supra, the measured outgassing which is dominated

by desorption / recycling at the antenna mouth, might be consistent with such low outgassing rates for the waveguides.

In order to extend the outgassing database to a more realistic LHCD antenna module, more advanced r.f. components were designed and fabricated for Test Module II, as a second step of the collaborative activities.

In the LHCD antenna module, the r.f. power has to be split either in the poloidal or in the toroidal direction (or in both directions) in such a way that the port area is used as much as possible to reduce the power density in the waveguides. In the JT-60U LHRF system, wide (12 waveguides) toroidal multi-junction modules are used [9]. $N_{//}$ flexibility (1.5 ~ 2.3) is obtained by tuning the klystron frequency (1.74 ~ 2.23 GHz). With such conditions, power has been coupled to the plasma up to a power density of 21 MW m^{-2}. Tore Supra antennas use a combination of 3-dB poloidal divider (hybrid junction) and rather narrow (4 waveguides) toroidal multi-junction. In this case, the $N_{//}$ flexibility (1.4 ~ 2.3) is performed by changing the phasing between modules at a fixed frequency (3.7 GHz). With these antennas, a 1MA plasma current has been driven for 1 minute with 3 MW of LH power (power density : 18 MW m^{-2}) [10].

For large antennas at high fixed frequency (≥5 GHz), poloidal power dividing systems having at least three outputs will probably be needed in combination with reasonably wide multi-junctions (~ 6 waveguides) to keep a control on the $N_{//}$. For this reason, we designed and developed different types of poloidal power dividers (3 secondary waveguides) and a rather large multi-junction module (3 x 6 waveguides). Moreover, this power dividing method has an advantage of simplifying LH system by decreasing number of transmission lines.

JAERI developed and manufactured one poloidal power divider to be labeled PPD, and the 3 x 6 multi-junction module. On the other hand, an E/H plane multi-junction to be labeled E/H MJ and a mode converter to be labeled MC, were developed and manufactured by CEA. For these components, low power tests were first performed, then r.f. properties, withstand voltage and outgassing were evaluated under high power and long pulse operation from March to November 1994.

This report will describe results of the test module II. In section 2, r.f. components are related. Low power test results of r.f. components and analysis results are presented in section 3 and 4, respectively. High power test results under long pulse operation are presented in section 5, and these results are discussed in section 6. The last section provides conclusion.

2. R.F. COMPONENTS

2.1 Background

For a stable high power LH injection into a steady-state tokamak, large $N_{//}$ controllability and low power density are required. In order to fulfill these requirements, it is needed to divide r.f. power in the poloidal and toroidal directions. Two types of power dividers were considered. The first type divider provides r.f. power into the secondary waveguides by using single eigen-mode in the divider. The second one serves r.f. power by means of multi eigen-modes. JAERI and CEA have decided to test three different poloidal dividers. One of the first type is labeled the E/H MJ (CEA), and two of the second type are labeled the PPD (JAERI) and the MC (CEA), respectively. All these power dividers were designed to be able to feed the E-plane multi-junction which consists in three rows of six secondary waveguides.

2.2 CEA E/H plane multi-junction and mode converter

Two types of poloidal dividers were built. The first, the E/H plane multi-junction (E/H MJ) which has only one eigen-mode (TE_{01}), was carried out. The E/H MJ takes advantage of the E-plane multi-junction to split the power in three reduced-section (10 x 76 mm^2) for secondary waveguides from a standard waveguide, as it is currently used on present-day LH antennas. Upper and lower secondary waveguides are twisted in the poloidal direction, and then each secondary waveguides are widened with a linear taper in order to lead to three quasi-standard waveguides 40 x 76 mm^2 lined on the same column. A step phase shifter in the central output waveguide insures the good 0 π 0 phasing in such a way that combination of the 3-waveguides produces the TE_{03} mode at the output. This component with length of 746 mm long is water cooled by channels located on the top and the bottom of the waveguides (Fig.1). The waveguides were made of Oxygen Free High Conductivity (OFHC) copper plates and the cooling pipes from OFHC copper extruded rods. Assembling was achieved by electron-beam welding. The copper-coated stainless steel input/output flanges were welded by the same technique. Pumping holes, drilled with a spacing of $\lambda_g/4$ and a diameter of 5 mm at mid-height of the main waveguide as well as the secondary waveguides, insure a good conductance and a low pressure gradient.

The second component is the combination of a raised cosine taper which enlarges the height from 76 to 192 mm and a quasi periodic TE_{01}-TE_{03} mode converter with a constant beat wave number along the propagation direction. In order to get a quasi perfect mode conversion efficiency, this MC includes 3.5 beat wavelengths. This component with length of 960 mm is water cooled by channels located on each large side (Fig.2). Fabrication was made with the same materials : OFHC copper for

the waveguides and cooling pipes, stainless steel for the flanges. The same assembling technique of e-beam welding was used as one for the E/H MJ. Large deformation of the small size of the waveguide occurred during fabrication process : a detailed metrology indicates a width of 40.68 ± 0.46 mm while 40.2 ± 0.2 mm is required, and a second piece was built with the required accuracy. A linear taper length of 250 mm was also fabricated to enlarge the internal height from 192 to 236 mm. This part is divided by three in the poloidal direction, which was made also of OFHC, and water-cooled.

In order to make tests in combination with JAERI components possible, a transition waveguide which connects CEA components of the width b=40 mm with JAERI components of width b=61 mm was fabricated from OFHC. The transition length is L =260 mm, and also water-cooled on top and bottom.

2.3 JAERI poloidal power divider and 3x6 multi-junction module

2.3.1 Design concept

CEA developed a mode converter with TE_{03} as mentioned in section 2.1. On the other hand, JAERI designed a poloidal power divider using three eigen-modes : TE_{01}, TE_{03}, TE_{05}. The JAERI poloidal power divider was developed under the following concepts :

- should be compact (as short as possible)
- should have good r.f. properties as low reflection and balanced power dividing

These r.f. properties must be realized in combination with the 3 x 6 multi-junction. A photograph of the JAERI components is shown in Fig.3.

2.3.2 r.f. components

Poloidal Power Divider (PPD)

JAERI fabricated PPD as shown in Fig. 4. Total length of the power divider is as short as 600 mm. Function of the power divider is to transmit r.f. power from input waveguide to following sub-waveguides with low reflection. This divider was made of DSC of 2 mm-thick plate, and was assembled with Ag-Cu brazing. The divider has flanges to connect with the other components at both ends and has cooling pipes to remove heat load and then to allow stationary conditions. The flanges and the cooling pipes made of stainless steel were attached by brazing.

The 3 x 6 Multi-junction Module (3x6 MJ)

Dimension of the 3 x 6 multi-junction module (3 x 6 MJ) is indicated in Fig.5 and 6. This 3 x 6 MJ is composed of two sections : a three poloidally-divided section

and the 3 x 6 MJ section as shown in the figures. The three divided section exists between PPD and 3 x 6 MJ, TE_{01} and TE_{11} modes can propagate in that section. The length of 100 mm in the section is required to decrease effect of higher modes at input junction, but this length is close to one guide wavelength of TE_{01} mode so that reflective waves at output junction may affect total r.f. behavior. Only TE_{01} mode can propagate in 3 x 6 MJ. Phase shifter of 60 deg is located in the middle stage. The 3 x 6 MJ was made of DSC as same as the poloidal power divider, but was fabricated by diffusion bonding method developed for assembling of Test module I. The 3 x 6 MJ has also flanges and cooling pipes.

Supplementary Phase Shifter(SPS)

A supplementary phase shifter (SPS) has to be added to adjust the total phase difference in poloidal direction to be 180 deg in order to ensure a good wave recombination when testing with E/H MJ or MC. Sketch of the SPS is shown in Fig.7. This phase shifter produces phase difference of 60 deg. It has to be noted that, on plasma, phase difference of the PPD in poloidal direction is not a constraint, because effect of the poloidal phase difference was not observed in LHCD experiments. This part was made of stainless steel with copper plating and was assembled with welding. It has also cooling pipes for CW operation.

3. R.F. PROPERTIES IN LOW POWER TEST

3.1 CEA components

3.1.1 E/H plane multi-junction (E/H MJ)

3.1.1.1 Theory

The scattering matrix of the E/H MJ was computed using LSE_{1n} modes and mode matching technique [11]. The tapers in the E-plane has been optimized using equivalent circuit for E-plane step [12]. The linear tapers are divided into a cascade of steps along the longitudinal direction.

3.1.1.2. Experiment

At 3.7 GHz, the standing wave ratio of -29.5 dB for a symmetric taper and -22 dB for a dissymmetric one were measured, while the calculated values were -25 dB and -22 dB, respectively. For the E/H MJ, the following main parameters were measured and compared to the theoretical values :

- the reflectivity at the input
- the power dividing ratio
- the relative phasing at the outputs

and the 3 x 6 MJ section as shown in the figures. The three divided section exists between PPD and 3 x 6 MJ, TE_{01} and TE_{11} modes can propagate in that section. The length of 100 mm in the section is required to decrease effect of higher modes at input junction, but this length is close to one guide wavelength of TE_{01} mode so that reflective waves at output junction may affect total r.f. behavior. Only TE_{01} mode can propagate in 3 x 6 MJ. Phase shifter of 60 deg is located in the middle stage. The 3 x 6 MJ was made of DSC as same as the poloidal power divider, but was fabricated by diffusion bonding method developed for assembling of Test module I. The 3 x 6 MJ has also flanges and cooling pipes.

Supplementary Phase Shifter(SPS)

A supplementary phase shifter (SPS) has to be added to adjust the total phase difference in poloidal direction to be 180 deg in order to ensure a good wave recombination when testing with E/H MJ or MC. Sketch of the SPS is shown in Fig.7. This phase shifter produces phase difference of 60 deg. It has to be noted that, on plasma, phase difference of the PPD in poloidal direction is not a constraint, because effect of the poloidal phase difference was not observed in LHCD experiments. This part was made of stainless steel with copper plating and was assembled with welding. It has also cooling pipes for CW operation.

3. R.F. PROPERTIES IN LOW POWER TEST

3.1 CEA components

3.1.1 E/H plane multi-junction (E/H MJ)

3.1.1.1 Theory

The scattering matrix of the E/H MJ was computed using LSE_{1n} modes and mode matching technique [11]. The tapers in the E-plane has been optimized using equivalent circuit for E-plane step [12]. The linear tapers are divided into a cascade of steps along the longitudinal direction.

3.1.1.2. Experiment

At 3.7 GHz, the standing wave ratio of -29.5 dB for a symmetric taper and -22 dB for a dissymmetric one were measured, while the calculated values were -25 dB and -22 dB, respectively. For the E/H MJ, the following main parameters were measured and compared to the theoretical values :

- the reflectivity at the input
- the power dividing ratio
- the relative phasing at the outputs

A phase shifter was located in the central waveguide, and the phase difference between central and lateral waveguides was designed to be 180 deg. As shown in Table 1, a fairly good agreement between measurements and calculations was obtained.

	Theoretical	Measured
Reflectivity (dB)	25.5	29.7
Power div. ratio (%)	33.0 33.7 33.0	33.6 31.1 32.8
Phasing (deg)	0 180 0	-87 105 -88

Table 1 Measured and theoretical r.f. properties of the 3-waveguide E/H plane multi-junction

3.1.2. CEA mode converter

3.1.2.1. Theory

The MC was studied using the telegraphist equation [13] in which was taken into account :

- the coupling coefficient between TE_{n0} modes.
- the backward and the forward wave for each mode.

The theoretical power in forward and backward direction for the different mode is given in Fig.8, which depends on the longitudinal direction[14,15].

3.1.2.2. Experiment

Three different methods are used to check r.f. properties:

- a) measurement of the total electric field by an electric probe
- b) measurement of the scattering matrix
- c) measurement of the far-field radiated pattern

a) Measurement of total electric field by an electric probe

From total electric field measurements, the mode content of the forward and backward waves can be solved. Linear equations system requires 2N measurements to solve this problem, assuming that N modes are propagating. Accordingly, the electric field is measured at N positions in the transverse direction, for two positions in the longitudinal direction. These measurements were performed on a three-waveguide poloidal junction (PJ), connected to the MC output and terminated with three matched loads. In Fig.9, the measurements of amplitude and phase versus the transverse direction are indicated by open dots. The solid line indicates the computed field which

is calculated from coefficients of each mode in forward and backward direction. It can be checked that the shape of the electric field, in amplitude and phase, corresponds to a quasi pure TE_{30} mode. Using the deduced coefficient of each modes for the forward and backward wave, the total electric field can be calculated as a function of the longitudinal coordinate in an oversized waveguide between the MC and the PJ. In order to evaluate total electric field pattern along the propagation direction (Fig.9), the ratio of the amplitudes at two peeks $y_1/a = 1/6$ and $y_2/a = 1/2$ is plotted as a function of the longitudinal coordinate (Fig.10). For these two poloidal locations y_1 and y_2, the phase difference expected to be 180 deg. It was observed that the ratio of amplitude and phase difference are quite constant. It showed that the power dividing ratio does not depend on an oversized spacer set between the MC and the PJ. In Fig.11, the dividing ratio is plotted as a function of the thickness of the spacer. The variation is small and is in agreement with the results given in Fig.10. From this mode content analysis, the measured mode conversion efficiency from the TE_{10} mode to the TE_{30} mode is 99 %, while the computed value is 98.7 %. The same measurements and calculations were done when the MC was radiating in free space. The same values were obtained, and this result showed a stable behavior of this MC with respect to boundary conditions.

b) Measurement of the scattering matrix of MC + PJ.

As for the scattering matrix of MC+PJ, main parameters were measured and compared to theoretical values. Results are given in Table 2.

	Measured	Theoretical
Reflectivity (dB)	18.5	17
	30.2	31.4
Power div. ratio (%)	33.1	35.2
	30.2	31.4
	66	-150
Phasing (deg)	-108	31
	65	-150

Table 2 Measured and theoretical R.F. properties of MC + PJ

- c) Measurement of the far-field radiated pattern of the MC

The E-plane electric field was measured with an electric probe in the far field of the MC. This probe can be moved in angle in the H-plane with a constant distance

between the output axis of the MC and the probe. The amplitude and the phase of the measured electric field were in very good agreement with values to be computed from the theoretical radiated pattern of the TE_{30} mode (Fig.12).

These results can give the following two main conclusions :

- Different techniques are useful as cross-check of conversion efficiencies,
- Experimental results agreed with theoretical values.

3.2 JAERI components

3.2.1 Outline of JAERI components

The set-up for JAERI components is shown in Fig.13. It is composed of the PPD, the 3 x 6 MJ and the SPS. S_{21} parameters measured by a network analyzer, as shown in Fig.13, are as follows :

Stage	Power dividing ratio	Phase	Phase difference
Top	32 %	-144 deg.	184 deg.
Middle	37 %	40 deg.	---------
Bottom	30 %	-146 deg.	186 deg.

Power reflection coefficient is less than 1 %.

3.2.2 The 3 x 6 multi-junction module

Measured phase differences of the 3 x 6 MJ in Fig.14, are as follows :

Between	Measured value	Design value
Top and middle stage	63 deg.	60 deg.
Middle and bottom stage	64 deg.	60 deg.

A reflection coefficient less than 1.2 % and r.f. losses less than 1.0 % were measured for each stage. These were in good agreement with the calculated r.f losses (0.85 %).

3.2.3 Supplementary Phase Shifter

The measured phase differences of the SPS (Fig.15), are as follows:

Between	Measured value	Design value
Top and middle stage	61 deg.	60 deg.
Middle and bottom stage	61 deg.	60 deg.

3.2.4 Poloidal Power Divider

Measured phase differences are reported in sections 3.2.2 and 3.2.3. The phase difference of the PPD were only calculated as follows :

Between	Calculated value
Top and middle stage	60 deg.
Middle and bottom stage	61 deg.

A poloidal dividing ratio was adjusted by inserting a non 3-divided spacer between the PPD and the 3 x 6 MJ. It was also found that the poloidal dividing ratio is sensitive to the length of the 3-divided section (Fig.16). These 2 parameters were varied and it was found that :

- when a spacer width of 2 mm is installed, the power dividing ratio is optimized to 33 ± 4 %.(Fig.17)
- when the three-divided length is increased from 100 to 127 mm, the power dividing ratio of the middle stage is improved from 45 % to 35 % (Fig.18).

3.2.5 JAERI components on short circuit

r.f. properties on short circuit were measured by adding a plate to the SPS outlet, as sketched in Fig.19. The dependence of the S_{11} parameter (reflectivity) on frequency is shown in Fig.20. An amplitude of -0.174 dB was measured at 3.7 GHz and consequently the r.f. losses reached 4 % of the incident power. On a matched load, r.f. losses were expected to be no more than half this value.

3.2.6 Development of poloidal power divider at JAERI

Before fabrication of high power components, mock-ups were designed at 2.2 GHz to study r.f. properties of poloidal power divider (PPD) at low power. The basic idea of the PPD is shown in Fig.21. r.f. power of the TE_{01} mode is injected from the input, the TE_{01} mode is gradually converted into TE_{03} and TE_{05} modes as transmitting in longitudinal direction in order to fulfill boundary conditions of PPD. Profile of r.f. power in PPD is governed by combination of these modes. By optimizing the configuration, the r.f. power profile can have 3 equal peaks at the output of PPD. The r.f. power may be transmitted into 3-divided waveguides with the same ratio.

In order to be compared to the 3.7 GHz PPD, total height at the output (which includes 2, 2-mm thick, septum) was scaled with the 2.2 GHz PPD in the ratio of the frequencies :

$$a_{2.2\ GHz} = (3.7/2.2) * a_{3.7GHz}$$

The longitudinal length was optimized from measurement results with the 2.2 GHz mock-up. As a preparation of 2.2 GHz-mock-up, r.f. properties were first carried out at 1.7 GHz with a network analyzer, since it is easier to understand behavior of PPD having TE_{01} and TE_{03} only. In this case, the r.f. properties are reproduced by a simple model such as :

- TE_{01}, TE_{03} forward wave only
- initial phase at inlet of the poloidal power divider

  0 deg for TE_{01} mode

  180 deg for TE_{03} mode
- amplitudes A_{01}, A_{03} are free parameters

Fitting parameters of A_{01} and A_{03} are found to be :

A_{01}=0.3, A_{03}=0.8 at inlet of PPD

A_{01}=0.6, A_{03}=0.6 at outlet of PPD

when comparing between measured and calculated r.f. properties.

By using this simple model, a PPD with TE_{01}, TE_{03} can be designed to provide r.f. power in three waveguides lined in poloidal direction as shown in Fig.22. Figure 22 indicates that total length should be 0.44 m for PPD of 0.18 m width to achieve the same power dividing ratio. In the case of 0.585 m in length, the PPD of 0.18 m in width may also provide good dividing ratio, but total length is unnecessary longer. Figure 23 shows r.f. profiles at the optimized PPD output (L=0.44m, X=0.18 m) width. Both amplitudes of TE_{01} and TE_{03} were the same and total power was 3 times of the amplitudes. Figure 24 illustrates r.f. power density profile in this PPD. Distribution of r.f. power was changing along longitudinal direction, the same amplitude was obtained at the output as mentioned above.

In the case of 2.2 GHz, it is more complex to analyze r.f. properties due to three propagating modes : TE_{01}, TE_{03}, TE_{05}. After R&D using some hand-made PPD's, a good prototype of a PPD was obtained as shown in Fig.25. Width of the PPD is 396.62 mm and length is 364 mm. Three following waveguides are terminated by loads. r.f. properties at 190 mm from junction in 3-divided waveguides is illustrated in Fig.26, reflection coefficient in input waveguide was 1.4 % and power dividing ratio was 35±4%. Phase difference in poloidal direction was 120±5 deg. By applying the simple model to the PPD, each mode conversion ratio at the end of power divider was obtained as shown in Table 3. This calculation result explains the experimental power dividing ratio as shown in Fig. 27, but phase difference was expected to be around 60 deg while phase difference was measured to be 120 deg. It should be pointed out that r.f. property is sensitive in oversized waveguide section of 3-divided waveguides. Both power distribution and phase distribution measured at different positions are changing in these section as shown in Fig.28. Higher modes

excited at a junction may affect r.f. properties. The measured phase distribution at Z = 95 mm from junction resembles the calculated one in Fig. 27.

Unfortunately, length of PPD for 3.7GHz is short by 8 mm compared with the correct one due to error in calculation ; length should be 364 x 2.2/3.7 ~ 216mm while that the PPD is indeed 208 mm. The deviation in electrical length is about 35 and 30 deg for TE_{01} and TE_{03} mode, respectively. This may affect extrapolation from 2.2 GHz PPD to 3.7 GHz PPD.

For the 3.7 GHz PPD, conversion efficiencies were obtained in the case of 3 experimental set-ups : 1) with the PPD connected to the PJ on load, 2) with the PPD radiating in free space, 3) with a 3-divided waveguide as on Fig.27, using Fourier transform method (Fig.29). These results are compared with results obtained from the 2.2 GHz mock-up (Table 3).

Mode	2.2 GHz mock up	with PJ	on free space	with 3-divided waveguide
TE01	53.0 %	55.4 %	44.4 %	51.5 %
TE03	31.4 %	31.6 %	52.2 %	33.6 %
TE05	15.5 %	13.1 %	3.4 %	12.9 %
TE07				2.0 %

Table 3. Conversion efficiency of PPD for different set-ups

When the boundary conditions are very different (radiating on free space), conversion efficiencies are strongly affected : this sensitivity indicates some resonant behavior of this component.

Like for the MC (Fig.9), the total electric field at the output of the PPD in an oversized waveguide as a function of the longitudinal direction was computed (Fig.30). The electric field at mid-height of the lower stage normalized to the electric field at the same position of the central stage is quite large but it exists a range of length in the longitudinal direction for which the phase difference is quasi constant. It must be noted that the experimental phase shift of 75 deg is verified. These results can be compared with the measurement of the power dividing ratio when the thickness of a spacer installed between the PPD and the 3 x 6 MJ is varied (Fig.17 and 18). The agreement is quite good.

Scattering matrix of this PPD was measured; the matrix is symmetric but is not unitary as shown in Table 4. This result shows that we have to obtain good coupling property with this type power divider, because reflective waves in particular when there are non-symmetric, lead to the r.f. losses in the system as indicated by a non-unitary matrix. (See next section 4.1 for scattering matrix in detail)

0.114, (61)	0.603, (-1)	0.575, (102)	0.596, (-1)
0.602, (3)	0.371, (153)	0.205, (-73)	0.631, (35)
0.582, (101)	0.200, (-70)	0.620, (160)	0.322, (-58)
0.589, (-4)	0.631, (35)	0.324, (-58)	0.247, (155)

Table 4. Scattering matrix of mock-up (2.2 GHz)

3.3 Combination system

3.3.1 JAERI components + CEA E/H plane multi-junction

A schematic drawing of the combination system in which that JAERI components are combined with CEA components, is shown in Fig.31. CEA components are composed of the E/H MJ and transition waveguide to adjust length in E-plane direction. Dependence of S_{21} parameter (amplitude and phase) on frequency at the 3 x 6 MJ temperature of 50 °C is shown on Fig.32. At 3.7 GHz, r.f. losses were affected by the resonant and a S_{21} amplitude of -2.198 dB was measured, which corresponds to r.f. losses of 40 %.

The dependence of resonant frequencies on temperature is indicated in Fig.33. The variation rate is -0.052 MHz / °C which can be easily explained. If a resonance occurs in a section of length l at a frequency f, and this section expands by Δl with temperature, the resonant frequency will shift by Δf related to Δl by :

$$\Delta f / f = \Delta l / l = - a \Delta T$$

therefore :

$$\Delta f / \Delta T = - a f$$

where a is the thermal expansion of the material.

For OFHC and DSC, a was almost the same and just vary from 17.0 to 17.7 x 10^{-6} when the temperature varied from 100 °C to 300 °C. For this range of temperature, $\Delta f / \Delta T$ varies from 0.0629 to 0.0655 MHz / °C. In Fig.33, the temperature of the 3 x 6 MJ is quoted, which is clearly not the part where resonance occurs. The temperature profile during baking (Fig.52) suggests that resonance occur either in the E/H MJ or PPD where baking temperature is lower by 20%. The 3.7010 GHz resonance is expected to occur at 3.7 GHz when the temperature is around 40 °C. The dependence of S_{21}, in amplitude and phase, on the module temperature is as follows:

Module temperature	amplitude	phase
20 °C	- 0.57 dB (12.0 %)	
100 °C	- 0.24 dB (5.4 %)	-4 deg.
200 °C	- 0.20 dB (4.5 %)	-43 deg.
300 °C	- 0.39 dB (8.6 %)	-62 deg.

The r.f. loss at the 3 x 6 MJ temperature of 200 °C decreases from 12 % to 5 % level of an incident power, since it becomes far from the resonant frequency. The phase variation rate due to the temperature rise was 0.29 deg / °C. The phase variation of 48 deg between 100 °C and 300 °C is equivalent to an expansion length of 14.2 mm.

3. 3. 2 JAERI components + CEA (40/61 + PJ + MC)

The S_{12} parameter was found (Fig.34) to be -0.24 dB at 3.7 GHz with 2 small resonance near 3.7 GHz at room temperature, one at 3.704 GHz (-0.35 dB) and the other, smaller, at 3.701 GHz. The measured reflection coefficient was -18 dB at 3.7 GHz. When the whole assembling is baked, the position of the resonance in frequency f moves with the temperature T to smaller frequency at the variation rate given by :

$$\Delta f / \Delta T = - 6.2\ 10^{-2}\ \text{MHz} / °C$$

This is very closed to the expected value, therefore, the resonant section is in the central part of the set-up, where the temperature is closed to the maximum temperature. The two small resonance observed at frequencies slightly higher than 3.7 GHz at room temperature are expected to be reached at 59 °C and 99 °C.

3.3.3. CEA mode Converter and E/H plane multi-junction

The r.f. loss of the assembling of the MC + PJ + E/H MJ was measured. The S_{12} parameter which gives the transmission efficiency is equal to -0.15 dB at 3.7 GHz and is nearly constant at room temperature on a bandwidth of ± 20 MHz (Fig.35). The reflection coefficient at the input was measured to be only 22 dB. The f=3.722 GHz resonance at 20 °C was shifted towards f=3.7 GHz at the rate :

$$\Delta f / \Delta T_{MJ} = - 6.5\ 10^{-2}\ \text{MHz} / °C$$

where T_{MJ} is the E/H MJ temperature. This is again very closed to the expected rate. It has to be noted that, in this case, the MC is just at a slightly lower temperature that of the E/H MJ one by 3 % and no conclusions on resonance location can be drawn. For T = 360 °C, resonance is expected at the working frequency f=3.7 GHz.

4. ANALYSIS OF LOW POWER TEST

4.1 Measurement of the scattering matrix

4.1.1. Scattering matrix

The scattering matrix of each component was first measured at 3.7 GHz. For all the components, the number of ports are 4. One is the input part, the others are the

The r.f. loss at the 3 x 6 MJ temperature of 200 °C decreases from 12 % to 5 % level of an incident power, since it becomes far from the resonant frequency. The phase variation rate due to the temperature rise was 0.29 deg / °C. The phase variation of 48 deg between 100 °C and 300 °C is equivalent to an expansion length of 14.2 mm.

3. 3. 2 JAERI components + CEA (40/61 + PJ + MC)

The S_{12} parameter was found (Fig.34) to be -0.24 dB at 3.7 GHz with 2 small resonance near 3.7 GHz at room temperature, one at 3.704 GHz (-0.35 dB) and the other, smaller, at 3.701 GHz. The measured reflection coefficient was -18 dB at 3.7 GHz. When the whole assembling is baked, the position of the resonance in frequency f moves with the temperature T to smaller frequency at the variation rate given by :

$$\Delta f / \Delta T = - 6.2\ 10^{-2}\ \text{MHz} / °C$$

This is very closed to the expected value, therefore, the resonant section is in the central part of the set-up, where the temperature is closed to the maximum temperature. The two small resonance observed at frequencies slightly higher than 3.7 GHz at room temperature are expected to be reached at 59 °C and 99 °C.

3.3.3. CEA mode Converter and E/H plane multi-junction

The r.f. loss of the assembling of the MC + PJ + E/H MJ was measured. The S_{12} parameter which gives the transmission efficiency is equal to -0.15 dB at 3.7 GHz and is nearly constant at room temperature on a bandwidth of ± 20 MHz (Fig.35). The reflection coefficient at the input was measured to be only 22 dB. The f=3.722 GHz resonance at 20 °C was shifted towards f=3.7 GHz at the rate :

$$\Delta f / \Delta T_{MJ} = - 6.5\ 10^{-2}\ \text{MHz} / °C$$

where T_{MJ} is the E/H MJ temperature. This is again very closed to the expected rate. It has to be noted that, in this case, the MC is just at a slightly lower temperature that of the E/H MJ one by 3 % and no conclusions on resonance location can be drawn. For T = 360 °C, resonance is expected at the working frequency f=3.7 GHz.

4. ANALYSIS OF LOW POWER TEST

4.1 Measurement of the scattering matrix

4.1.1. Scattering matrix

The scattering matrix of each component was first measured at 3.7 GHz. For all the components, the number of ports are 4. One is the input part, the others are the

output parts in the power division. The S_{ij} parameters of the scattering matrix S are :

S_{11}	S_{12}	S_{13}	S_{14}
S_{21}	S_{22}	S_{23}	S_{24}
S_{31}	S_{32}	S_{33}	S_{34}
S_{41}	S_{42}	S_{43}	S_{44}

The following properties must be checked :

- $S_{ij} = S_{ji}$.(symmetric matrix)
- S x S* = I if no r.f. loss (S* is the adjoint matrix of S)
- $|S_{12}| = |S_{13}| = |S_{14}|$ (power dividing ratio)
- $S_{23} = S_{34}$ (coupling coefficient between the lateral and the central output waveguides)
- $S_{22} = S_{44}$ (reflection coefficient at the output waveguides when all the ports are matched)

4.1.2 JAERI poloidal power divider

For the PPD connected to the 40/61 transition waveguide, the measured scattering matrix is given in table 5. The first number was normalized by the amplitude of electric field, $|S_{ij}|$, and the second (in parenthesis) indicated the phase, $<S_{ij}$, in degrees.

4.7910^{-2}, (-8)	0.551, (113)	0.625, (-177)	0.516, (107)
0.544, (112)	0.524, (-167)	0.367, (-62)	0.305, (-156)
0.632, (-179)	0.371, (-61)	0.394, (41)	0.371, (-59)
0.511, (107)	0.305, (-156)	0.367, (-60)	0.531, (-112)

Table 5. Scattering matrix of JAERI PPD with PJ

Main features of this matrix are as follows :

- Phase difference between central output and 2 lateral outputs ($<S_{12}$-$<S_{13}$ and $<S_{14}$-$<S_{13}$) is around 75 deg.
- Energy conservation ($\Sigma S_{ij} \cdot S_{ji}^{*}=1$) is not fulfilled specially for j = 2, 3 and 4.
- Power dividing ratios are unbalanced, but other symmetries are quite well verified.

This can be explained that even mode is excited at the lateral output waveguide, since the coupling between even and odd mode is null.

The scattering matrix of total assembling of JAERI components (PPD + 3 x 6 MJ + SPS) with the same CEA 61/40 transition is given in table 6.

0.06021, (7)	0.537, (-159)	0.556, (25)	0.507, (-162)
0.531, (-158)	0.708, (73)	0.141, (-34)	0.305, (122)
0.549, (25)	0.136, (-34)	0.136, (99)	0.11, (0)
0.507, (-162)	0.295, (123)	0.112, (2)	0.676, (2)

Table 6 Scattering matrix of JAERI components + 40/61 transition

It is seen here that the phase difference between the central and the lateral output waveguide is around 180 deg. However, energy conservation ($\Sigma S_{ij} \cdot S_{ji}^{*}=1$) is not fulfilled. The main effect is dependent on the power dividing ratio. Because S_{12} parameter is substantially changed from 0.63 to 0.55, though the reflection due to the 3 x 6 MJ is less than 1% .

4.1.3 CEA E/H plane multi-junction module

For the E/H MJ, the scattering matrix is given in table 7.

0.0632, (-106)	0.575, (8)	0.562, (-153)	0.568, (4)
0.589, (9)	0.407, (104)	0.327, (-12)	0.468, (69)
0.556, (-151)	0.316, (-11)	0.524, (-154)	0.346, (-10)
0.582, (5)	0.478, (70)	0.359, (-11)	0.402, (103)

Table 7. Scattering matrix of CEA E/H plane multi-junction

The same measurements applied to the MC+ PJ leads to the scattering matrix given in table 8.

0.119, (-99)	0.549, (66)	0.575, (-108)	0.549, (65)
0.562, (67)	0.473, (40)	0.295, (-113)	0.355, (125)
0.588, (-108)	0.295, (-114)	0.478, (76)	0.288, (-107)
0.556, (66)	0.351, (124)	0.285, (-107)	0.489, (97)

Table 8. Scattering matrix of CEA mode converter + PJ

In the 2 previous cases it can be seen that :

- the symmetries are quite well verified.
- the r.f. losses are higher for the second, third and fourth line.

4.2 Analysis of stability with respect of the reflected power

This was first performed on the 2.2 GHz mock-up. Effect of reflection from sub-waveguide was studied with the measured S-matrix. The S•S* is given in table 9 :

diagonal terms are closed to unity, but non-diagonal terms are not zero. This non unitary S-matrix may leads to complicated phenomena. Therefore we have to confirm that the non unitary S-matrix can reproduce r.f. property when power is reflected from the sub-waveguides. In order to verify, then r.f. properties were measured when small reflected power exists as shown in Fig. 36.

1.062	0.016	0.391	0.026
0.016	0.941	-0.227	0.231
0.391	-0.227	0.873	-0.348
0.026	0.231	-0.348	0.911

Table 9. Non unitary S∗S-matrix at the 2.2 GHz mock-up.*

Typical data are illustrated in Fig. 37. In this case reflected power from one sub-waveguide was set at ~4.4%, while phase of the reflective wave was changed by phase shifter. Power dividing ratio varied as the phase changes, even though reflective power was low. In the same figure, calculation results are shown using non unitary S-matrix. It seems that measured results are consistent with calculated ones with a non-unitary S-matrix. It should be pointed out that r.f. property is sensitively affected by small reflection power and r.f. property also depends on phase of the reflection power when reflected power is non-symmetric as shown Fig. 38.

Expected performance with plasma was examined using non unitary S-matrix. At first, reflection in each row was homogeneous, reflection coefficient was 3 % in each sub-waveguide. Power dividing ratio were not so much changed : 32% (upper stage), 35 % (middle), and 32 % (lower). In the homogenous case, reflection coefficients were 1.4, 3.0, and 7.2 % for the 3 stages. Power dividing ratio were then more affected due to reflections : 36, 34, and 27 % for the 3 stages.

For the 3.7 GHz components, a comparison between the different power dividers was made. Using the scattering matrix obtained experimentally, electric fields for the forward and backward wave in each port are calculated for changing the amplitude or the phase of reflection coefficient on the output waveguides. The aim is as follows :

- to furthermore understand behavior of the dividing ratio in the case that the distance between the PPD and the 3 x 6 MJ is changed by inserting a 3-waveguide spacer.
- more generally, to evaluate the sensitivity of the PPD due to reflected power from a plasma.

From theoretical view, a necessary criterion to validate the computation was obtained by calculating the power balance of the multi-pole $P_{out} - P_{in}$. This balance is null if there is no r.f. loss, and negative if r.f. loss exists in the system. A positive value would indicate it works as an amplifier. Experimental matrixes suffer from 2 main defects :

- They are not symmetric (Sij ≠ Sji)
- They are not unitary S x S* ≠ 1

Even the matrix is symmetrized by taking the average value in amplitude and phase, the criterion is still not verified in the case that the reflection coefficient changes on the output waveguides. The difference is often found positive. To overcome this difficulty, there are at least two possibilities :

- to compare the measured matrix to the theoretical matrix.
- to normalize the measured matrix so as to meet the condition of S x S* = 1

It was checked that a good agreement between electric fields by this new matrix and the measured ones are obtained, when a short circuit plate is moved in one output waveguide on the CEA components. Furthermore, we checked variation of the power dividing ratio when a 3-divided waveguide section was inserted between the PPD and the 3 x 6 MJ (Fig.18). In this case, electric fields in every port using the matrix of the PPD were computed. The reflective electric field of 0.1 was used, since reflective power from the 3x 6 MJ of 1 % was measured. Phase of the reflection coefficient for each output waveguides were changed by thickness of the three-waveguide spacer. In Fig.39, this phase is labeled fro. The thickness is converted into electric length using TE_{10} wavelength and the ratio of electric fields in the middle and top/bottom outputs is plotted versus fro. The crosses indicate measured values. When theoretical curve was computed using the phase difference of 270 deg between the mild stage and the top/bottom stage for the backward wave, a good agreement between theoretical and measurements was obtained.

The stability of the PPD, E/H MJ and MC were compared by the same way. The effect on amplitude and phase for the forward and backward waves at the 3 output waveguides is plotted as a function of the phase of the reflection coefficient. It was assumed that the amplitude and the phase of the reflection coefficient were the same for the three outputs. Power reflection was fixed at 1%, phase to be labeled fro was variable. The calculation was also made for the whole JAERI component set, though the reflected field at the output of the PPD was different in this case (Fig.40).

For the PPD, the unbalance of incident electric fields in the 3 stages is large. The amplitudes are 0.50, 0.70 and 0.50, when specific fro is near 180 deg. Phase

variation for the forward waves is no more than 10 deg. These results were consistent with those of the 2.2 GHz mock-up when the fro is far from 180 deg.

For the E/H MJ, the unbalance is slightly fro-dependent. In the worst case, the amplitudes are 0.60, 0.54, 0.60, phase variations are low(<10 deg).

For the MC + PJ, the unbalance is now weakly fro-dependent and is low. The amplitudes are typically 0.54, 0.58, 0.54. Phase variations are also low (<10 deg).

The behavior of these power divider was evaluated in the case that r.f. power was coupled to plasmas. The same calculations were carried out with much higher power reflection coefficients. It is assumed that the reflection of 2, 5, 8 % is unbalanced, the corresponding phase was : fro, 0, 20 deg (Fig. 38). In this case, the amplitude unbalance is strongly enhanced for all components and is maximized when phase of output 1 is in opposition with phase of outputs 2 and 3 (fro ≈180 deg).

For PPD, the amplitudes of 0.65, 0.60 and 0.55 were obtained, the phase variation of 10 deg was indicated. This is, roughly, the unbalance measured on the 2.2 GHz mock-up in the case of unbalanced reflection (1.4, 3.0 and 7.2 %). In the case of E/H MJ, the amplitudes of 0.45, 0.6 and 0.65 for the worst case and the phase variation of about 15 deg were obtained. For MC, the amplitudes of 0.50, 0.55 and 0.70 were indicated while the phase variation was of the order of 10 deg.

As a conclusion, when the reflection coefficient is low (1 % in power), MC is the more stable component with respect of the reflected field variation. However, when the power reflection coefficients increase, the unbalance of the electric fields in the three outputs becomes very large for all components. On plasma, these power dividers will have to be operated with low reflection.

5. HIGH POWER TEST

5.1 Experimental set-up

High power tests were performed in a new vacuum tank (Fig.41) . This tank is larger (V=0.34 m^3, L=3.5 m) and can be baked up to 450 °C. The transmission line includes a high r.f. power switch which allows klystron test on a dummy load. The cooling of the transmission line has been slightly improved. r.f. tests were achieved either with the components to be tested terminated by a short-circuit plate, or with the components connected at the output to a dummy load. Schematic drawings of case 1 and case 2 are given in Figs.42 and 43, respectively. Details on the test bed facility are given in appendix 1.

In the first case, a 3-dB power divider (hybrid junction) is inserted in the transmission line to insure low power reflection to the klystron. The maximum (resp average) electric field strength with a short-circuit plate is 2 (resp.1.4) times higher

variation for the forward waves is no more than 10 deg. These results were consistent with those of the 2.2 GHz mock-up when the fro is far from 180 deg.

For the E/H MJ, the unbalance is slightly fro-dependent. In the worst case, the amplitudes are 0.60, 0.54, 0.60, phase variations are low(<10 deg).

For the MC + PJ, the unbalance is now weakly fro-dependent and is low. The amplitudes are typically 0.54, 0.58, 0.54. Phase variations are also low (<10 deg).

The behavior of these power divider was evaluated in the case that r.f. power was coupled to plasmas. The same calculations were carried out with much higher power reflection coefficients. It is assumed that the reflection of 2, 5, 8 % is unbalanced, the corresponding phase was : fro, 0, 20 deg (Fig. 38). In this case, the amplitude unbalance is strongly enhanced for all components and is maximized when phase of output 1 is in opposition with phase of outputs 2 and 3 (fro ≈180 deg).

For PPD, the amplitudes of 0.65, 0.60 and 0.55 were obtained, the phase variation of 10 deg was indicated. This is, roughly, the unbalance measured on the 2.2 GHz mock-up in the case of unbalanced reflection (1.4, 3.0 and 7.2 %). In the case of E/H MJ, the amplitudes of 0.45, 0.6 and 0.65 for the worst case and the phase variation of about 15 deg were obtained. For MC, the amplitudes of 0.50, 0.55 and 0.70 were indicated while the phase variation was of the order of 10 deg.

As a conclusion, when the reflection coefficient is low (1 % in power), MC is the more stable component with respect of the reflected field variation. However, when the power reflection coefficients increase, the unbalance of the electric fields in the three outputs becomes very large for all components. On plasma, these power dividers will have to be operated with low reflection.

5. HIGH POWER TEST

5.1 Experimental set-up

High power tests were performed in a new vacuum tank (Fig.41) . This tank is larger (V=0.34 m^3, L=3.5 m) and can be baked up to 450 °C. The transmission line includes a high r.f. power switch which allows klystron test on a dummy load. The cooling of the transmission line has been slightly improved. r.f. tests were achieved either with the components to be tested terminated by a short-circuit plate, or with the components connected at the output to a dummy load. Schematic drawings of case 1 and case 2 are given in Figs.42 and 43, respectively. Details on the test bed facility are given in appendix 1.

In the first case, a 3-dB power divider (hybrid junction) is inserted in the transmission line to insure low power reflection to the klystron. The maximum (resp average) electric field strength with a short-circuit plate is 2 (resp.1.4) times higher

than that in the case of a test on load with low reflection. Even though the module injection power is limited to half of the klystron output power by the 3-dB hybrid junction, the maximum electric field for the same klystron output is increased by 1.4 and is therefore effective to estimate the withstand-voltage. However, high power level may be limited by differential thermal expansion of the two sections connected to the hybrid junction, causing unbalanced phases and, possibly, the klystron switching off.

r.f. measurements are available at the output of the klystron and at the input of the vacuum tank. In the second case, the r.f. measurements are also available at the output of the tank. The different waveguides in vacuum (mode converter, multi-junction, phase shifter, transition, connection waveguides....) were equipped with thermocouples to record temperature evolution. In particular, power division ratio was studied by measurement of the temperature increase rate dT/dt for the different stages in the poloidal direction, when the waveguides were uncooled.

Gas pressure is also available from a Penning gauge and a Bayart-Alpert gauge. Outgassing flux were estimated, as for Test Module II, by switching off the vacuum pump (build-up method) which leads to more reliable values when the outgassing is low. Analysis of outgassing rates is more difficult than for Test Module I, because the complexity of the set-up (different sections with various power density and losses) leads to a large temperature gradient. It is known that outgassing rate increases quasi-exponentially with temperature. For the on-load tests, the following method was applied. An exact exponential dependence on the outgassing rate on the temperature, was assumed. Moreover, it was assumed that the outgassing rates of each section lay on the same line (i.e. same initial outgassing rate and same slope). The free parameter was adjusted to fit the total experimental outgassing flux.

5.2 CEA E/H plane multi-junction on short circuit

The E/H MJ was connected to the input r.f. window via a standard connection waveguide (L= 765 mm). Four thermocouples are installed on the multi-junction : one on the E-plane multi-junction section where the losses are expected to be the highest ($1.46\%.m^{-1}$ at 200 °C) and one on each of the 3 secondary waveguides to check the power division.

Baking at 200 °C for 60 + 60 h was achieved and baking temperature lowered to 100 °C in order to get low initial conditions for outgassing. r.f pulse length was extended first to Tmax = 200 °C, then to Tmax=450 °C.

At high power ($P_{klystron}$ > 300 kW), power injection is limited by the increasing reflection power at the klystron due to unbalanced expansion of the transmission lines : at 320 kW, the klystron is switched off 340 s after r.f. injection

when the reflected power exceeds the set point (20 kW) as indicated in Fig.44. However, the module could be heated up to 410 °C. At higher power ($P_{klystron}$= 430 kW, P_{module}=200 kW), limitation is even more severe and the maximum temperature is 380 °C.

Power division, deduced from thermocouples measurements, was excellent (Fig.45) : for the different powers, the unbalance was less than 10 % and the heating rate increases linearly with the injected power (Fig.46).

During power injection, outgassing increased quasi exponentially when the module temperature increases from 100 to 450 °C (Fig.47). For outgassing rate evaluation, the entire E/H MJ surface (0.72 m^2) was taken into account. Outgassing flux from the connection waveguide is neglected and the input temperature is taken for reference, despite the much lower measured temperatures at the outputs. The outgassing rate is therefore underestimated. Due to the rather low baking temperature (200 °C), the outgassing rate is quite high for the first shots but decreases almost by one order of magnitude during the experiment from 5-6 x 10^{-5} to 8 x 10^{-6} Pa m^3 $s^{-1}m^{-2}$ at 200 °C. Outgassing measurements at 200, 300 and 400 °C are plotted for the different shots in Fig.48. The rather high outgassing rate at high temperature is due to the low baking temperature (300 °C) and the small number of shots. The conditioning provided by the accumulation of r.f. injection can be evaluated by the integrated injected energy : in equivalent conditions, outgassing rate measured at 400 °C is consistent with measurement done on test module I (Fig.49).

All these measurements indicated a good power handling capability, a good power division with no local overheating due to non linear effects (resonance).

5.3 JAERI components with short circuit

The experimental set-up of JAERI components with short circuit is shown in Fig.42. The vacuum tank and JAERI components were baked at 200 °C for 125 hours to get outgassing rate quasi-saturation, and then the baking temperature was decreased to 100 °C. r.f. conditioning was first done using short pulses of 10 msec length with a duty circle of 1/11 for 1 sec. The r.f. power from 50 kW to 225 kW was injected into the components.

After r.f. conditioning, a withstand-voltage test was performed using a pulse length of 2 sec. Breakdowns was not observed, even though the maximum power of 225 kW was injected. At the 225 kW level, the maximum electric field strength at secondary waveguide of 72 x 8.5 mm reached near 3.9 kV /cm.

The withstand-voltage test was also performed using a long pulse of more than 100 sec. It was found that JAERI components, fabricated by diffusion bonding method, could withstand the maximum long operation of 520 sec at the r.f. power of

70 kW, the maximum r.f. power of 120 kW (average value) during 280 sec. Time trajectory of klystron output power, module injection power and pressure of the vacuum tank are indicated in Fig.50. It is also found that breakdowns due to an excessive outgassing do not occur, even though the pressure is increased from 1.8 x 10^{-4} to 0.1 Pa. This final high pressure was due to the much higher temperature of the PPD Input (T= 365 °C) than baking temperature (200 °C). Outgassing fluxes, with the module temperature at 200°C, range from 8 x 10^{-6} to 1.1 x 10^{-5} Pa m^3 s^{-1}.

In the case of an r.f module injection power of 120 kW (average r.f. power), a temperature rise of 0.25 °C/s was measured on the outer wall of the 3 x 6 MJ which the r.f. power loss was evaluated to be 1.7 %.

5.4 JAERI components + CEA E/H plane multi-junction

The experimental set-up of JAERI components, combined with the E/H MJ and transition waveguide, is shown in Fig.43. r.f. power was transmitted from the PPD to the E/H MJ. The outside walls of these components were equipped with thermocouples.

Before outgassing flux during r.f. power injection was evaluated, these components and the vacuum tank were baked at 200, 300 and 450 °C, respectively. When saturation of outgassing fluxes was obtained, baking temperature was decreased to 100 °C, in each case. Outgassing fluxes at 100 °C without r.f. injection is used as the reference background flux. Dependence of outgassing flux on the baking duration is shown in Fig.51, and each temperature distribution of the vacuum tank during each baking treatment is shown in Fig.52. Baking temperature was defined as the maximum temperature of the vacuum vessel. The background fluxes at 100 °C after 200, 300 and 450 °C baking were 5.5 x 10^{-7}, 3.0 x 10^{-7} and 2.0 x10^{-7} Pa m^3 s^{-1}, respectively. The dependence of outgassing flux on r.f. injection energy in each baking treatment is shown in Fig.53. These data were measured when the module was uncooled and the temperature maintained below the baking temperature. It indicates that high baking treatment is effective to reduce outgassing.

Temperature rises during r. f. injection of 300 kW (# 10699), measured by thermocouples on outside walls of these components, are shown in Fig.54. From a 2-D thermal analysis code, it was checked that, because of the high thermal conductivity of DSC, temperature gradients, in a poloidal section of the 3 x 6 multi-junction module, are very small : though r.f. loss at inside septum are two times higher than that at outside septum, temperature difference is only 4 °C after an r.f injection time of 250 sec. Consequently, the measured temperature rise is very close to the maximum temperature and temperature measurements fit the calculated temperatures with r.f. losses of 0.85 %.

For this shot, at the end of the 210 sec injection time, temperatures, for each section, are as follows :

	Temperature [°C]	Outgassing area [m^2]
JAERI PPD Input	320	0.197
JAERI PPD Output	250	0.195
3 x 6 MJ	180	1.273
SPS	150	0.431
CEA E/H MJ Input	250	0.38
CEA E/H MJ Output	180	0.38
Connection WG	230	0.56

Using the method described in sect. 5.1, the outgassing rate of each section was evaluated to fit the total measured outgassing flux of 7.24×10^{-6} Pa m^3 s^{-1}. These outgassing rates are consistent with those of the module test I within a factor of 2.5 (Fig.55).

5.5 CEA mode converter + CEA E/H plane multi-junction

5.5.1 Baking and r.f. conditioning

The whole system is baked at 400 °C during 60 hours. Outgassing rate at this temperature decreased from 3.2×10^{-5} to 9×10^{-6} Pa m^3 s^{-1} m^{-2}. At 100 °C, outgassing rate was 5.10^{-8} Pa m^3 s^{-1} m^2. For pulse length of 2 seconds, a power at the klystron of 440 kW was obtained after less than 10 pulses of conditioning.

5.5.2 Long pulse operation

Three shots were performed without cooling. Two of them were done with a power of 200 kW at the klystron and a pulse length of 900 sec and one with a power of 350 kW at the klystron during 400 sec.

When the temperature in the 3 x 6 MJ was less than 340 °C, the temperature rise during r.f. injection was strictly identical to that for the 3 waveguides of the E/H MJ. The same behavior was also observed for the three thermocouples on the MC. Therefore, a good dividing ratio is assessed for both these components. The measured temperature rises, for an incident power of 300 kW at the input, was 0.051 °C s^{-1} for the MC and 0.22 °C s^{-1} for the E/H MJ. By taking into account the of losses of the TE_{30} mode for the MC, and TE_{10} mode for the E/H MJ, rates of 0.075 °C s^{-1} and 0.16 °C s^{-1} were obtained, respectively. For klystron output powers of 200 and 300 kW, Fig 56 and 57 show the time evolution of the temperatures (MC and E/H MJ) and the pressure. Incident and reflected power at the klystron are also plotted. Pressure

slowly increases when the temperature rises. The two peaks are due to outgassing rate measurement by the build-up method.

When the temperature at the input of the E/H MJ reached 340 °C, a non linearity was observed in the temperature increase. The temperature of the MC (input and outputs) was then 240 °C. From the low power test, the first resonance is expected around 360 °C, and then one can say this resonance is caused by the E/H MJ. This is confirmed by observing the temperature evolution in time : the E/H MJ temperature grows non linearly. During r.f. shots, outgassing measurements were carried out. For a typical shot the following temperatures are recorded :

	Temperature [°C]	Outgassing Surface [m^2]
MC input	250	0.38
MC outputs	250	0.38
E/H MJ input	400	0.36
E/H MJ outputs	300	0.36
Connection WG	260	0.56

Using the technique explained in sect. 5.1, it is found that 65 % of the outgassing flux comes from the input of the E/H MJ. From this section, the outgassing rate is 5×10^{-7} Pa m^3 $s^{-1}m^{-2}$ at a temperature of 200 °C and 1.8×10^{-5} Pa m^3 $s^{-1}m^{-2}$ at 400 °C.

5.6 JAERI components + CEA mode converter

JAERI components were tested in combination with the MC. The experimental set-up, sketched in Fig.58, was tested first with the r.f. power injected from the PPD side, then from the MC side. Nineteen long pulses (Thf = 400-1800 s) of r.f. were applied either with no cooling or with water cooling.

5.6.1 Baking and r.f. conditioning

Before the first set of experiment (injection from PPD), the system was baked at 300 °C for 75 hours and the final outgassing at 300 °C, was 2.9×10^{-6} Pa $m^3 s^{-1} m^{-2}$. Then the temperature was decreased from 300 to 100 °C and the tank was maintained at this temperature during the experiment. Outgassing rate decreased from 1.3 to 0.9 x 10^{-7} Pa m^3 $s^{-1}m^{-2}$. These values are equivalent to the ones obtained during the test of module I and first test of JAERI components with E/H MJ (Fig.51). The same procedure conditioning was performed : 2400 short pulses (10 ms) and 50 longer pulses (2 sec.) allowed to transmit 400 kW without breakdowns.

5.6.2 Power division

The power dividing ratio, in the 3 stages of a divider, can be given by :

$$(\Delta T/\Delta t)/\ \Sigma(\Delta T/\Delta t).$$

This is calculated, from the available thermocouples measurements, in different sections : the PPD (Fig.59), the 3 x 6 MJ, the SPS (Fig.60) and the MC (Fig.61). Results of these measurements are given in table 10.

Components	Injection	Top	Central	Bottom	Shot #
PPD	PPD	0.35	0.35	0.30	18023
	PPD	0.35	0.35	0.30	18108
	MC	0.345	0.345	0.31	18485
3 x 6 MJ	PPD	0.34	0.34	0.31	18023
SPS	PPD	0.35	0.35	0.30	18108
MC	PPD	0.34	0.32	0.34	18023
	PPD	0.34	0.32	0.34	18108
	MC	0.345	0.315	0.345	18485

Table 10. Power dividing ratio of the different components deduced from thermocouples measurements

A fairly good power balance was measured in all cases, with a lower power injected in the bottom waveguide (10-15 %) for the JAERI components, while the power of the central waveguide of the MC is slightly lower (5-10 %).

The two small resonance which were measured at room temperature during the frequency scan (f = 3.701 and 3.704 GHz) (see sect. 3.3.2) induce a transitory large increase of losses, specifically in the SPS and the CEA / JAERI transition, but also in the PPD (Fig.62). From the low power test, these resonance was expected when the resonant section is at 59 °C and 99 °C. These resonance did not affect, in most cases, high power transmission capability.

5.6.3 r.f. losses

When the r.f. components were cooled by water, the global r.f. losses during r.f. injection were evaluated from calorimetric measurements. Two output thermocouples are available : one is at the output of the pipes cooling the top of the waveguides and the other at the output of the pipes cooling the bottom of the waveguides. The slight unbalance, measured from thermocouples attached to the waveguides (Table 8), is confirmed : r.f. losses of the upper section with respect to the lower section is in the ratio of 0.54 / 0.46. Moreover, the resonance (T=59 °C) increases the global r.f. losses by about 10 %. Global r.f. losses were measured in two different cases :

- r.f. injection from PPD with the tank at 100 °C
- r.f. injection from MC with the tank at 20 °C

The energy removed by the water was calculated in the case of very long pulses for which stationary temperatures are reached (Fig.63). The associated power P_{calor} can be easily obtained. Corrections for radiated power between the tank and the waveguides were made to get the r.f. power loss (P_{loss}). Different powers are given in table 11.

Shot #	Ttank (°C)	P_{hf} (kW)	thf (s)	P_{calor} (kW)	P_{loss} (kW)	P_{loss}/Ph (%)
18102	100	240	1950	7.3	6.0	2.5
18475	20	250	860	5.4	6.2	2.5
18482	20	300	1640	6.6	7.7	2.6

Table 11. Calorimetric measurements of the global losses

To compare these calorimetric measurements to low level S_{12} parameter, losses of the connections and the r.f. windows have to be added (< 0.5 %). The global loss of the system was evaluated to be : $P_{loss} / P_{hf} = 3.0 \pm 0.7$ % $= 0.13 \pm 0.03$ dB. This value is substantially lower than the S_{12} parameter measured at low level (T=20 °C) : $S_{12} = 0.24 \pm 0.05$ dB (off the resonance). However, error bars indicated that these two evaluations of r.f. loss are not inconsistent.

5.6.4 Outgassing

Outgassing was measured as that mentioned above up to 400 °C when the water cooling was not used. The following temperatures were measured for the different sections (Fig.60 & 61):

	Temperature[°C]	Outgassing Surface [m^2]
PPD input	405	0.197
PPD outputs	280	0.195
SPS	130	0.431
3x6 MJ	220	1.273
MC input	230	0.38
MC outputs	230	0.38
Connection WG	250	0.48

With the same technique, outgassing rate of the different sections was evaluated : outgassing flux of the input of the PPD represents 55% of the total measured flux. In Fig.64, the outgassing rate of the hottest part, the PPD input, is plotted as a function of shot number, at 200, 300 and 400°C.

When these new results were compared with the outgassing rate obtained from the previous experiment, it was found that for the same integrated injected energy, the outgassing rate is higher by at least one order of magnitude. However, in the high power test of module I, temperature of the waveguides reached 500 °C and a strong decrease of the outgassing rate from shot to shot was observed. For this experiment, temperature exceeded 300 °C only for the 2 shots indicated on Fig. 65. It is therefore more realistic to compare these new results with the first shot performed on test module I. In this case, the discrepancy is only a factor of 2-3.

5.6.5 Steady state operation

For the first installation of the PPD with the E/H MJ, it was found that the 3.701 GHz resonance (see section 3.3.1), made steady state operation with water cooling impossible : even at low power ($P_{r.f.}$ = 56 kW). Temperature of the input of the poloidal power divider rises to 220 °C in 2 minutes. Calorimetric measurements indicated a total loss of 8-11 %. The Phase Shifter was then disconnected from the CEA / JAERI transition and an undivided 2-mm thick spacer was removed. Low power level measurements indicated an improvement of r.f. properties with no resonance at 3.7 GHz.

In such conditions, with water cooling of the waveguides, quasi-stationary conditions were obtained during very long r.f. injection time : 1500 s after r.f. injection ($P_{r.f.}$ = 300 kW), the temperature rise rate is below 1×10^{-2} °C s^{-1} and the maximum temperature is 110 °C (Fig.66). The pressure is stationary at P = 8.0×10^{-6} Pa. The stationary outgassing rate was measured for different r.f. power levels leading to different equilibrium temperatures. These results were compared with similar results on Test Module I : in this case again the new results are higher by a factor of 3-5 (Fig.67) despite the same initial outgassing at 20 °C (1.3×10^{-8} Pa m^3 $s^{-1}m^{-2}$).

6. ANALYSIS OF HIGH POWER TEST

Five set-ups were tested at high power : 2 on short-circuit, mainly to check the high electric field withstand of basic components (E/H MJ and PPD in combination with the 3 x 6 MJ) and 3 in transmission on a dummy load to check r.f. properties of the 3 different poloidal dividers in combination with the module. Outgassing evolution of these set-up was also studied in the same time, either by letting the components

With the same technique, outgassing rate of the different sections was evaluated : outgassing flux of the input of the PPD represents 55% of the total measured flux. In Fig.64, the outgassing rate of the hottest part, the PPD input, is plotted as a function of shot number, at 200, 300 and 400°C.

When these new results were compared with the outgassing rate obtained from the previous experiment, it was found that for the same integrated injected energy, the outgassing rate is higher by at least one order of magnitude. However, in the high power test of module I, temperature of the waveguides reached 500 °C and a strong decrease of the outgassing rate from shot to shot was observed. For this experiment, temperature exceeded 300 °C only for the 2 shots indicated on Fig. 65. It is therefore more realistic to compare these new results with the first shot performed on test module I. In this case, the discrepancy is only a factor of 2-3.

5.6.5 Steady state operation

For the first installation of the PPD with the E/H MJ, it was found that the 3.701 GHz resonance (see section 3.3.1), made steady state operation with water cooling impossible : even at low power ($P_{r.f.}$ = 56 kW). Temperature of the input of the poloidal power divider rises to 220 °C in 2 minutes. Calorimetric measurements indicated a total loss of 8-11 %. The Phase Shifter was then disconnected from the CEA / JAERI transition and an undivided 2-mm thick spacer was removed. Low power level measurements indicated an improvement of r.f. properties with no resonance at 3.7 GHz.

In such conditions, with water cooling of the waveguides, quasi-stationary conditions were obtained during very long r.f. injection time : 1500 s after r.f. injection ($P_{r.f.}$ = 300 kW), the temperature rise rate is below 1×10^{-2} °C s^{-1} and the maximum temperature is 110 °C (Fig.66). The pressure is stationary at P = 8.0×10^{-6} Pa. The stationary outgassing rate was measured for different r.f. power levels leading to different equilibrium temperatures. These results were compared with similar results on Test Module I : in this case again the new results are higher by a factor of 3-5 (Fig.67) despite the same initial outgassing at 20 °C (1.3×10^{-8} Pa m^3 $s^{-1}m^{-2}$).

6. ANALYSIS OF HIGH POWER TEST

Five set-ups were tested at high power : 2 on short-circuit, mainly to check the high electric field withstand of basic components (E/H MJ and PPD in combination with the 3 x 6 MJ) and 3 in transmission on a dummy load to check r.f. properties of the 3 different poloidal dividers in combination with the module. Outgassing evolution of these set-up was also studied in the same time, either by letting the components

heating up to 400 °C or with cooling in order to get stationary conditions.

On the short circuit, the tested components (E/H MJ and JAERI components) showed good electric withstand : 200 kW and above could be injected corresponding to the maximum electric field of about 7 kV/cm at the input of the E/H MJ and the PPD, and 3.6 kV/cm in the multi-junction module and at the outputs of the E/H MJ and PPD.

On the dummy load, small resonance (S_{21} = - 0.35-0.5 dB) occur in the most set-ups and induce strongly, but transient, non-linearity in the r.f. losses (Fig.62), but high r.f. power transmission capability was not affected in the most cases up to a power density level of 120 MW m^{-2} at the inputs of the poloidal dividers (PPD, E/H MJ, MC) and 31 MW m^{-2} at the multi-junction module. However, for the first set-up (JAERI components + E/H MJ) the rather strong resonance (S_{21} = -2.2 dB) makes high power transmission impossible and steady state operation with water cooling cannot be performed.

Away from these resonance's, power dividing ratio of the dividers deviates only by little from the ideal case : for PPD, it is typically 0.30, 0.35 and 0.35 (Table 1) when going from the lower stage to the upper stage, in very good accordance with small signal measurements (Fig.17), while for E/H MJ and MC, typical values are 0.34, 0.32 and 0.34 (table 1) and even ideal power splitting is achieved when the MC was tested in combination with the E/H MJ (Fig 57).

The r.f losses are deduced from calorimetric measurements for the case of JAERI components with MC; total losses are 2.5 ± 0.7 % (Table 2) which is slightly below small signal measurements (5 ± 1 % - Fig.34), but consistent with calculated losses (2.2 %), assuming 'normal' losses in each components. From this calorimetric loss measurement, it can also been inferred that r.f. loss in each power divider (PPD and MC) is below 1.5 %.

Evaluation of outgassing rate is more difficult than that for test module test I because of the large temperature gradients. However, the same strong pre-baking temperature, T_{bake}, dependence was observed : when T_{bake} was increased from 300 °C to 450 °C, outgassing during r.f. transmission, was reduced by almost one order of magnitude (Fig.53). As in the previous experiment (module test I), outgassing rate was also found to vary quasi-exponentially with the waveguide temperature during r.f. transmission (Fig.47) leading, very roughly, to an increase of outgassing of, almost, one order of magnitude when temperature is incremented by 100 °C.

For the different set-ups, outgassing rate was in the 10^{-6} Pa m^3 s^{-1} m^{-2} range at 300 °C and the 10^{-5} Pa m^3 s^{-1} m^{-2} range at 400 °C. However it has to be noticed, that higher outgassing rates may be obtained when the temperature of the components exceeds over the pre-baking temperature during r.f. injection (Fig.65). Compared with results from module I [8], there is a fairly good accordance within a factor of 2-3,

which is acceptable, when considering the uncertainty on outgassing rate estimations.

Stationary outgassing could be obtained, with water cooling, for the JAERI components with the MC : the low outgassing rates, in the 10^{-7} Pa m^3 s^{-1} m^{-2} range, are again consistent with the previous results, when considering the large differences in experimental conditions (Fig.67). Extrapolation for a real antenna cooled with hot pressurized water suggests an outgassing rate in the lower 10^{-6} Pa.m^3 s^{-1} m^{-2} range.

7. CONCLUSION

As a second step of the collaborative activities, in order to extend the outgassing database to a more practical LHCD antenna module, more advanced r.f. components were designed and fabricated for the Test Module II. JAERI developed and manufactured one poloidal power divider and the 3 x 6 multi-junction module, while two poloidal power dividers, a E/H plane multi-junction and a mode converter were developed and manufactured by CEA.

For the PPD, E/H MJ and MC, the scattering matrix measured in the small signal tests indicated that reflection coefficients at the front end of the antenna with the plasma have to be rather uniform for the different rows in order to have a well-worked antenna, and then it is essential to attain the reflection coefficient less than a few %.

All these poloidal dividers have a good capability to split high r.f. powers equally in three and the r.f. losses are, in the most cases, small. However, in every experimental set-up, resonant phenomena was observed frequently and a transient anomalous loss (S_{21}=0.3~0.5 dB) was induced. Since the resonant phenomena may strongly limit the r.f. power transmission capability, it is important, for an LH antenna using such poloidal power dividers, that electric lengths of the r.f. components are properly determined to avoid the resonance in the range of operating temperature.

Despite the difficulties to calculate the outgassing rate for the complex systems (two poloidal dividers connected to the multi-junction module), an reliable evaluation of the outgassing rate was made. The outgassing rates were consistent with results from test module I. In particular the strong dependence of outgassing on temperature was further documented.

Steady state operation (300 kW-1000 sec) of the 3 x 6 multi-junction module to be connected to the PPD and MC with water cooling was successfully demonstrated. The maximum temperature of 100 °C, the outgassing rate of ~10^{-7} Pa m^3 $s^{-1}m^{-2}$. For a real on-plasma antenna, with temperature around 200 °C, the outgassing rate will be in the 10^{-6} Pa m^3 $sec^{-1}m^{-2}$ range.

which is acceptable, when considering the uncertainty on outgassing rate estimations.

Stationary outgassing could be obtained, with water cooling, for the JAERI components with the MC : the low outgassing rates, in the 10^{-7} Pa m^3 s^{-1} m^{-2} range, are again consistent with the previous results, when considering the large differences in experimental conditions (Fig.67). Extrapolation for a real antenna cooled with hot pressurized water suggests an outgassing rate in the lower 10^{-6} Pa.m^3 s^{-1} m^{-2} range.

7. CONCLUSION

As a second step of the collaborative activities, in order to extend the outgassing database to a more practical LHCD antenna module, more advanced r.f. components were designed and fabricated for the Test Module II. JAERI developed and manufactured one poloidal power divider and the 3 x 6 multi-junction module, while two poloidal power dividers, a E/H plane multi-junction and a mode converter were developed and manufactured by CEA.

For the PPD, E/H MJ and MC, the scattering matrix measured in the small signal tests indicated that reflection coefficients at the front end of the antenna with the plasma have to be rather uniform for the different rows in order to have a well-worked antenna, and then it is essential to attain the reflection coefficient less than a few %.

All these poloidal dividers have a good capability to split high r.f. powers equally in three and the r.f. losses are, in the most cases, small. However, in every experimental set-up, resonant phenomena was observed frequently and a transient anomalous loss (S_{21}=0.3~0.5 dB) was induced. Since the resonant phenomena may strongly limit the r.f. power transmission capability, it is important, for an LH antenna using such poloidal power dividers, that electric lengths of the r.f. components are properly determined to avoid the resonance in the range of operating temperature.

Despite the difficulties to calculate the outgassing rate for the complex systems (two poloidal dividers connected to the multi-junction module), an reliable evaluation of the outgassing rate was made. The outgassing rates were consistent with results from test module I. In particular the strong dependence of outgassing on temperature was further documented.

Steady state operation (300 kW-1000 sec) of the 3 x 6 multi-junction module to be connected to the PPD and MC with water cooling was successfully demonstrated. The maximum temperature of 100 °C, the outgassing rate of ~10^{-7} Pa m^3 $s^{-1}m^{-2}$. For a real on-plasma antenna, with temperature around 200 °C, the outgassing rate will be in the 10^{-6} Pa m^3 $sec^{-1}m^{-2}$ range.

Acknowledgments

The authors would like to express their thanks to all members of the RF Facility Division and RF Heating Laboratory of JAERI, and LHRF group and secretaries at CEA-Cadarache, for their continuous support. In particular, they are grateful to J. Achard for the r.f. measurements and S. Poli for mechanical assistance. They would also like to acknowledge Drs. R. Aymar, D. Escande, R. Gravier, T. Nagashima, M. Ohta, S. Shimamoto and M. Yoshikawa for their encouragement of collaborative activities.

Reference

[1] Ikeda Y. et al., High power Lower Hybrid Current Drive Experiments in JT-60U, IAEA-CN-60/A-3-I-1, Seville, Spain, 26 Sep.-1Oct., 1994.
[2] Tore Supra team, Recent results on Tore Supra, IAEA-CN-60/A-1-II-1, Seville, Spain, 26 Sep.-1Oct., 1994.
[3] The JET team, Lower hybrid current drive in JET and reactor application, IAEA-CN-60/A-3-I-2, Seville, Spain, 26 Sep.-1Oct., 1994.
[4] R. Decoste et al., Biased divertor performance under LH current drive and heating conditions on the TdeV Tokamak, IAEA-CN-60/A-4-II-8, Seville, Spain, 26 Sep.-1Oct., 1994.
[5] Maebara S. et al., Outgassing of the lower hybrid current drive antenna on JT-60U, Fusion Engineering and Design 30 (1995) 253-259
[6] G. Rey et al., Proc. 15th Symp. Fusion Technology, Vol.1, Utrecht, 1988, p.514.
[7] Seki M. et al., Outgassing measurement of the waveguide module for a steady state LHCD antenna, Fusion Engineering and Design 30 (1995) 357-367.
[8] M. Goniche et al, Very long pulse high RF power test of a LH frequency antenna module, Rep. EUR-CEA-FC-1511. M. Seki et al., Performance test of a lower hybrid waveguide under long-high r.f. power transmission, JAERI-Research 96-025.
[9] Ikeda Y. et al., Simple multi-junction launcher with oversized waveguides for lower hybrid current drive on JT-60U, Fusion Engineering and Design 24 (1994) 287-298.
[10] D. Van Houtte et al, One minute pulse operation in the Tore Supra Tokamak, Nuc.Fus. Vol.33 (1993) No.1, 137-141.
[11] R. E. Collin, Field theory of guided waves, p 412, IEEE press, Field theory of guided waves.
[12] N. Marcuvitz, Waveguide Handbook, p 307, Mc Graw Hill.

Acknowledgments

The authors would like to express their thanks to all members of the RF Facility Division and RF Heating Laboratory of JAERI, and LHRF group and secretaries at CEA-Cadarache, for their continuous support. In particular, they are grateful to J. Achard for the r.f. measurements and S. Poli for mechanical assistance. They would also like to acknowledge Drs. R. Aymar, D. Escande, R. Gravier, T. Nagashima, M. Ohta, S. Shimamoto and M. Yoshikawa for their encouragement of collaborative activities.

Reference

[1] Ikeda Y. et al., High power Lower Hybrid Current Drive Experiments in JT-60U, IAEA-CN-60/A-3-I-1, Seville, Spain, 26 Sep.-1Oct., 1994.
[2] Tore Supra team, Recent results on Tore Supra, IAEA-CN-60/A-1-II-1, Seville, Spain, 26 Sep.-1Oct., 1994.
[3] The JET team, Lower hybrid current drive in JET and reactor application, IAEA-CN-60/A-3-I-2, Seville, Spain, 26 Sep.-1Oct., 1994.
[4] R. Decoste et al., Biased divertor performance under LH current drive and heating conditions on the TdeV Tokamak, IAEA-CN-60/A-4-II-8, Seville, Spain, 26 Sep.-1Oct., 1994.
[5] Maebara S. et al., Outgassing of the lower hybrid current drive antenna on JT-60U, Fusion Engineering and Design 30 (1995) 253-259
[6] G. Rey et al., Proc. 15th Symp. Fusion Technology, Vol.1, Utrecht, 1988, p.514.
[7] Seki M. et al., Outgassing measurement of the waveguide module for a steady state LHCD antenna, Fusion Engineering and Design 30 (1995) 357-367.
[8] M. Goniche et al, Very long pulse high RF power test of a LH frequency antenna module, Rep. EUR-CEA-FC-1511. M. Seki et al., Performance test of a lower hybrid waveguide under long-high r.f. power transmission, JAERI-Research 96-025.
[9] Ikeda Y. et al., Simple multi-junction launcher with oversized waveguides for lower hybrid current drive on JT-60U, Fusion Engineering and Design 24 (1994) 287-298.
[10] D. Van Houtte et al, One minute pulse operation in the Tore Supra Tokamak, Nuc.Fus. Vol.33 (1993) No.1, 137-141.
[11] R. E. Collin, Field theory of guided waves, p 412, IEEE press, Field theory of guided waves.
[12] N. Marcuvitz, Waveguide Handbook, p 307, Mc Graw Hill.

[13] H-S. Unger, Circular waveguide of improved design, the Bell system technical journal, July 1958, p 899.
[14] Ph. Bibet, X. Litaudon, D. Moreau, IAEA Technical Committee Meeting on RF launches for plasma heating and current drive, Naka (Japan), 10-12 Nov. 1993.
[15] Ph. Bibet, T. K. Nguyen et al, Experimental and theoretical results concerning the development of the main r.f. components for next TS LHCD antennae, Proceedings of the 18th SOFT, Karlsruhe (Germany) 22-26 August 1994.

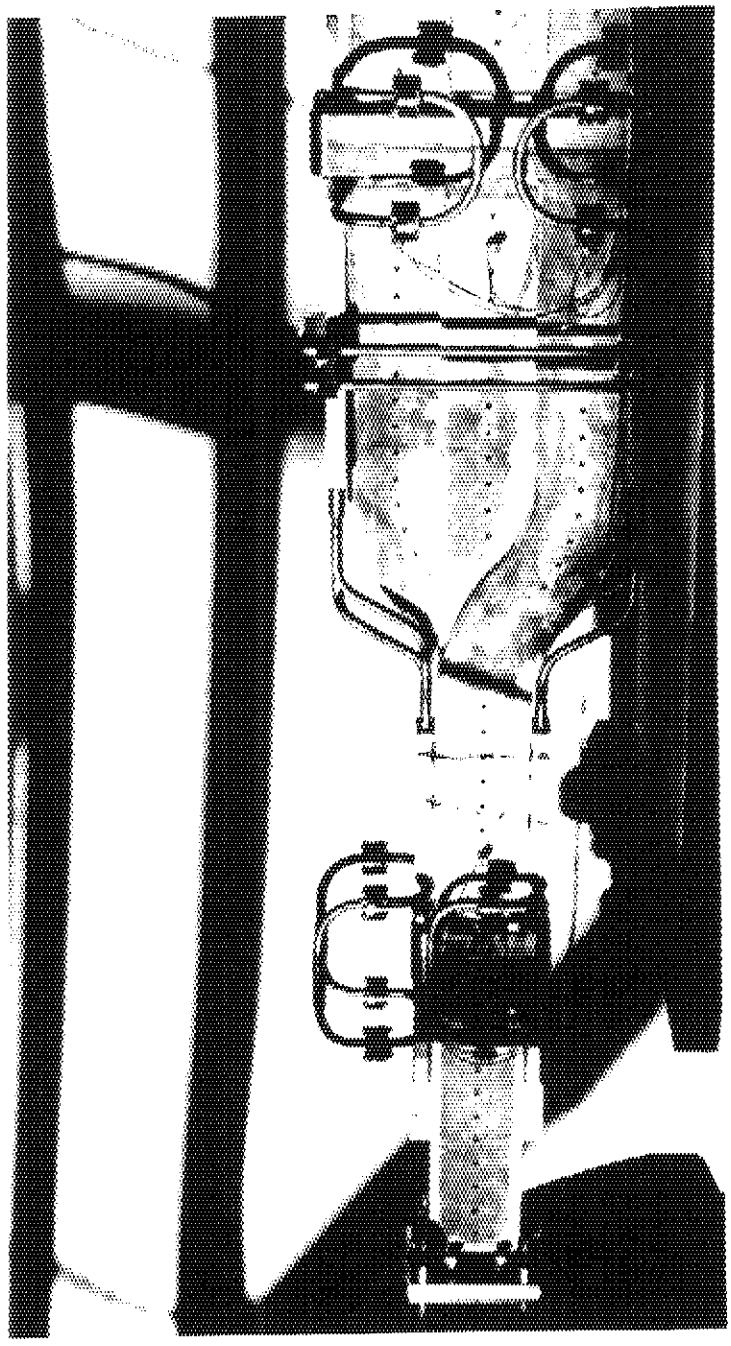

Fig. 1 Photograph of CEA E/H plane multi-junction.

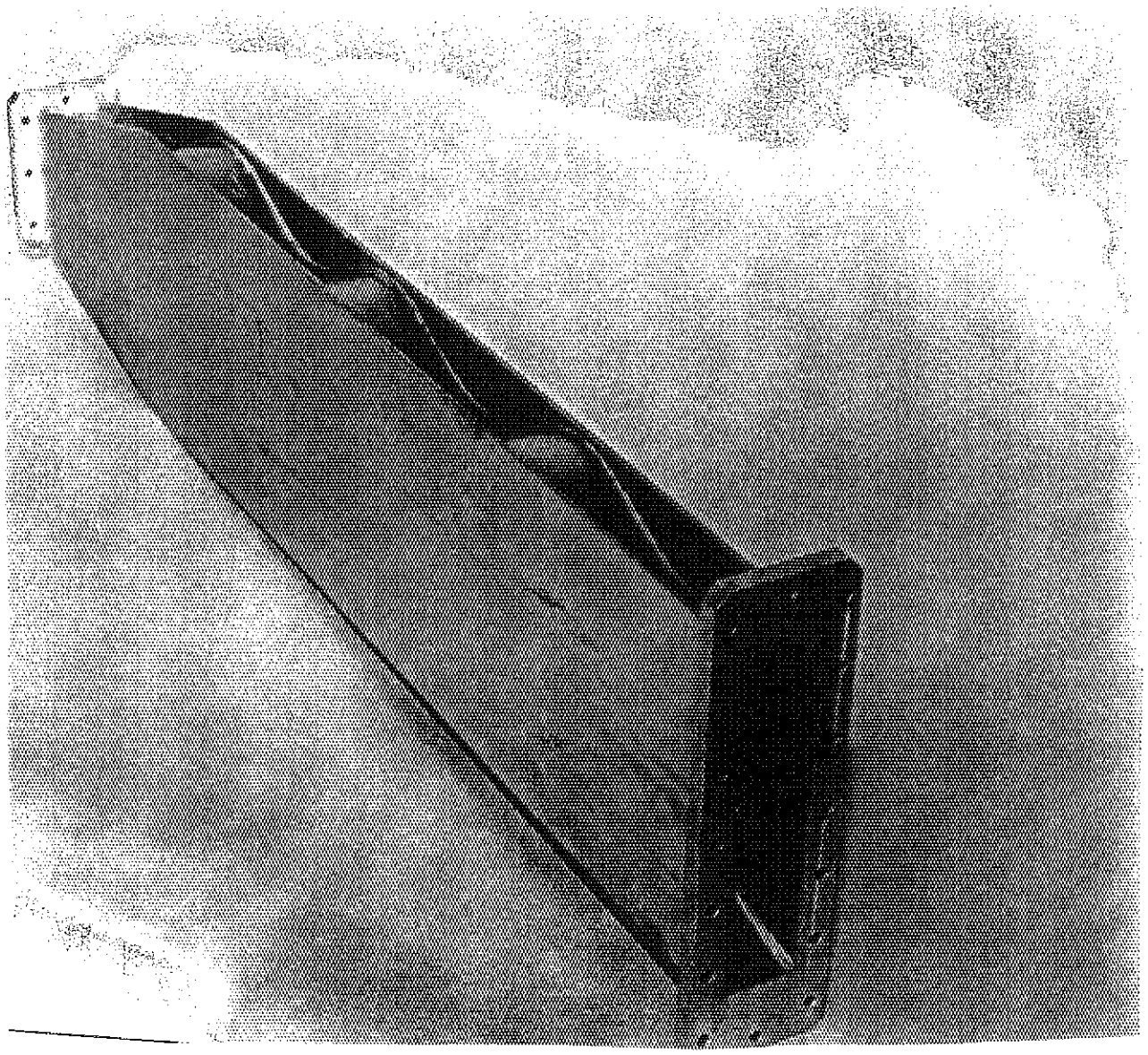

Fig. 2 Photograph of CEA mode converter.

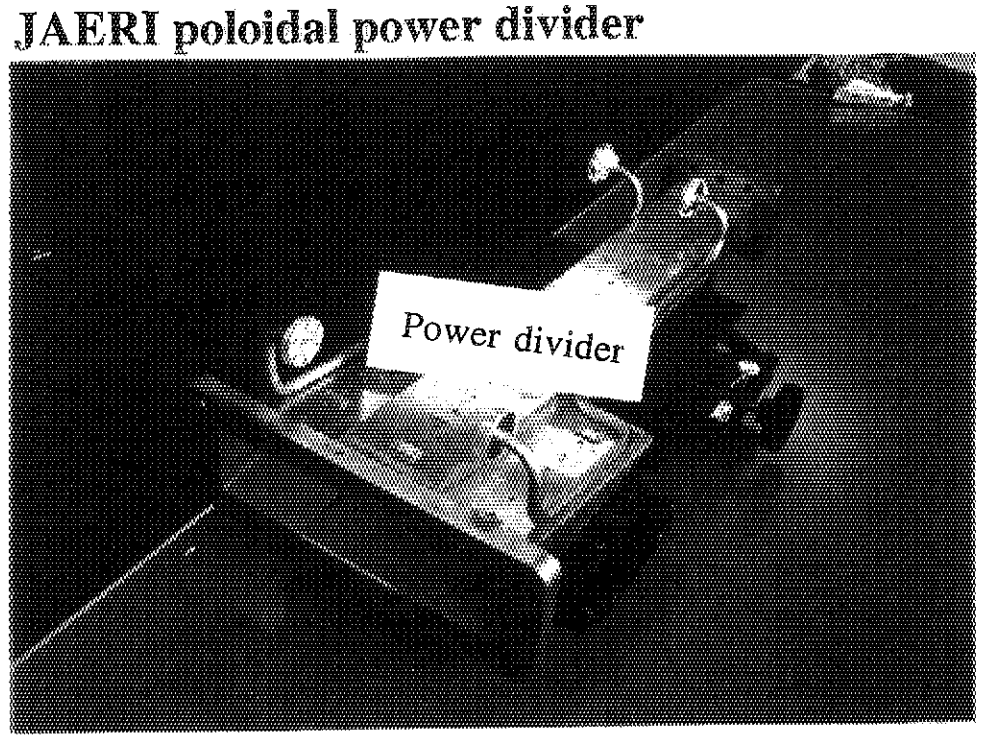

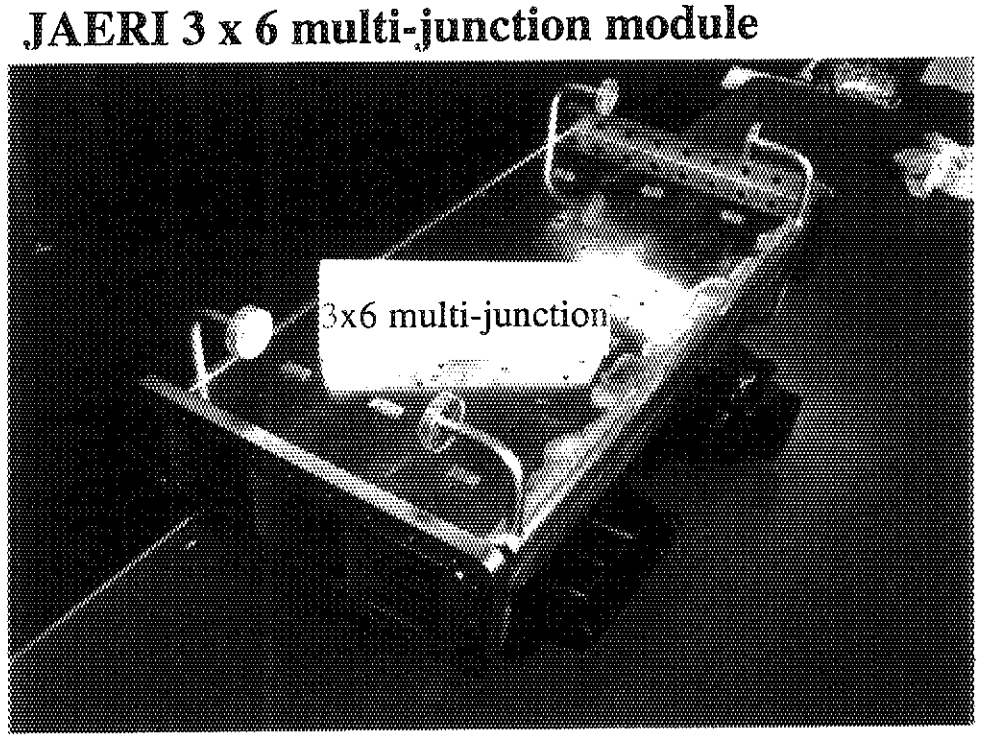

Fig. 3 Photograph of JAERI components.

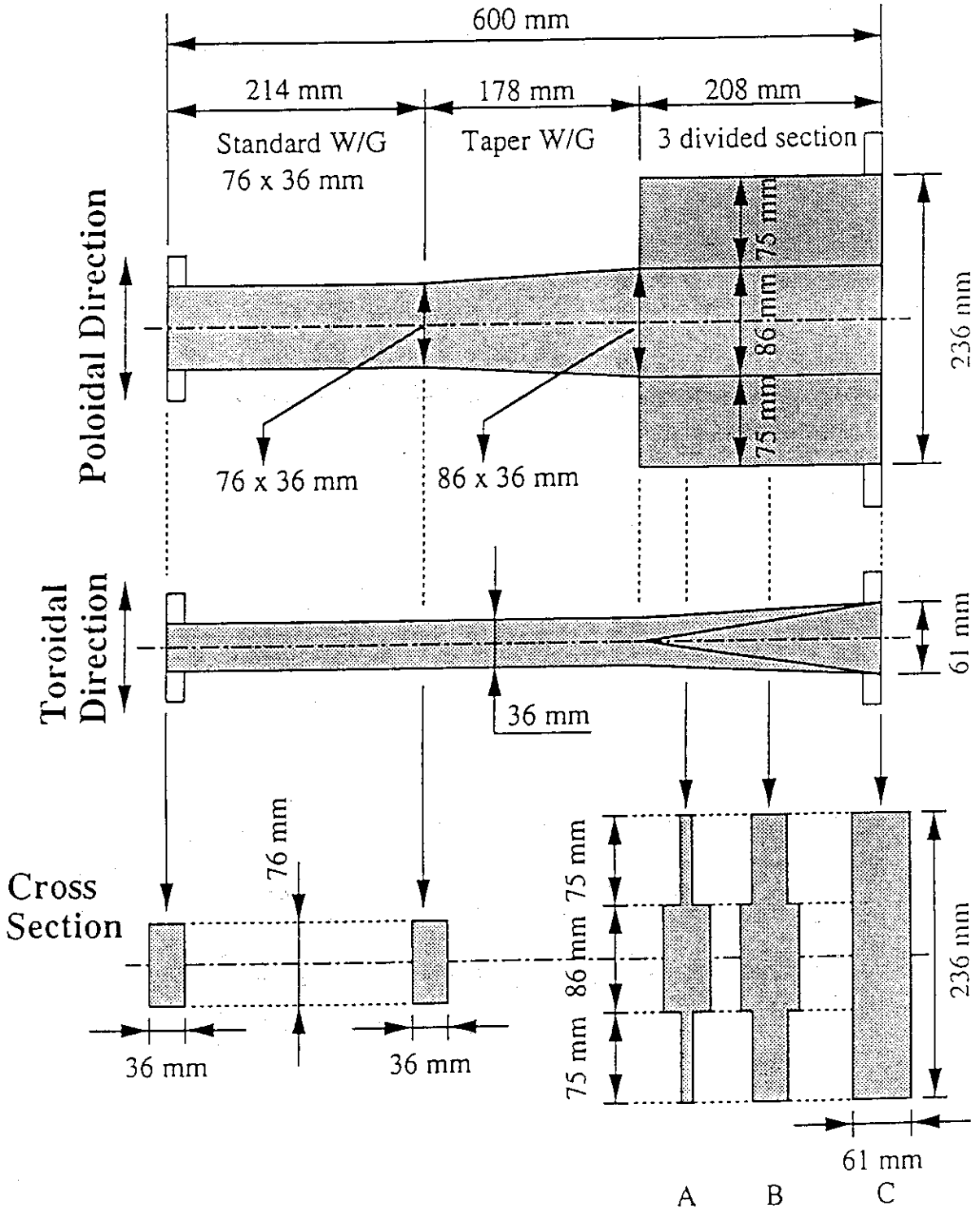

Fig. 4 Dimension of JAERI poloidal power divider.

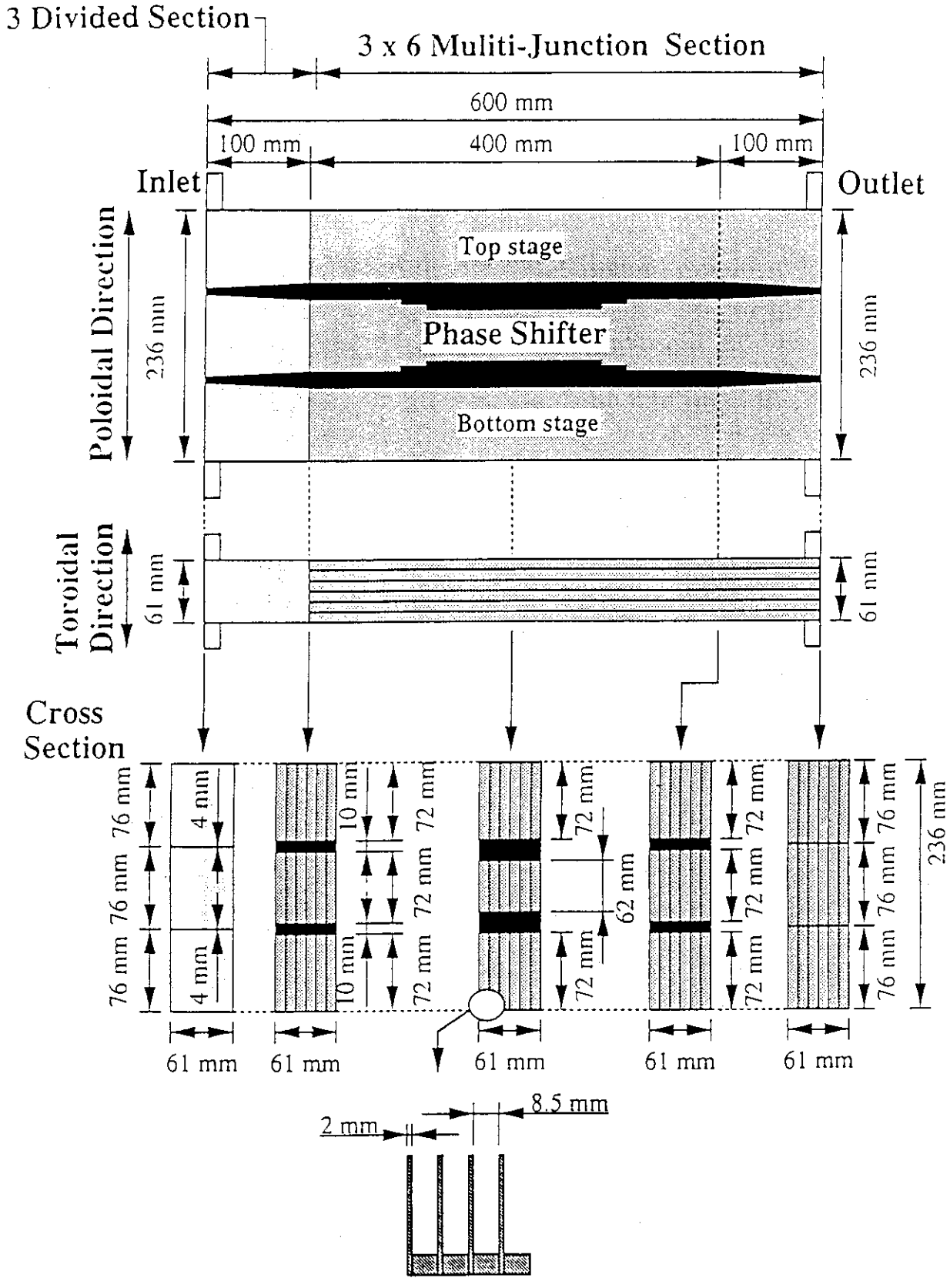

Fig. 5 Dimension of JAERI 3×6 multi-junction module.

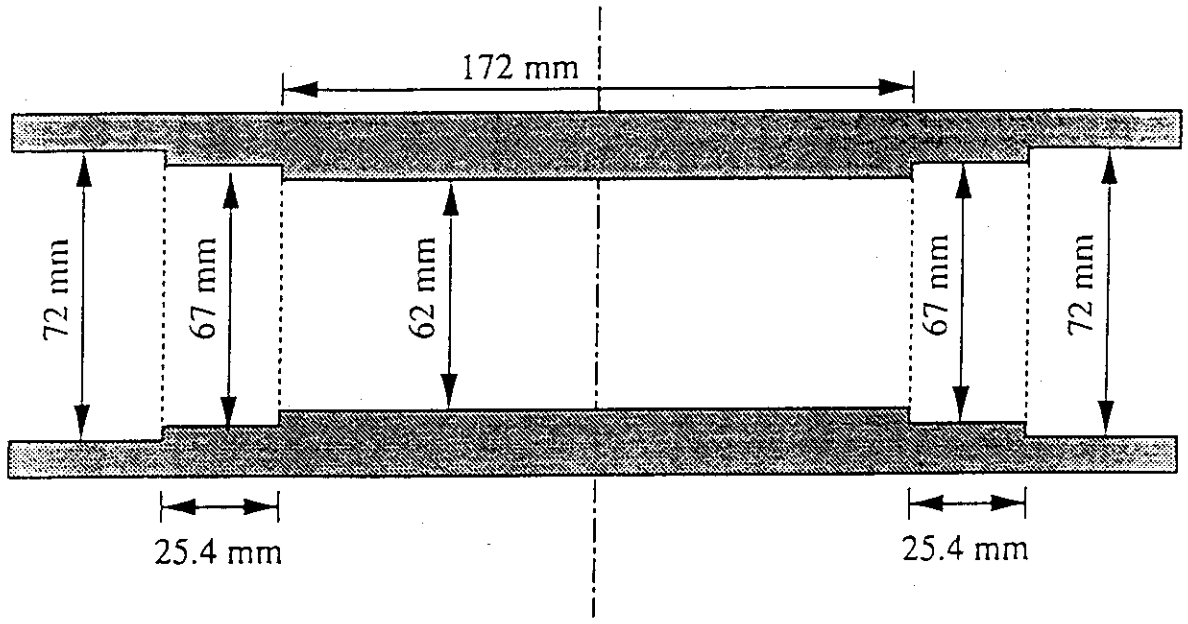

Fig. 6 The phase shifter of JAERI 3×6 multi-junction module.

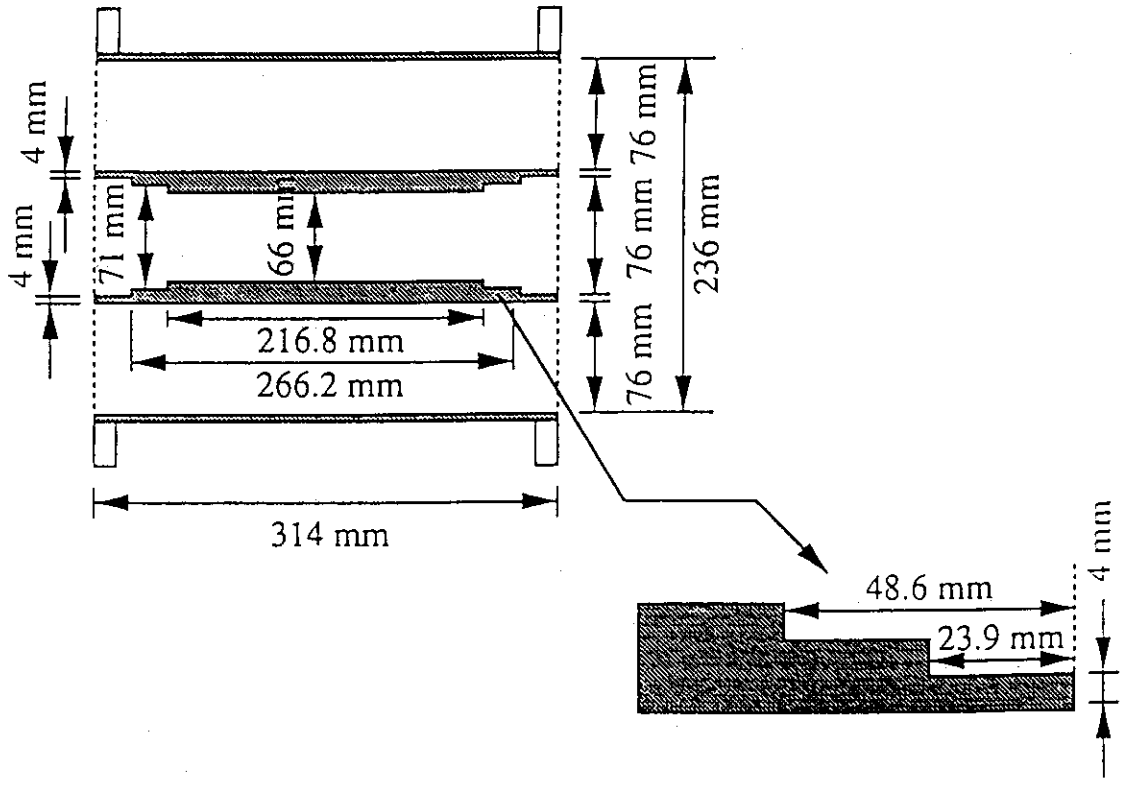

Fig. 7 JAERI supplementary phase shifter.

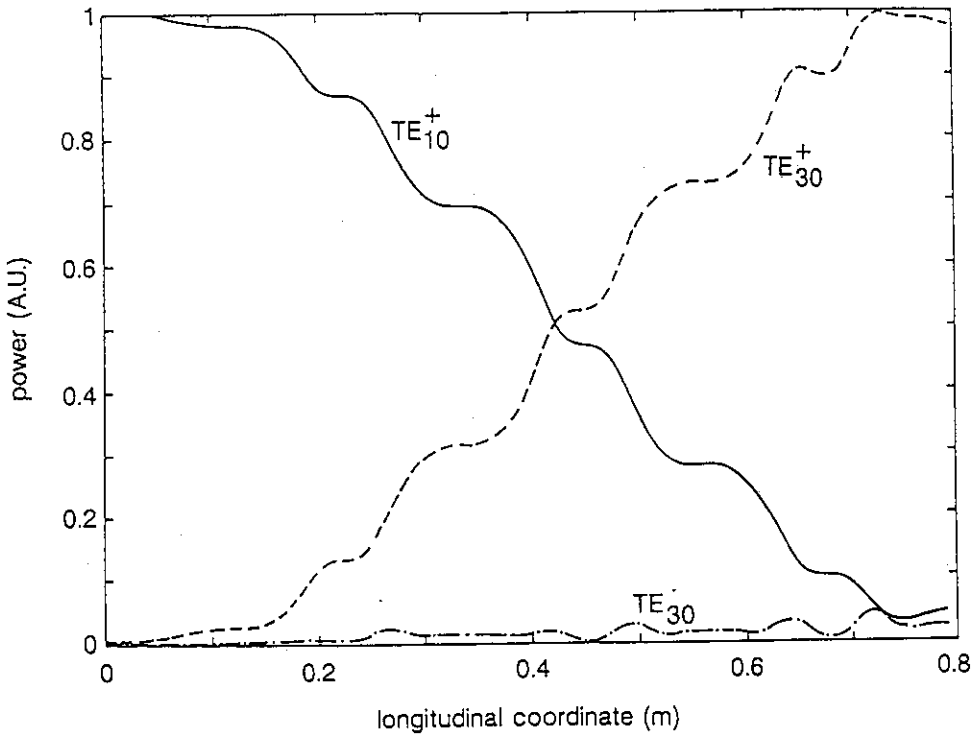

Fig. 8 Power amplitude of the forward (+) and backward (−) propagating modes, along the longitudinal direction, inside the CEA mode converter.

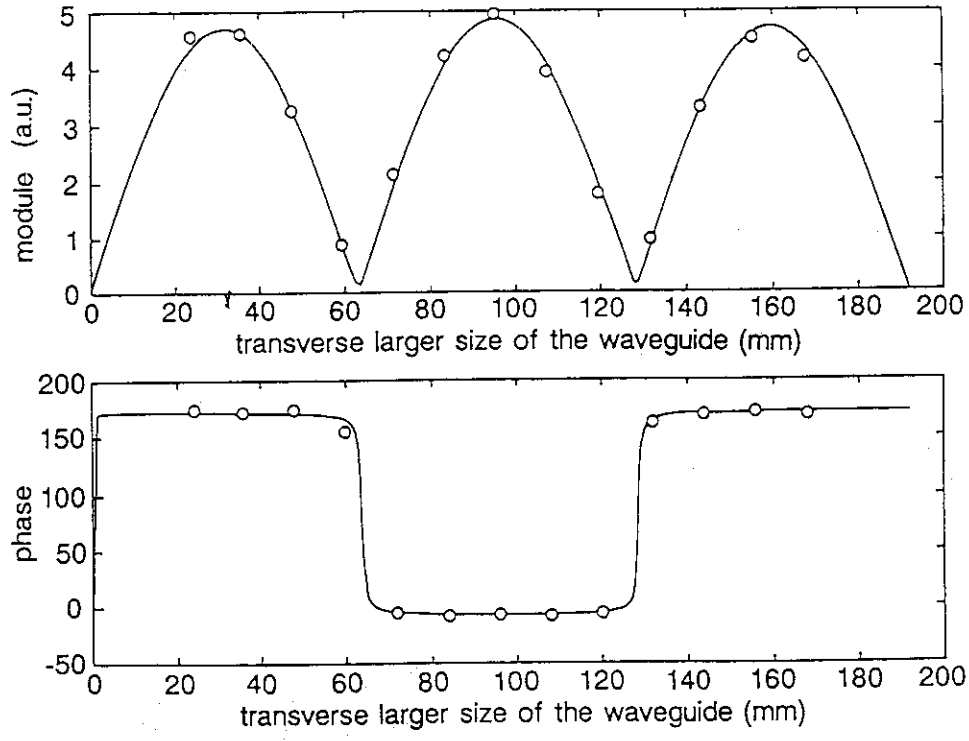

Fig. 9 Amplitude and phase of the total electric field measured with an electric probe, in the transverse direction, in an oversized waveguide set at the mode converter output. The dots are for experimental values, the line are obtained theoretically after the computation of the different coefficient for the propagating modes in the forward and backward direction deduced from measurement.

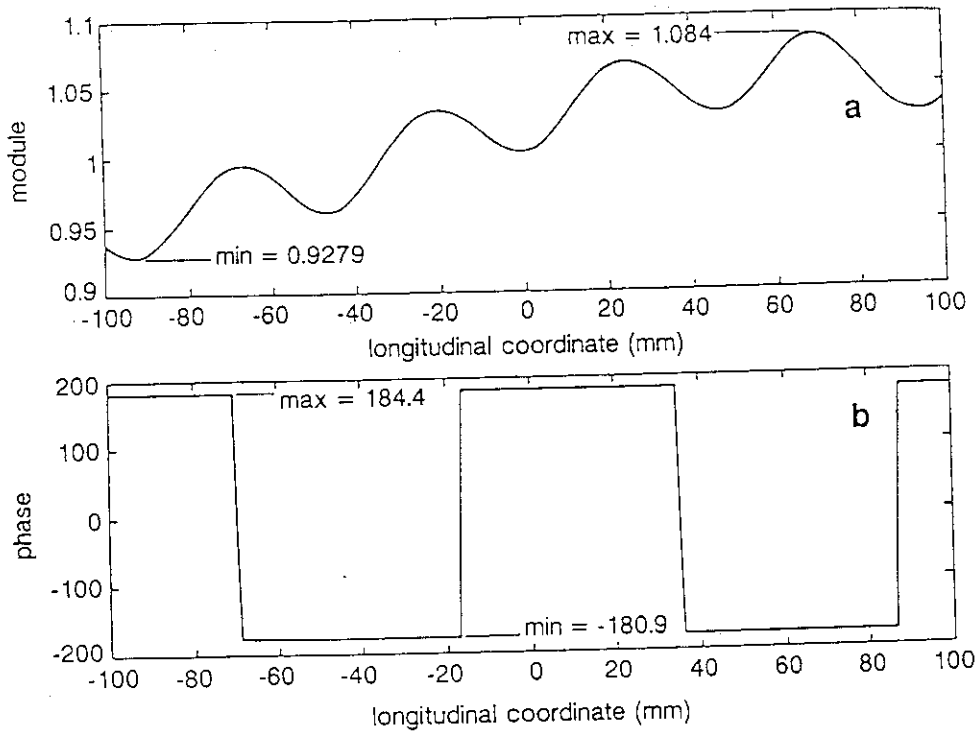

Fig. 10 Ratio of the amplitude of the total electric field in the middle of the transverse size of the waveguide to the one at a point situated at 1/6 of the transverse size and difference of phase at the 2 same places versus the longitudinal direction inside an oversized waveguide at the output of the CEA mode converter.

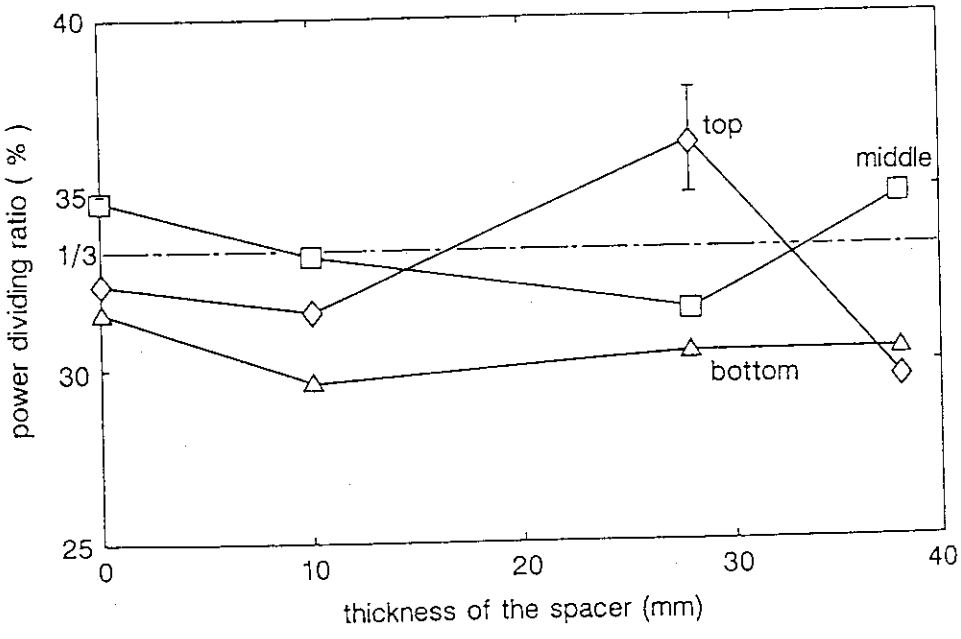

Fig. 11 Variation of the CEA (MC+PJ+3×4 multi-junction) power dividing ratio when oversized spacers of different thickness are set between the MC and the PJ.

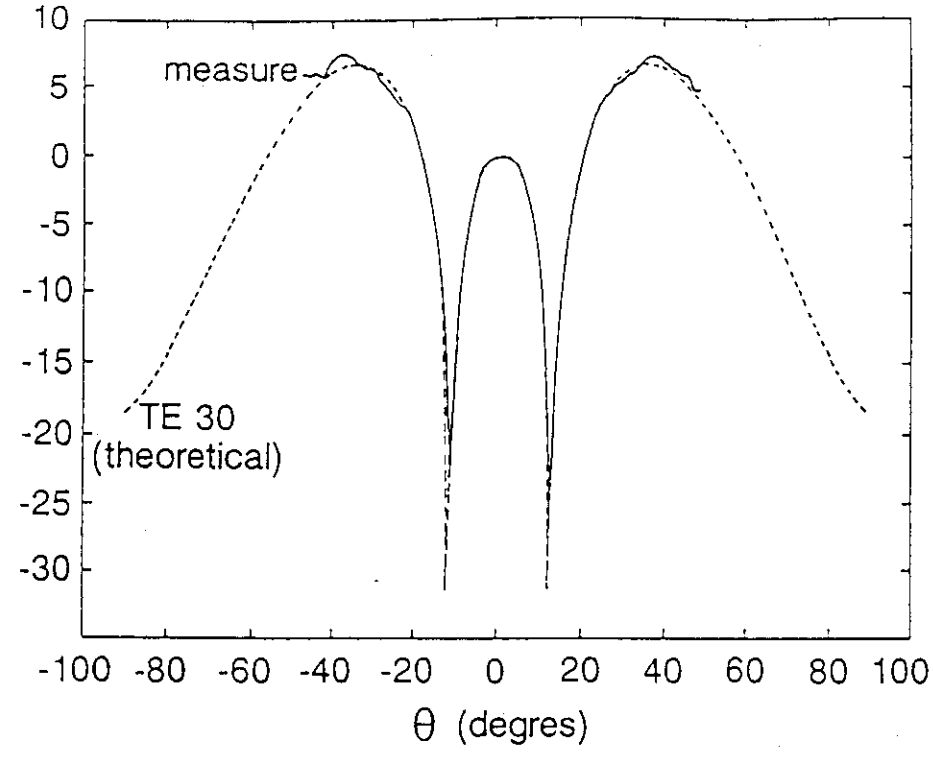

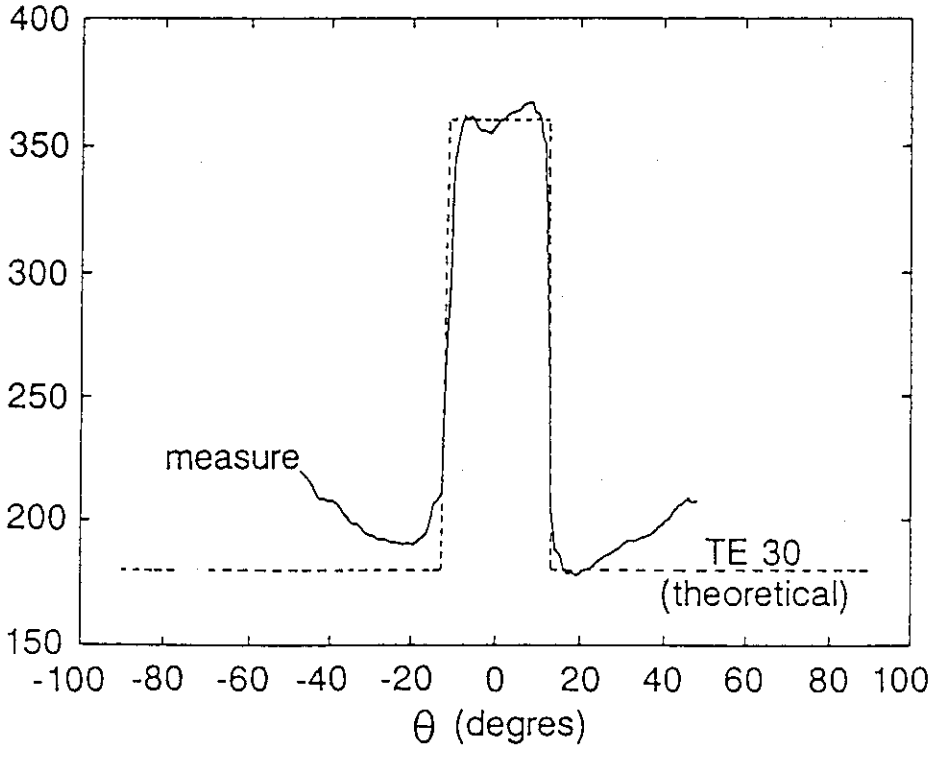

Fig. 12 Comparison of the measured radiating pattern of the CEA MC measured in the far field with the theoretical one of the TE_{30} mode. Amplitude and phase versus the angle in the H plane between the MC axis and the direction of measurement.

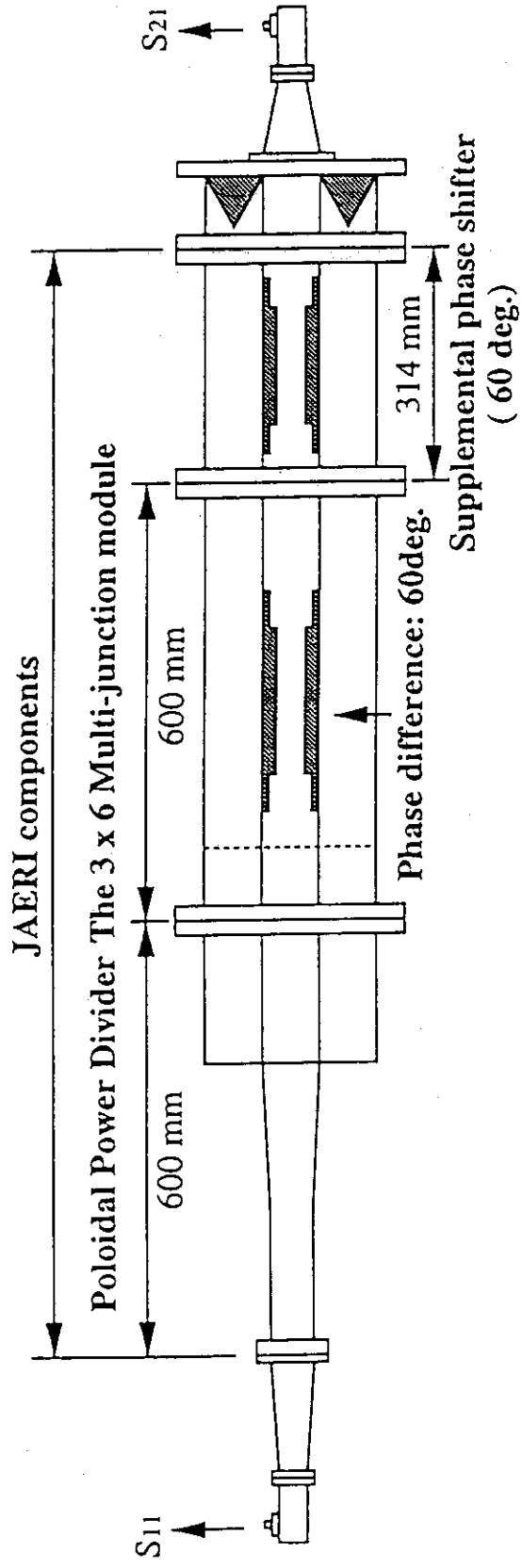

Fig. 13 Schematic drawing of the set-up on a low power test for JAERI components.

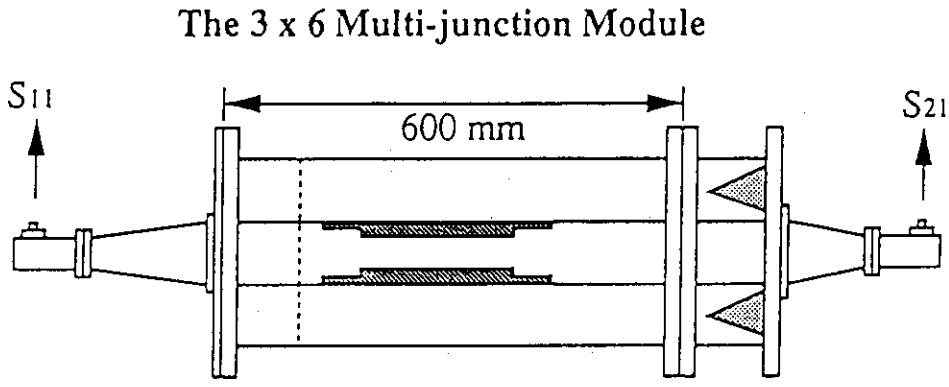

Fig. 14 Schematic drawing of the set-up on a low power test for the 3×6 multi-junction module.

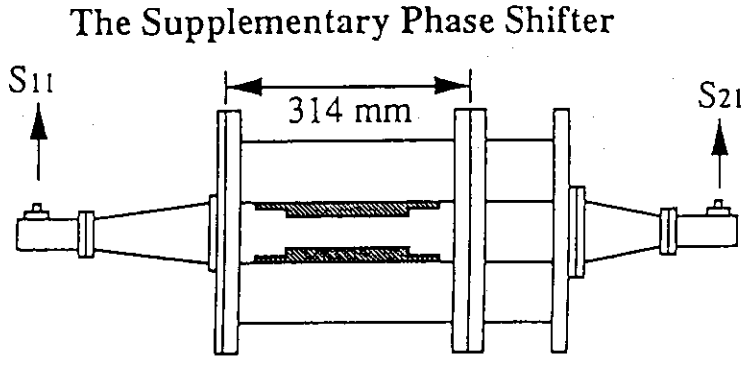

Fig. 15 Schematic drawing of the set-up on a low power test for the supplementary phase shifter.

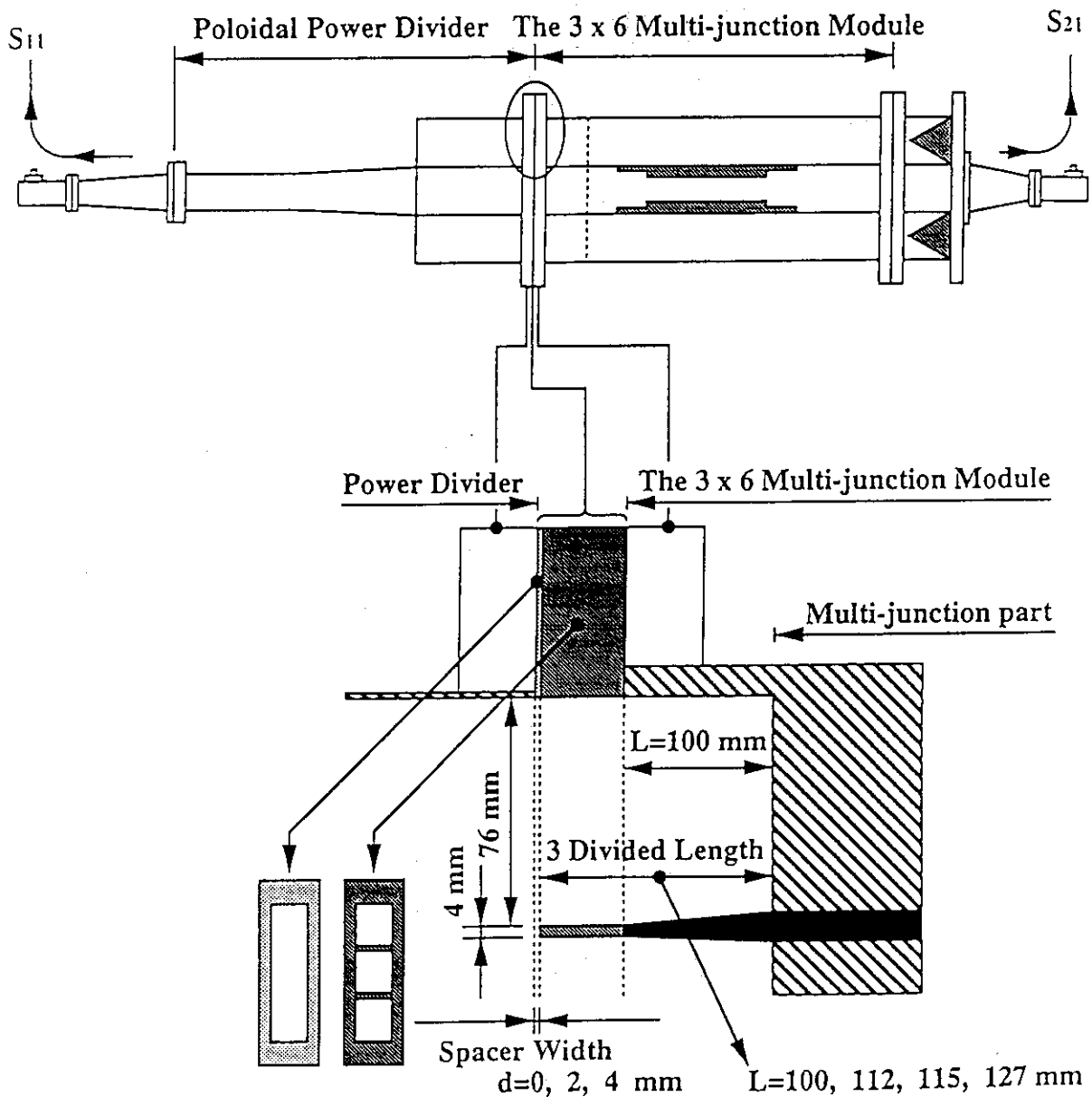

Fig. 16 Schematic drawing of the adjustment part for the power dividing ratio.

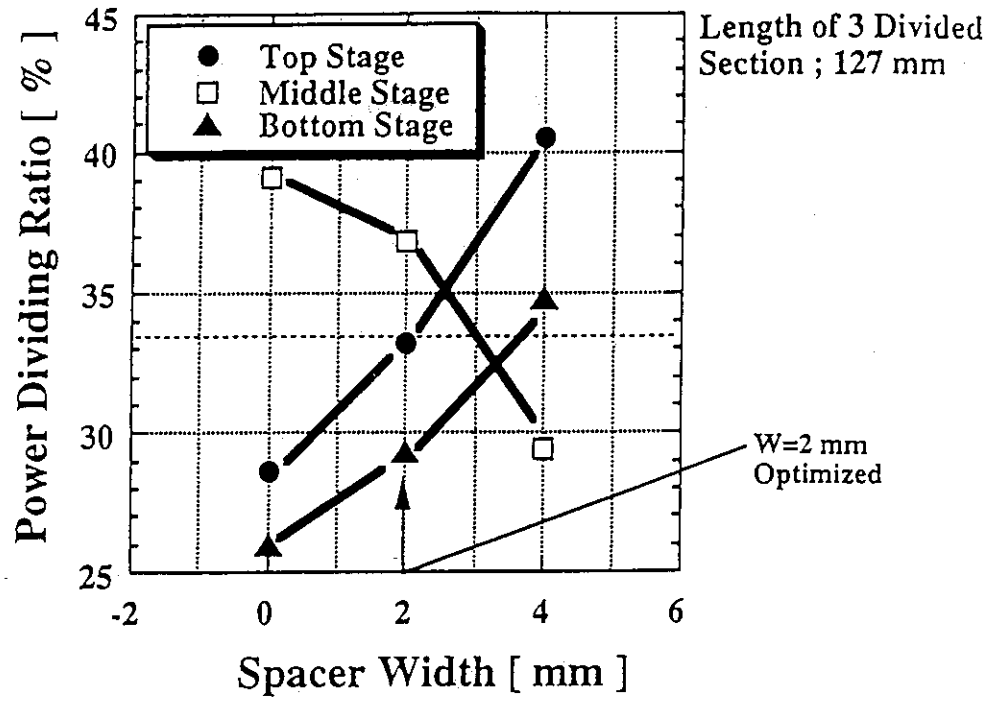

Fig. 17 The dependence of the power dividing ratio on the spacer.

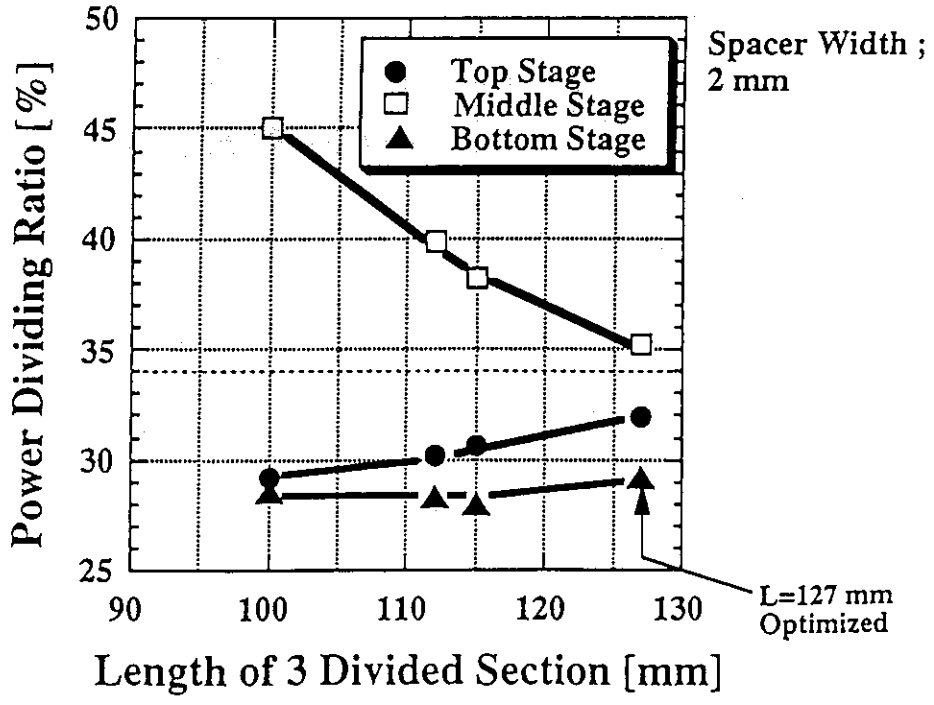

Fig. 18 The dependence of the power dividing ratio on the length of 3 divided section.

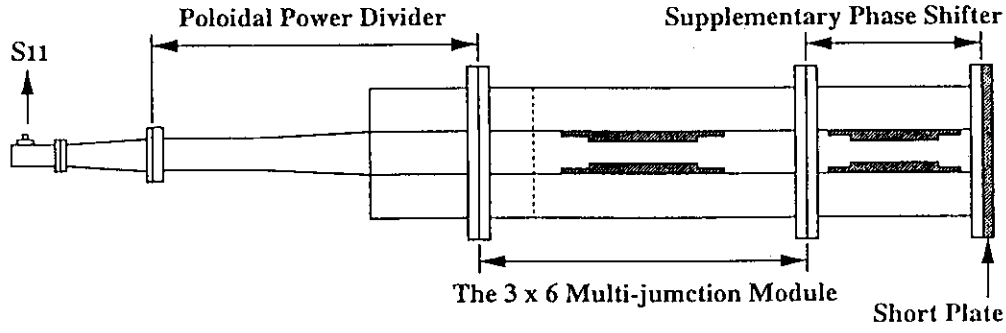

Fig. 19 Schematic drawing of the set-up on a low power test for JAERI components on short circuit.

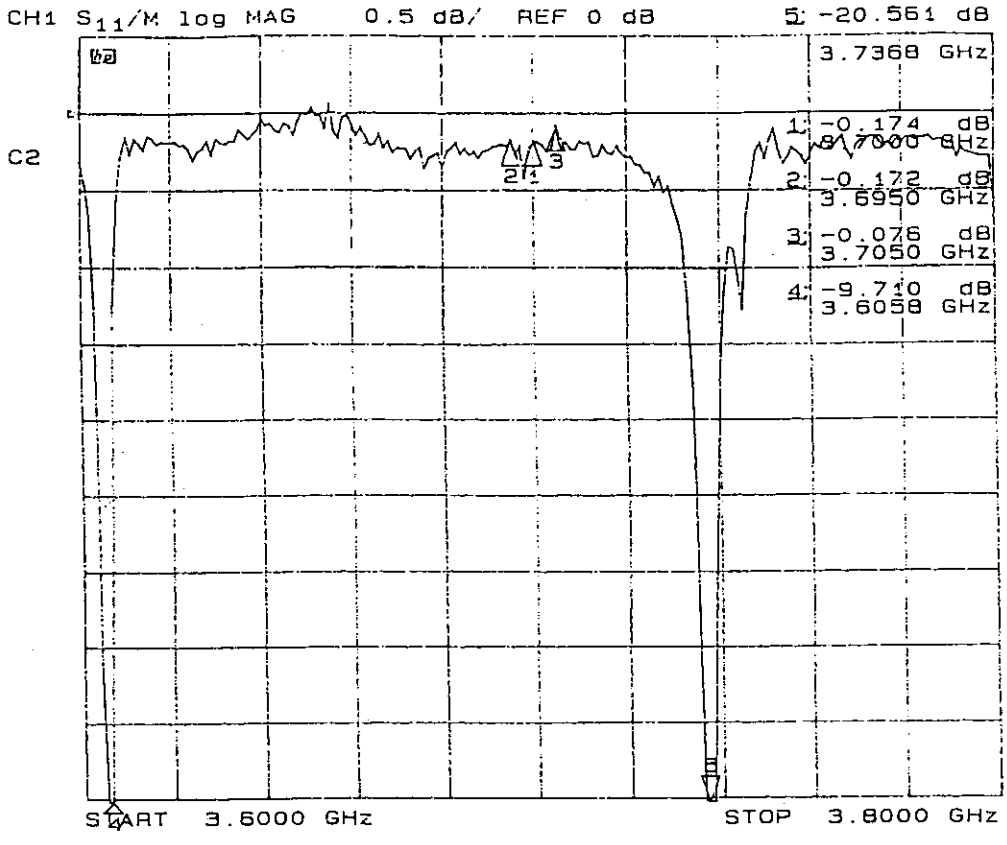

Fig. 20 S_{11} parameter of JAERI components on short circuit versus frequency.

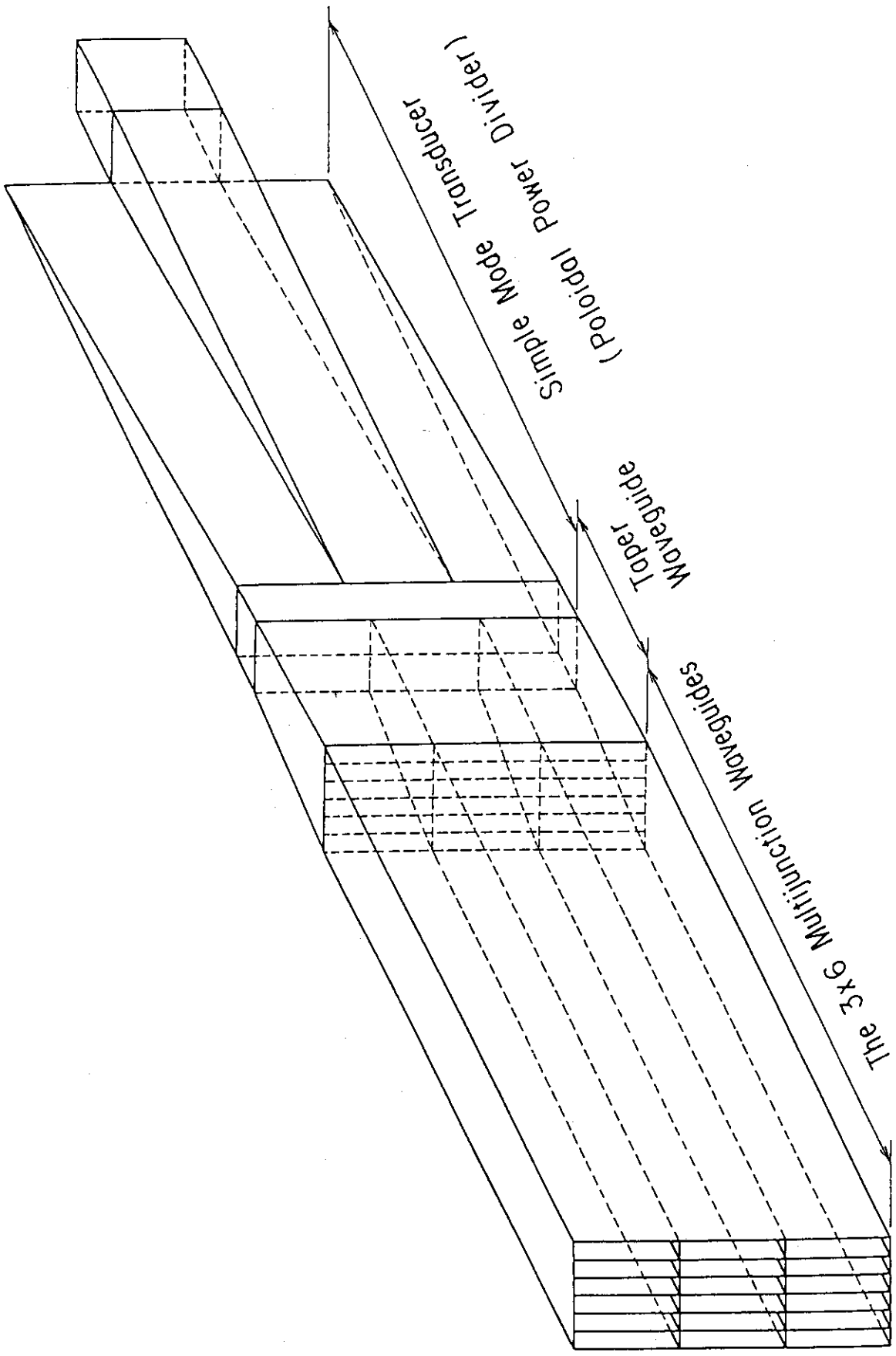

Fig. 21 Conceptual design of poloidal power divider.

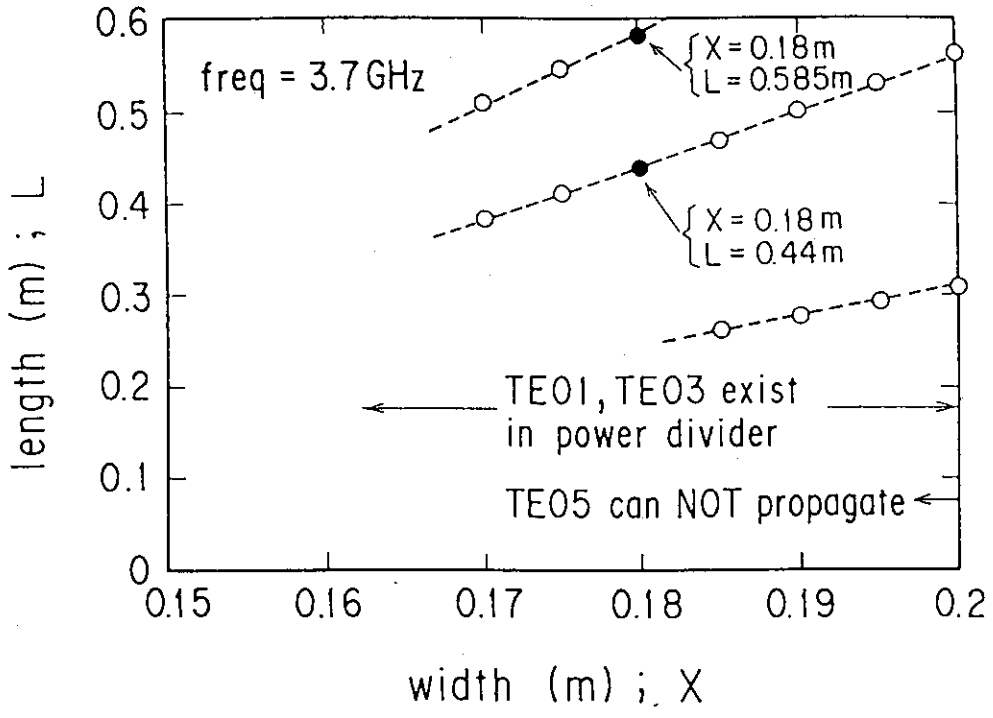

Fig. 22 Length of poloidal power divider versus width in E-plane for good dividing ratio. A poloidal power divider $TE_{01,03}$ is designed by this relation.

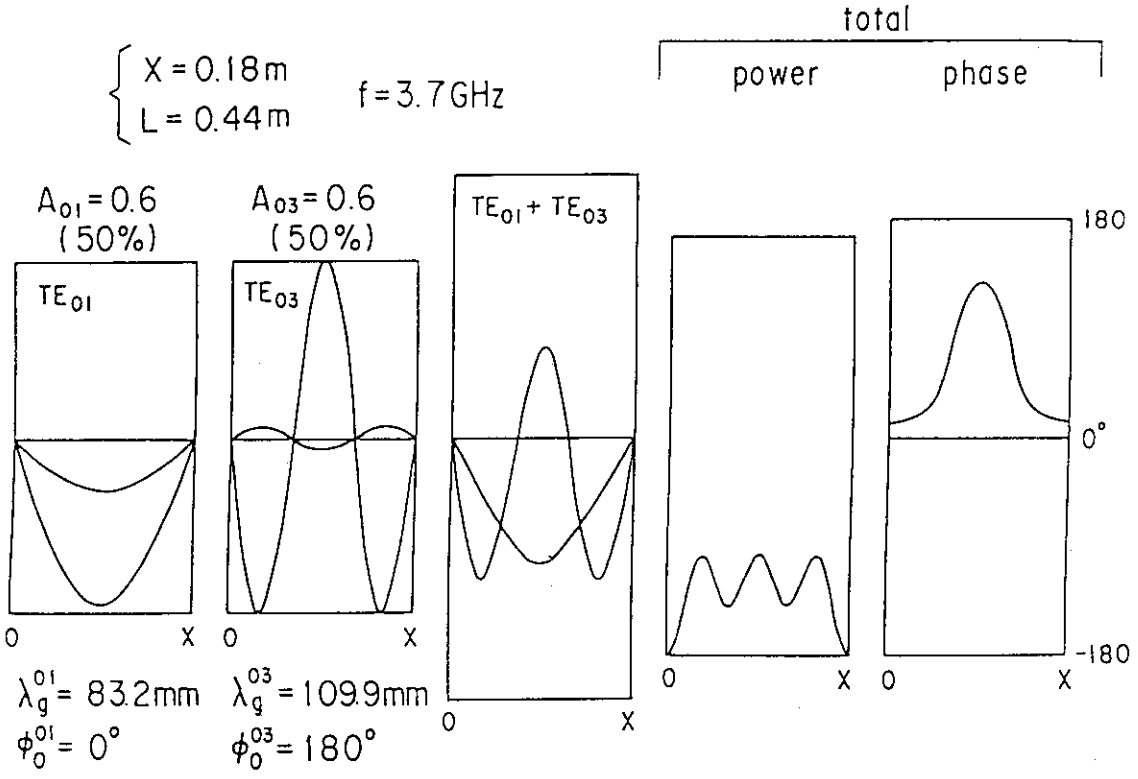

Fig. 23 Analysis of r.f. property using the simple model. TE_{01} and TE_{03} modes are shown at the end of PPD. Profile of r.f. power is well explained.

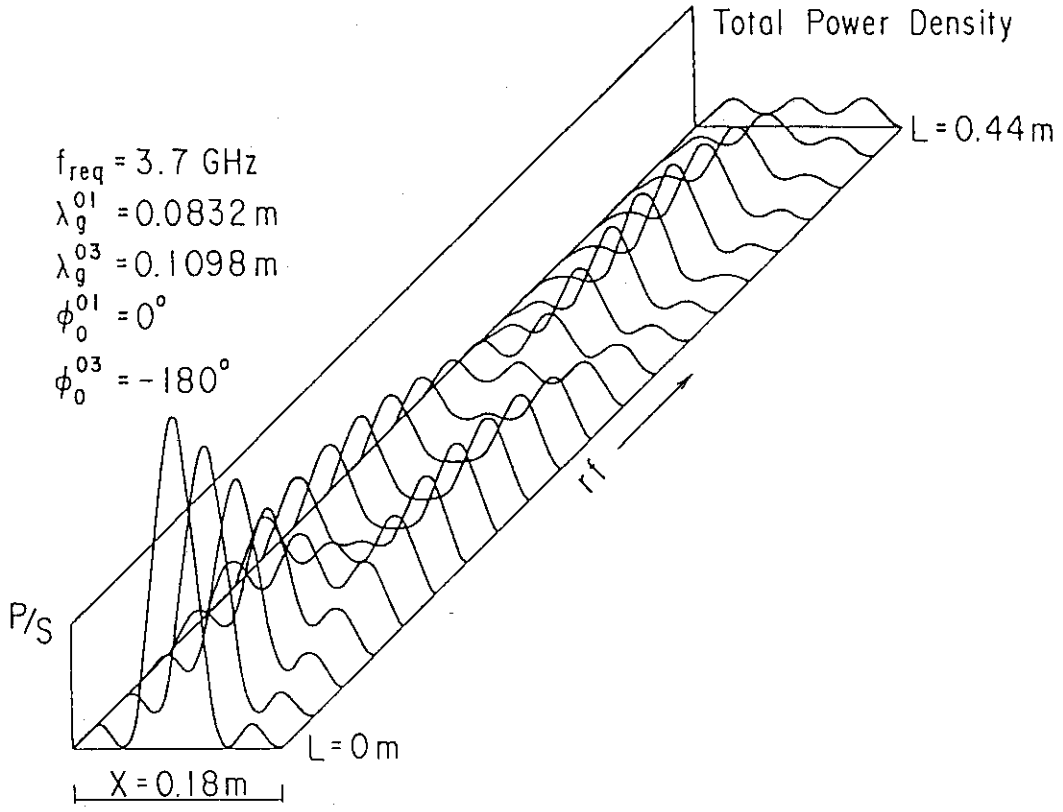

Fig. 24 A poloidal power divider with $TE_{01,03}$ modes is shown. r.f. power density is drawn in the down-side figure. Good power dividing ratio is expected from the same peaks in power density.

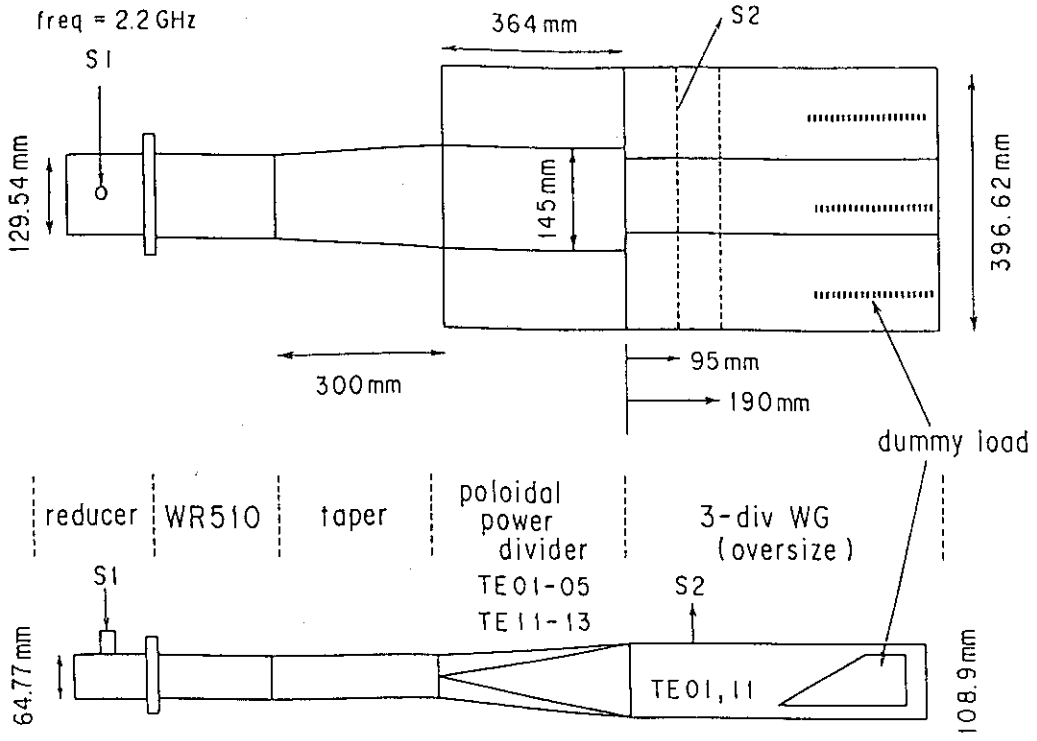

Fig. 25 A poloidal power divider with $TE_{01,03,05}$ is developed in 2.2 GHz for R&D. Three waveguides lined in poloidal direction have no sub-waveguide in it for convenience. Power and phase are measured at z = 95, 190 mm from a junction using r.f. probe connected with a network analyzer.

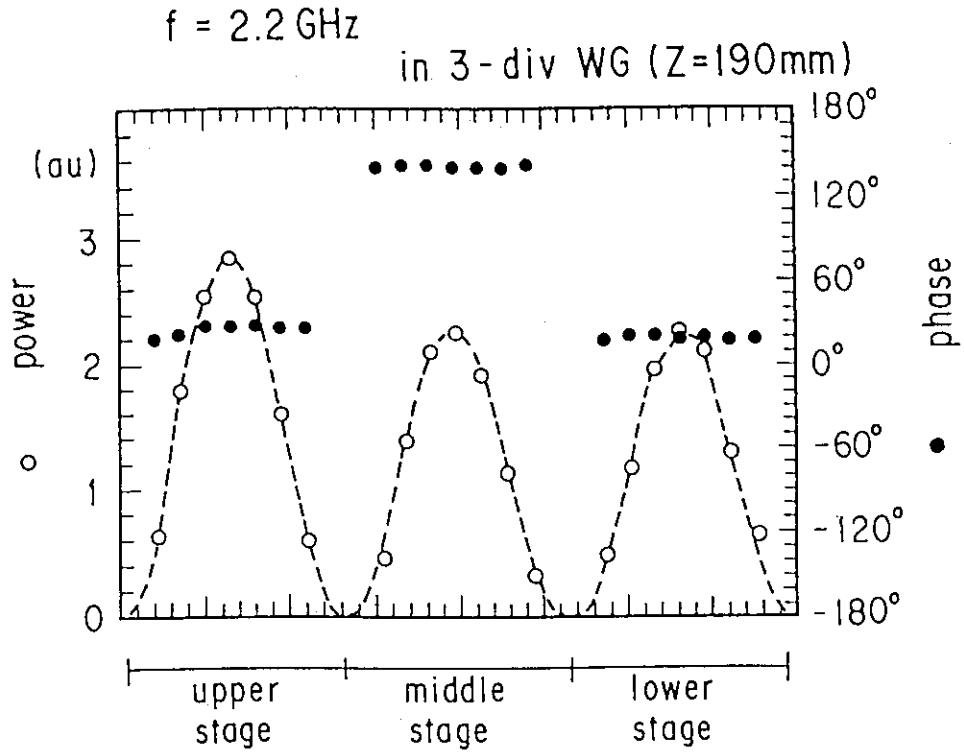

Fig. 26 Both power density and phase distribution are plotted at z = 190 mm. Power dividing ratio is ~1/3, phase difference is ~120 deg. Reflection in input waveguide is low as 1.4 %.

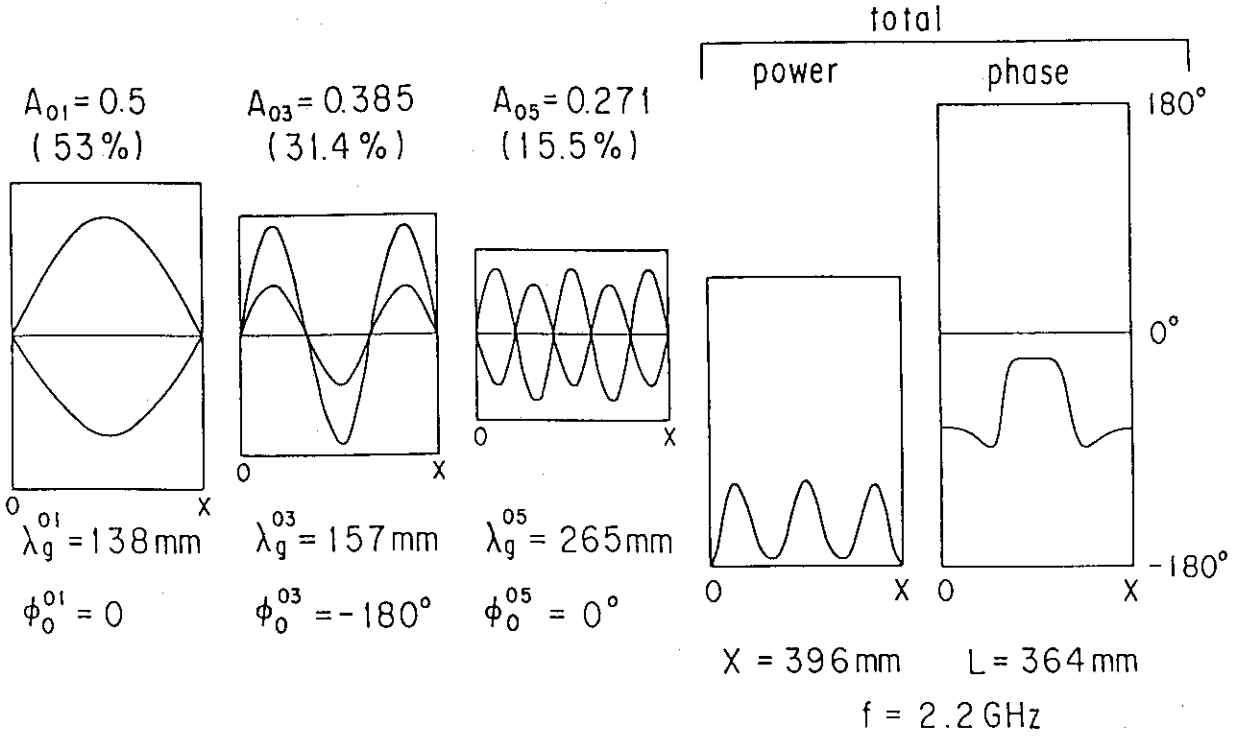

Fig. 27 R.f. property is analyzed by a simple model, amplitude of $TE_{01,03,05}$ is shown at the end of the poloidal power divider. Total power and phase are also drawn.

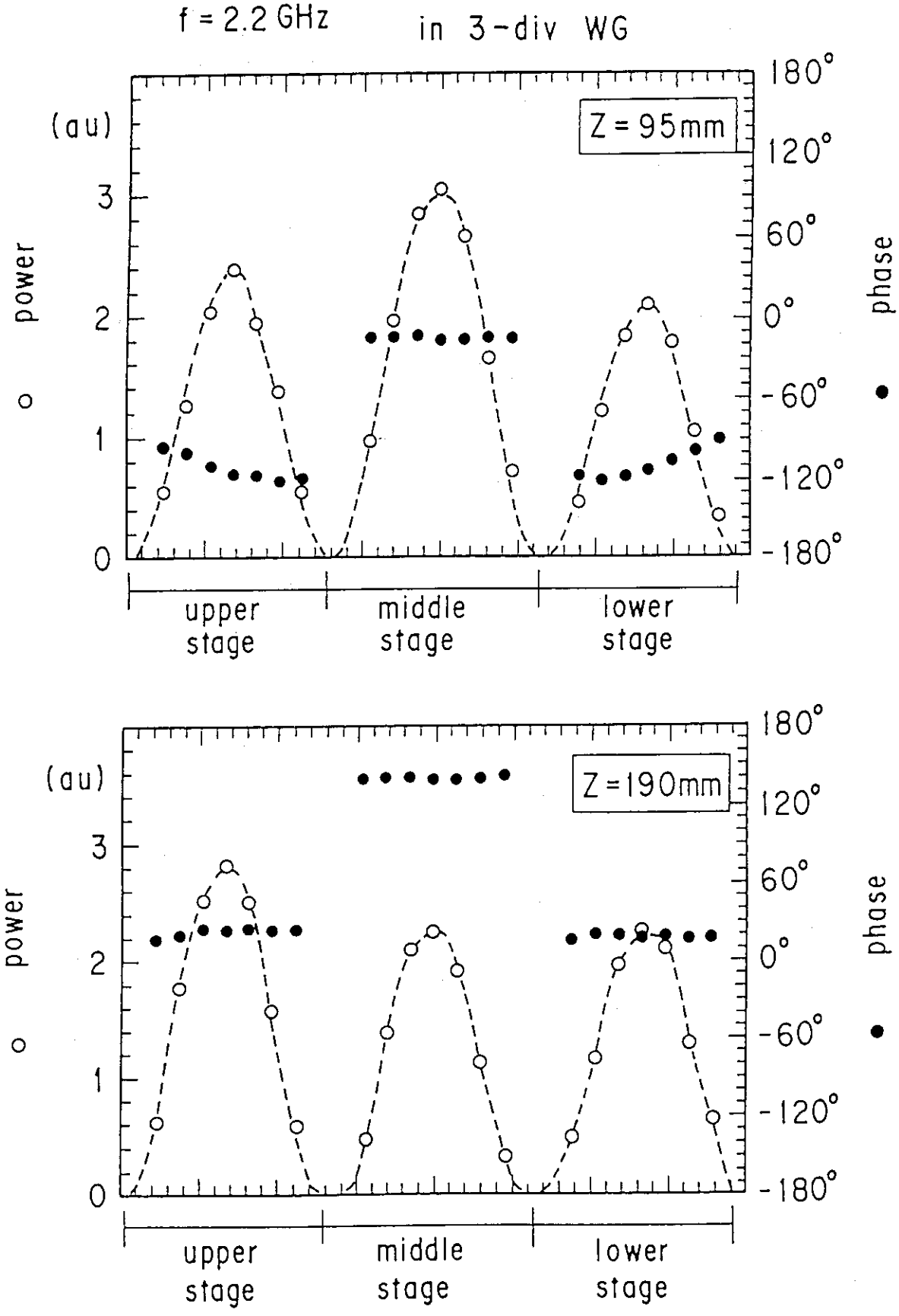

Fig. 28 Result of Fourier analysis is indicated.

$$Func = \sum_i Ai \cdot \cos(ix) + B_i \cdot \sin(ix)$$

A(0) = 0
B(0) = 0
A(1) = 0
B(1) = 0.4112
A(2) = 0
B(2) = 0
A(3) = 0
B(3) = -0.3317
A(4) = 0
B(4) = 0
A(5) = 0
B(5) = 0.2057
A(6) = 0
B(6) = 0
A(7) = 0
B(7) = -0.0823
A(8) = 0
B(8) = 0

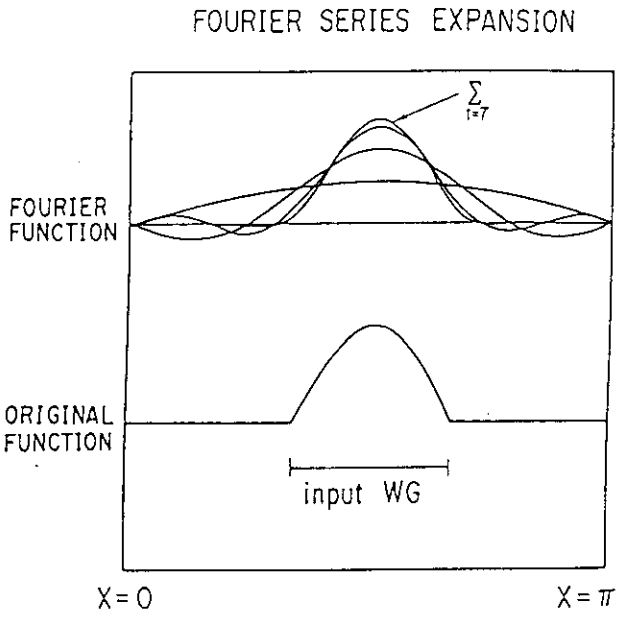

Fig. 29 Effect of higher mode at a junction on r.f. property is shown. Phase distribution measured at z = 95 mm suggests higher mode in sub-waveguide. Power is different between at z = 95 and z = 190 mm.

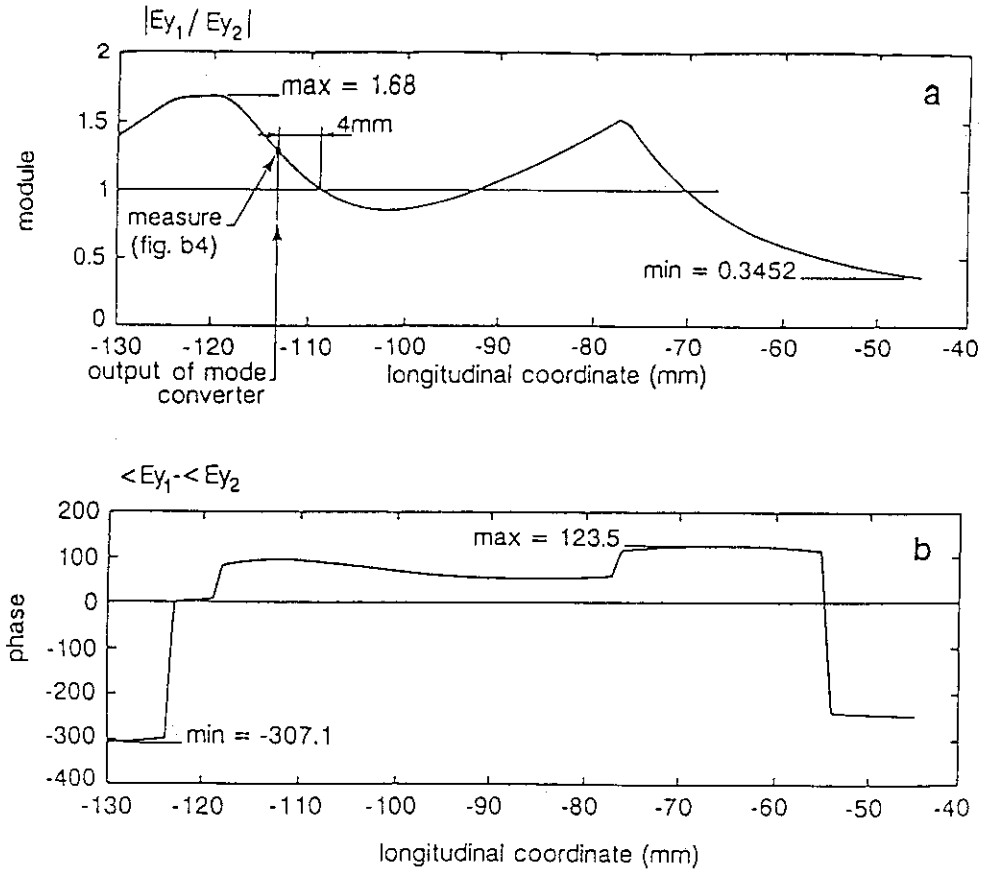

Fig. 30 The same Fig. 10 but with JAERI PPD.

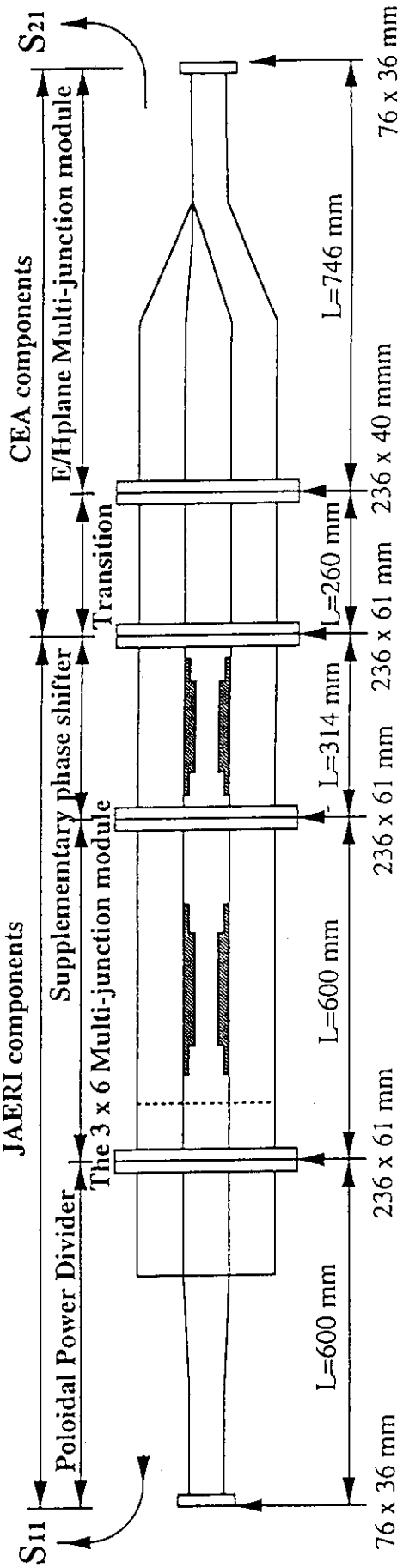

Fig. 31 Schematic drawing of the set-up on a low power test for JAERI components + CEA E/H plane multi-junction module.

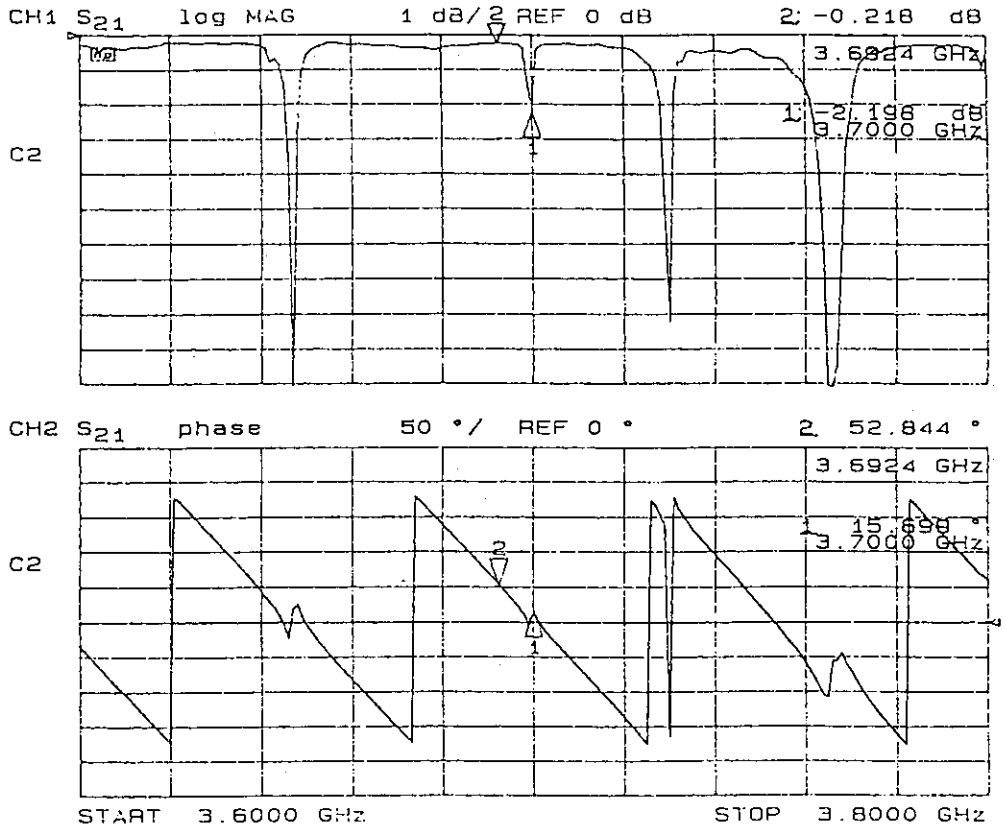

Fig. 32 S_{21} parameter at the 3 × 6 multi-junctin module temperature of 50 ℃ in JAERI components + CEA E/H plane MJ versus frequency.

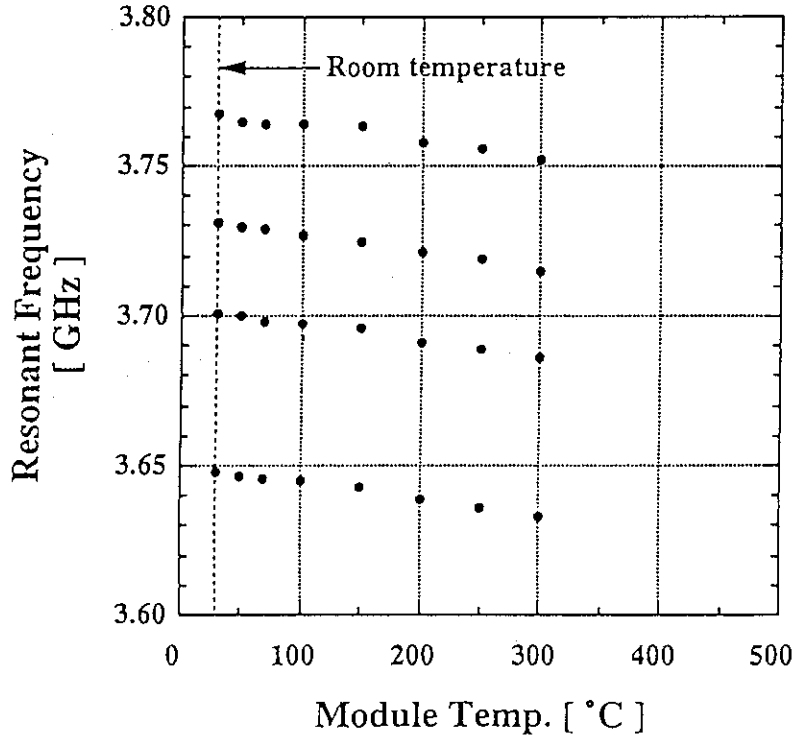

Fig. 33 The dependence of the resonant frequency on the module temperature.

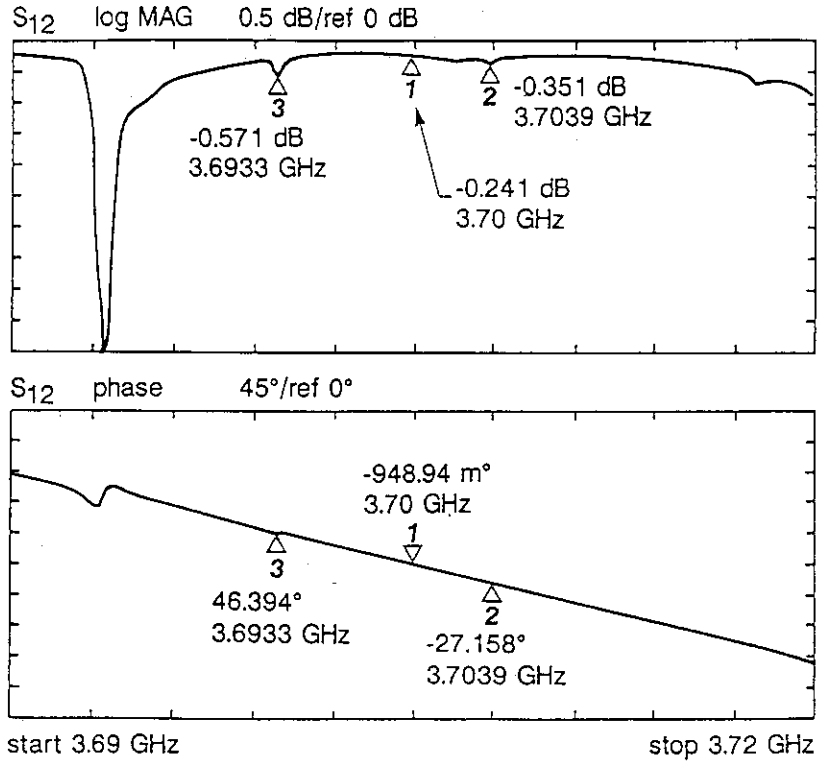

Fig. 34 Amplitude and phase of S_{12} parameter of JAERI components + CEA (61/40 + PJ + MC) versus frequency.

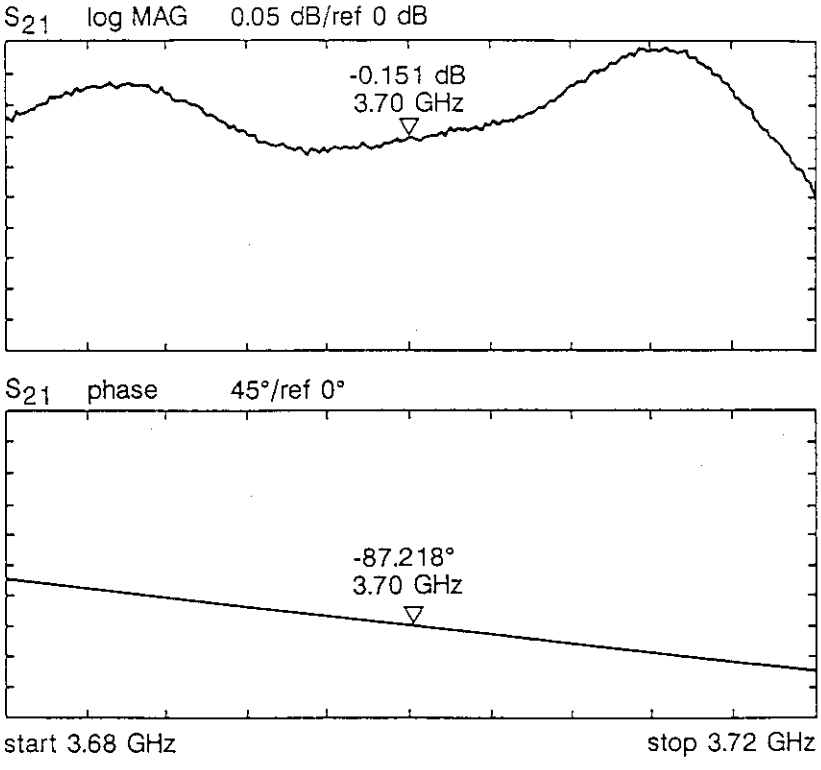

Fig. 35 Amplitude and phase of S_{12} parameter of CEA MC + E/H plane multi-junction.

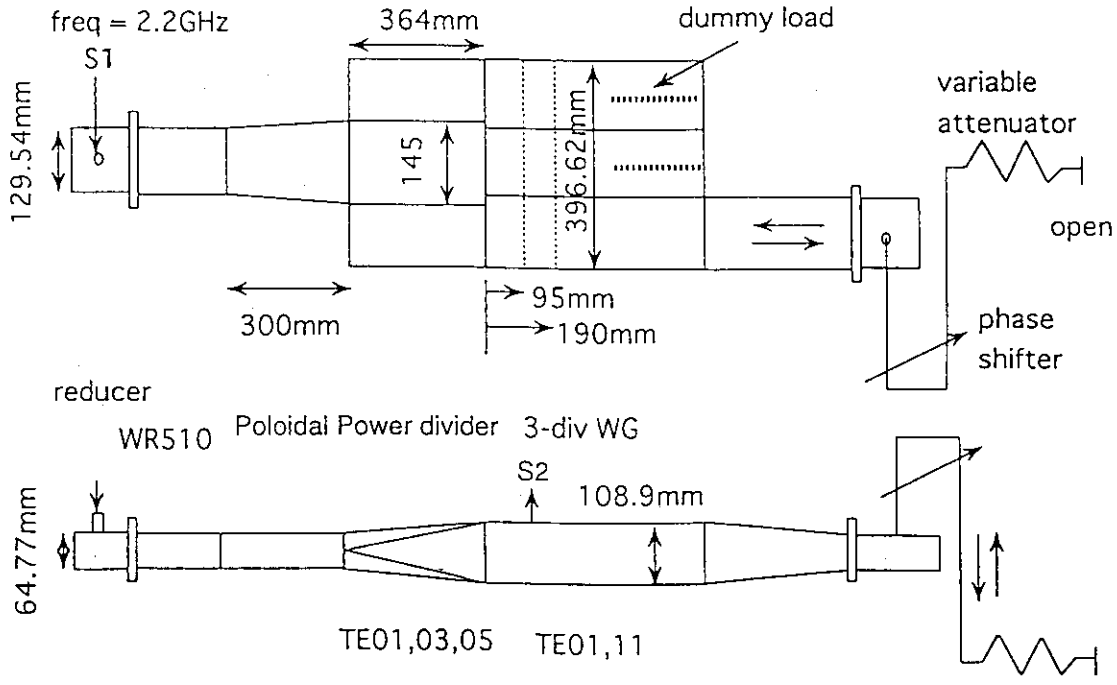

Fig. 36 The experimental set-up of the 2.2 GHz mock-up. Effect of reflection is measured under non unitary system using phase shifter and variable attenuator.

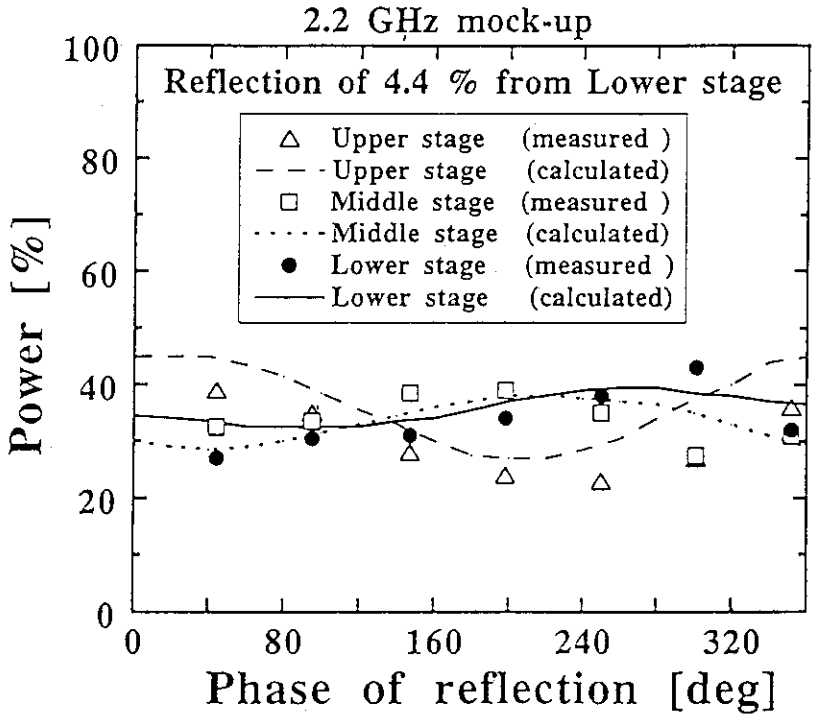

Fig. 37 Power dividing ratio as a function of phase of reflective power. Reflection coefficient is 4.4 % in lower stage. Measured power dividing ratio in each stage is plotted. Calculated power ratio using non unitary S-matrix is also drawn.

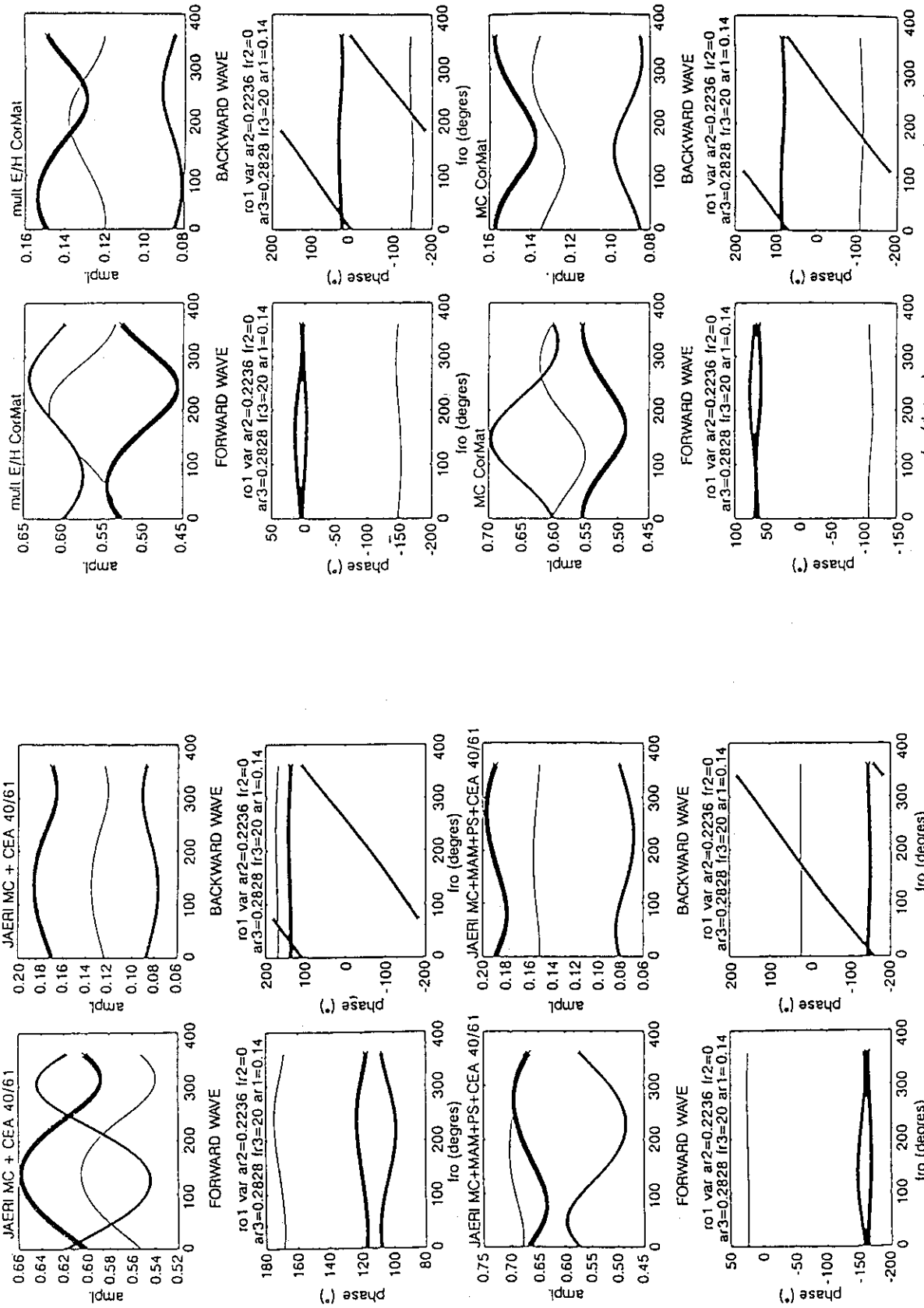

Fig. 38 Calculated power ratio using non unitary S-matrix, same curves as Fig. 40 with inhomogeneities in reflection coefficients, is drawn. : Amplitudes of reflection coefficients are taken to be 2, 5, 8 % for resp. top, central, bottom outputs, where phase are fro, 0, 20°.

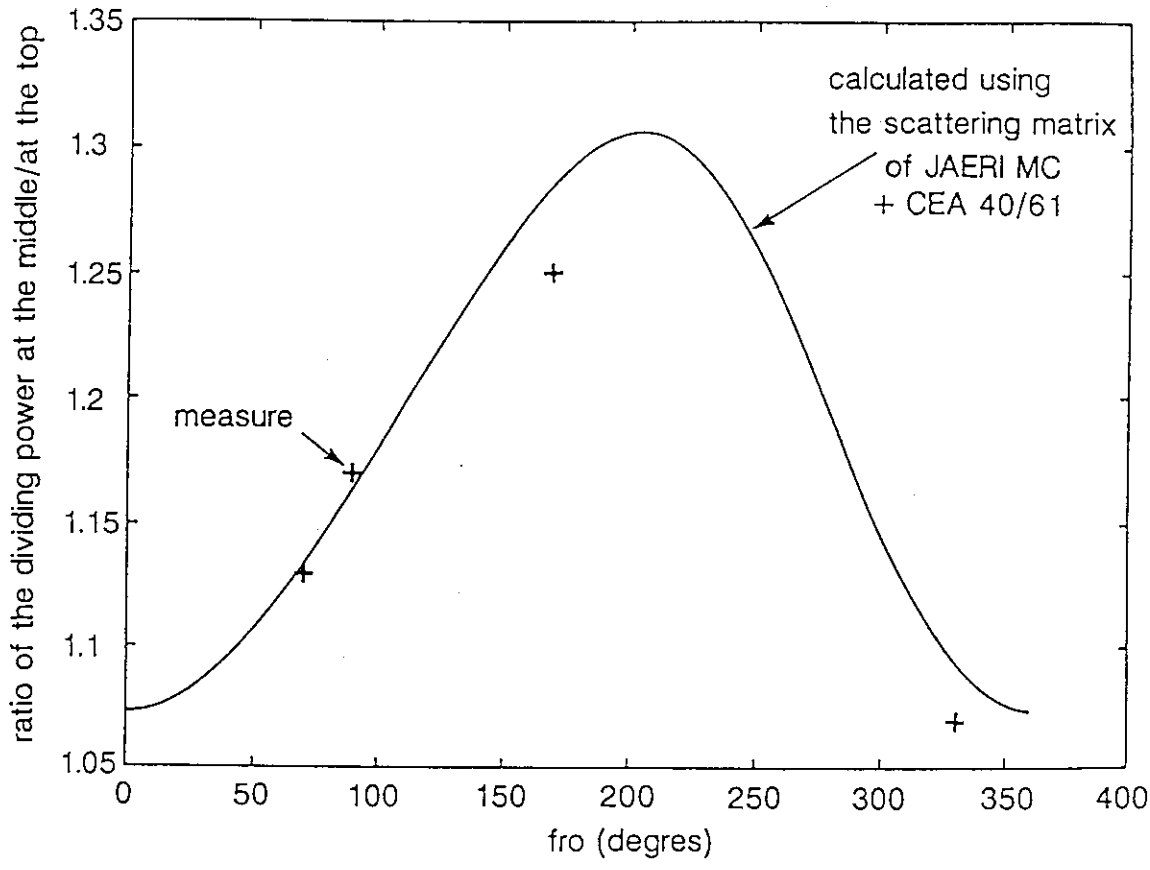

Fig. 39 Ratio of the amplitudes of the electric field in the middle output and the top／bottom output : a) Experimental points (+) when the width of an oversized spacer between PPD and the multi-junction is changed (from Fig. 18). b) Calculation (plain curve) with the modified scattering matrix of PPD. A reflective power of 1 % is assumed for the 3 output waveguides.

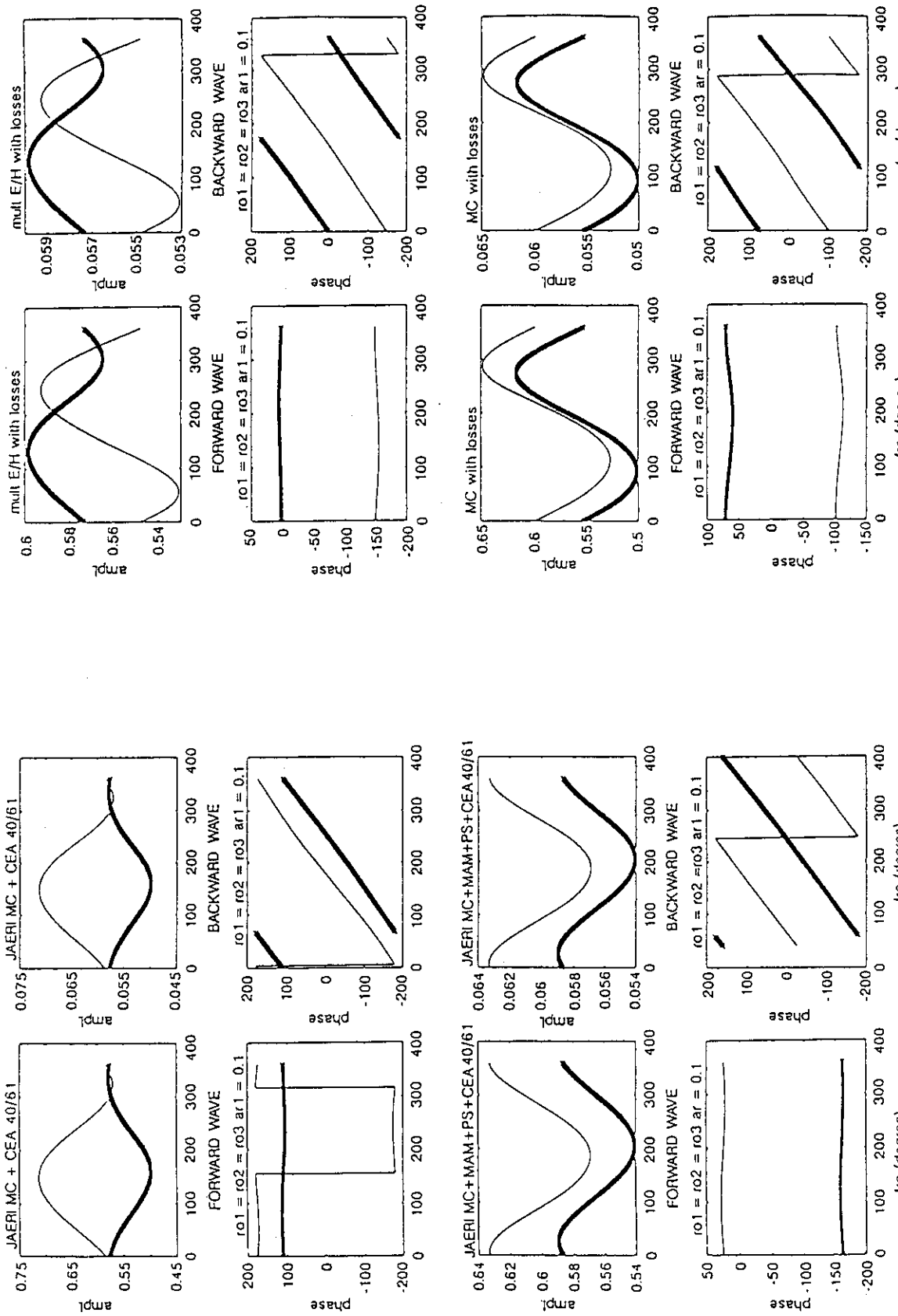

Fig. 40 Amplitude and phase of the forward (+) and backward (－) waves for the central output (thin line) and the top and bottom outputs (thick lines). in the case of : 1) PPD, 2) JAERI components, 3) E/H MJ, 4) MC. The reflection power of 1 % is assumed for all output waveguides, the phase to be labeled fro is the varying x-axis parameter. The geometric symmetries of the components are taken into account.

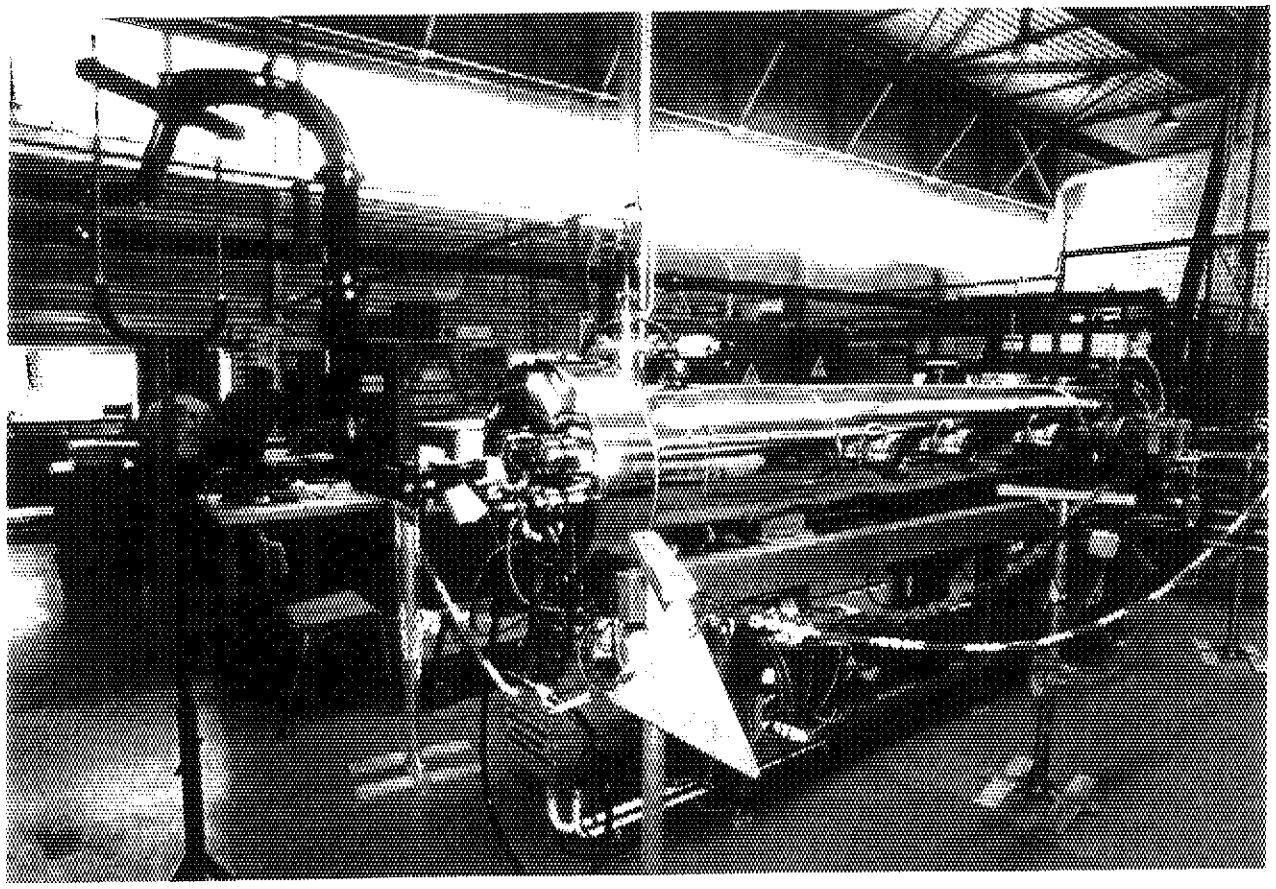

Fig. 41 Photograph of the vacuum tank.

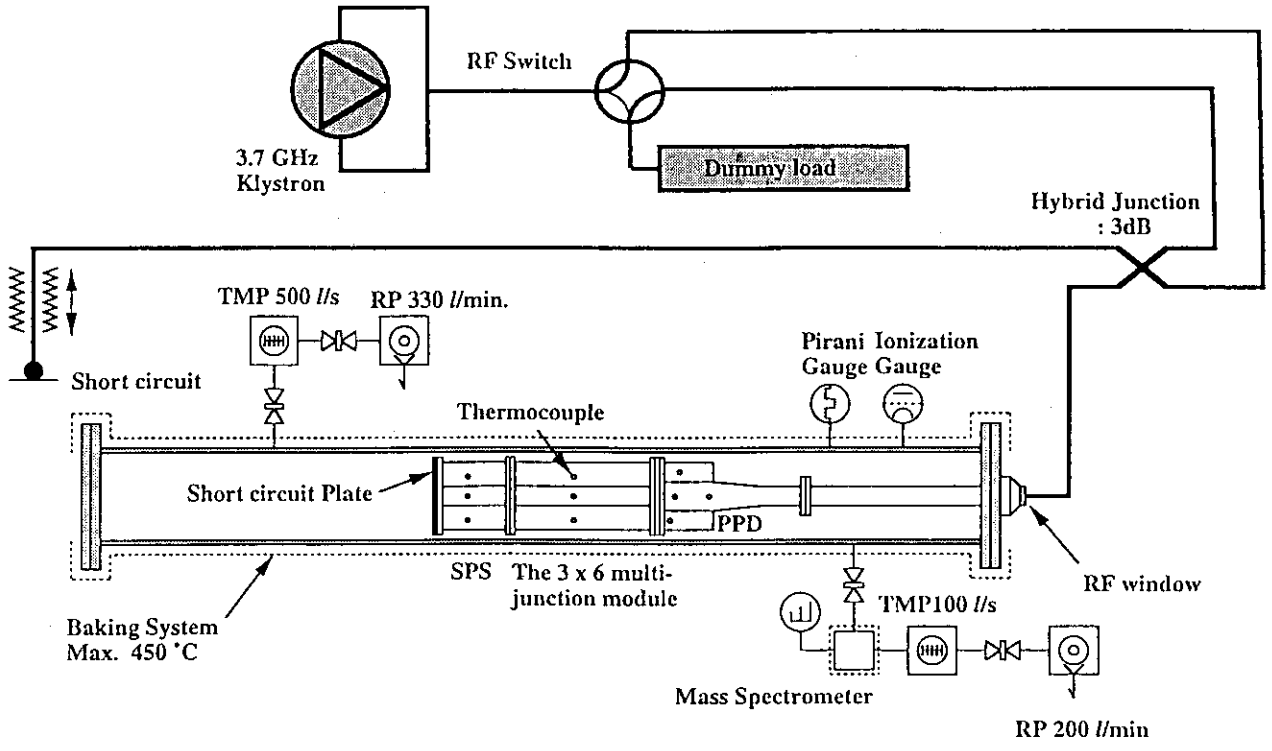

Fig. 42 Schematic drawing of the experimental set-up for high power test on short-circuit.

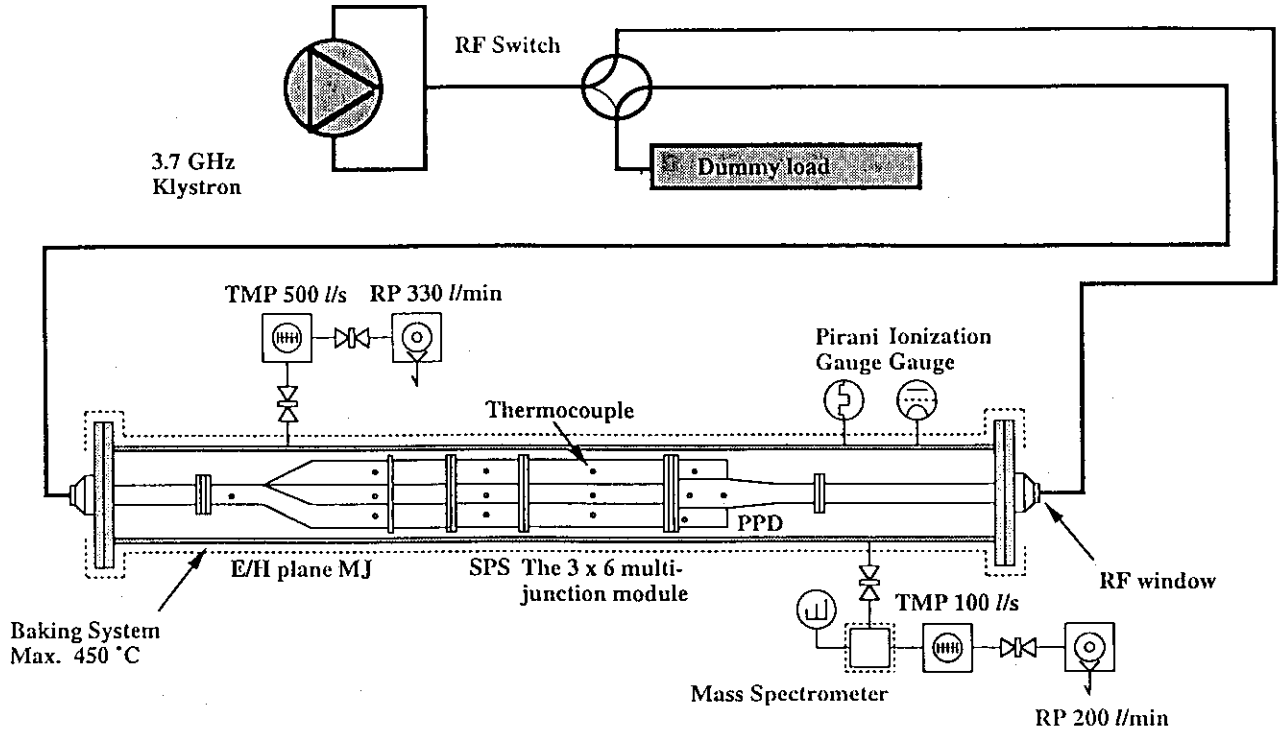

Fig. 43 Schematic drawing of the experimental set-up for high power test on load.

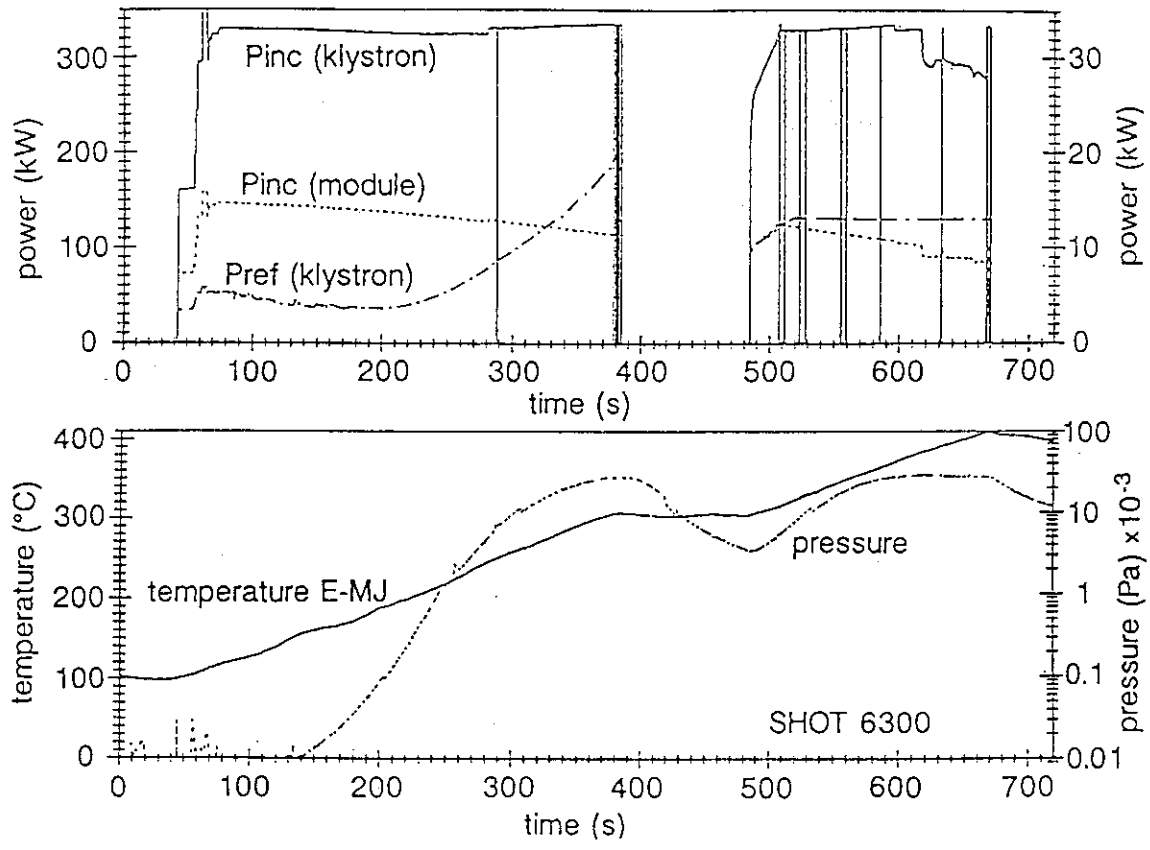

Fig. 44 R.f. powers (incident and reflected), temperature and pressure vs. time during high power test if the multi-junction on short (Shot 6300).

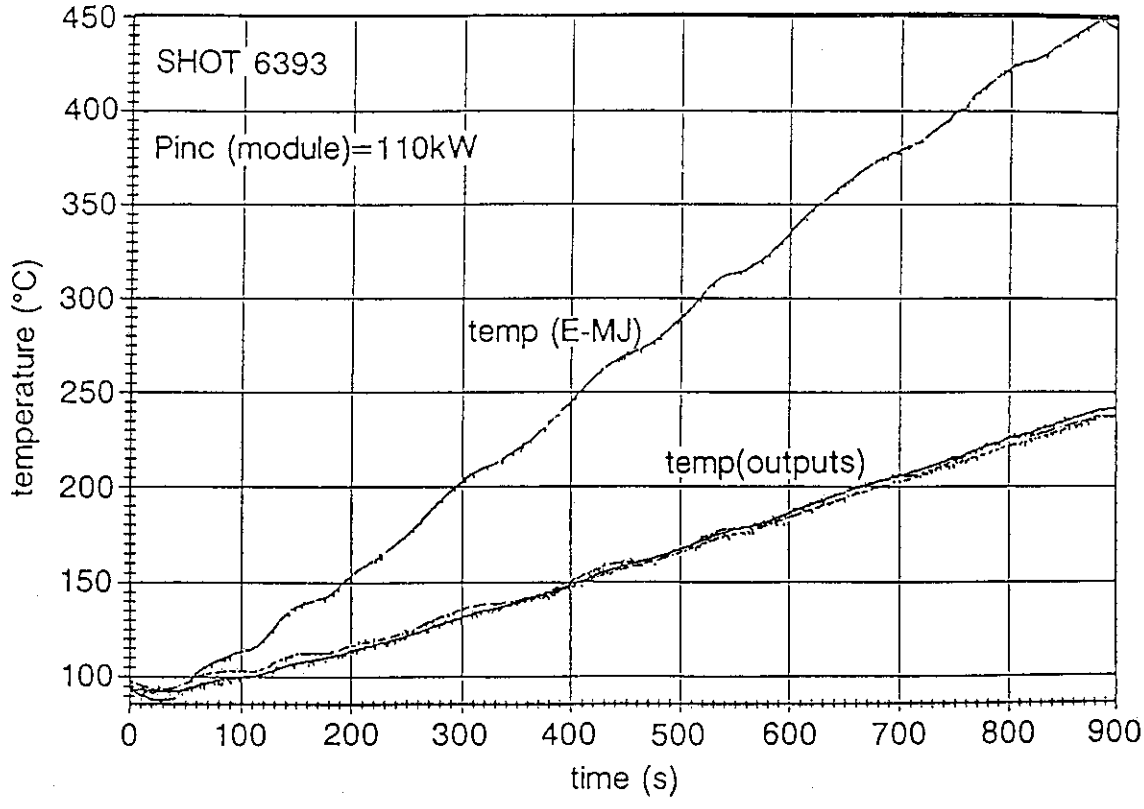

Fig. 45 Temperature of the E／H plane multi-junction at the input and outputs (Shot 6393-Prf = 110kW).

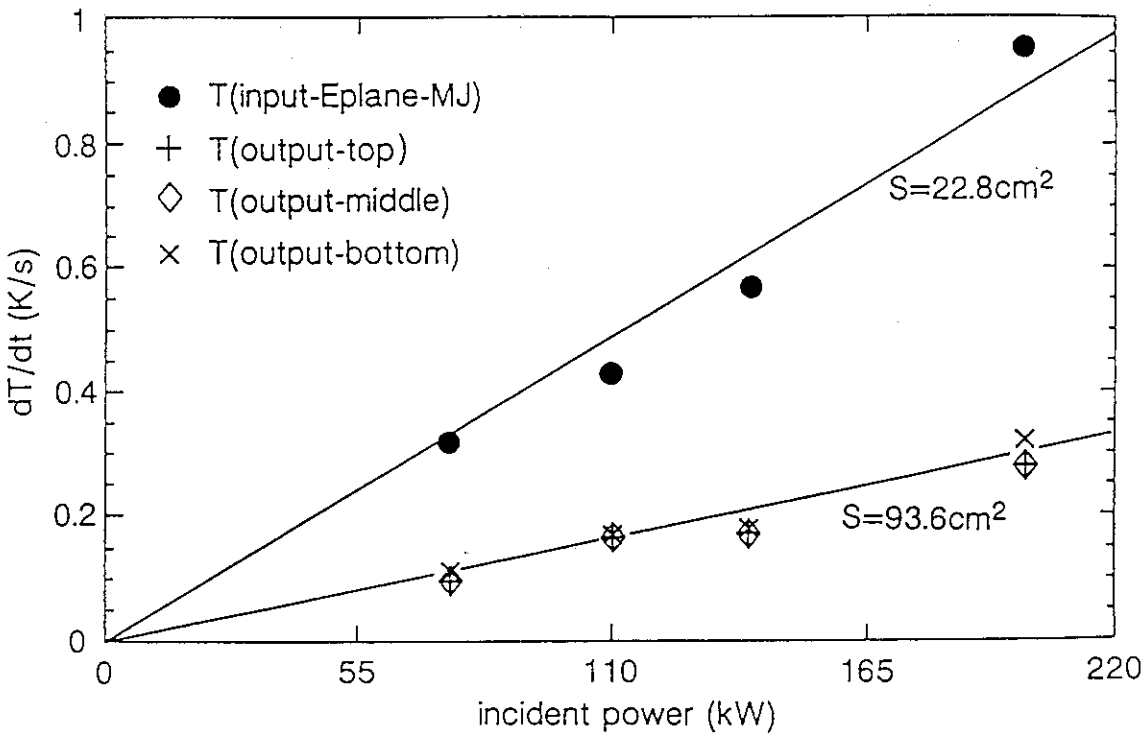

Fig. 46 Temperature rise rate vs. RF power at the input (close circles) and the outputs of the E／H plane multi-junction.

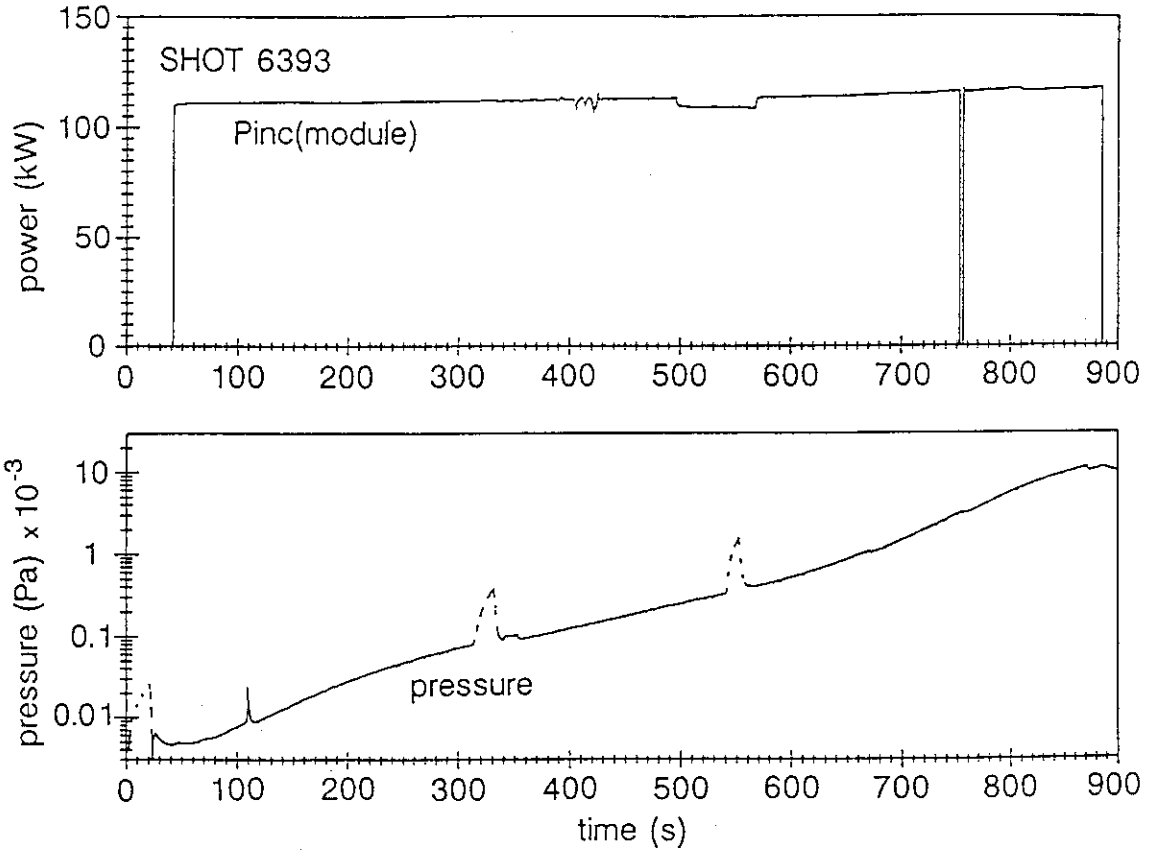

Fig. 47 RF incident power and pressure (log scale) vs. time during test of the E／H plane multi-junction on short-circuit. Final temperature is 450 ℃.

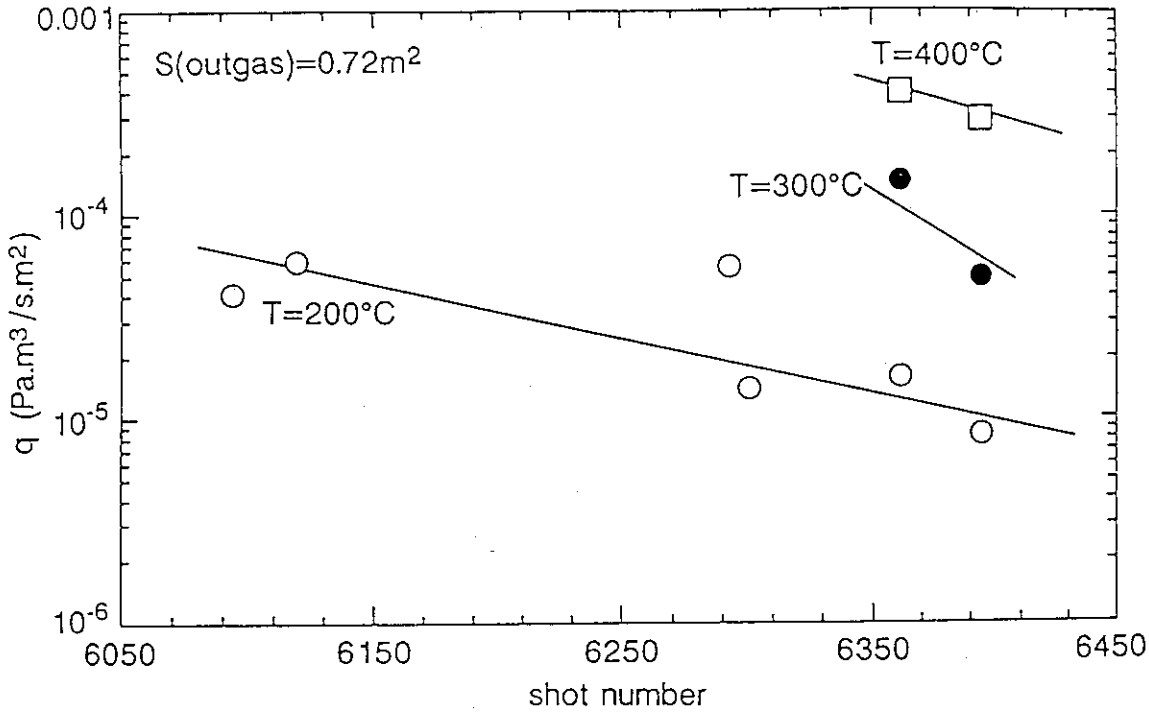

Fig. 48 Outgassing rate of the E/H plane multi-junction on short short-circuit at 200, 300 and 400 ℃.

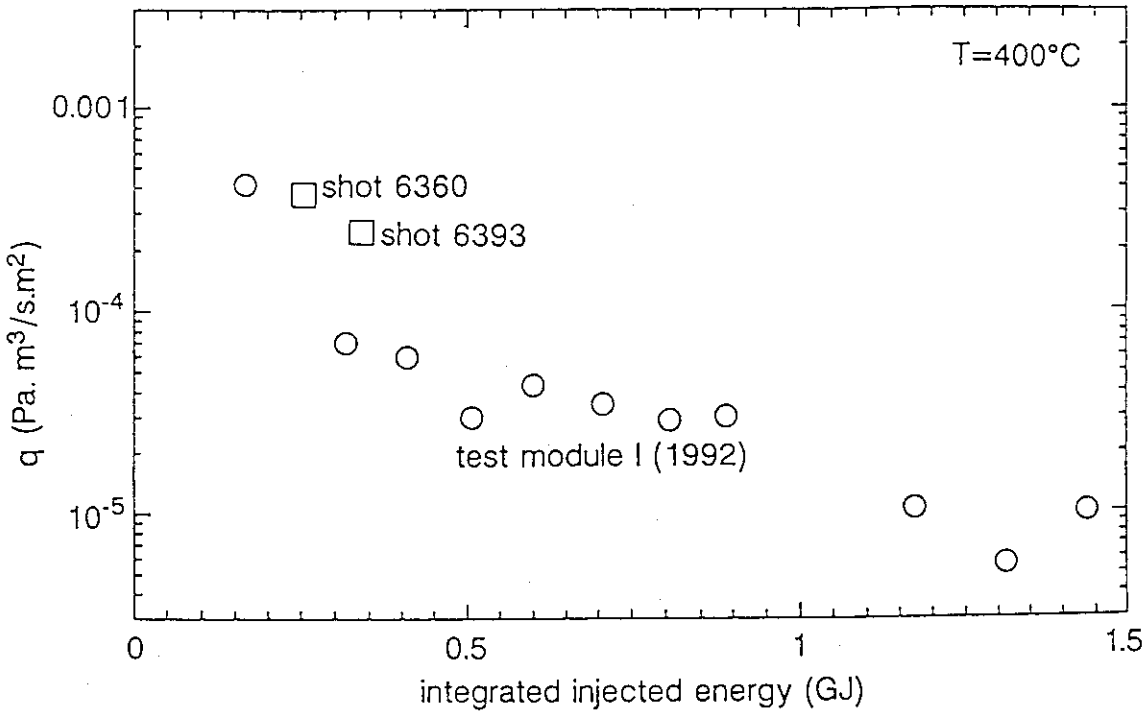

Fig. 49 Comparison of the outgassing rate of test module I and the E/H plane multi-junction at 400 ℃.

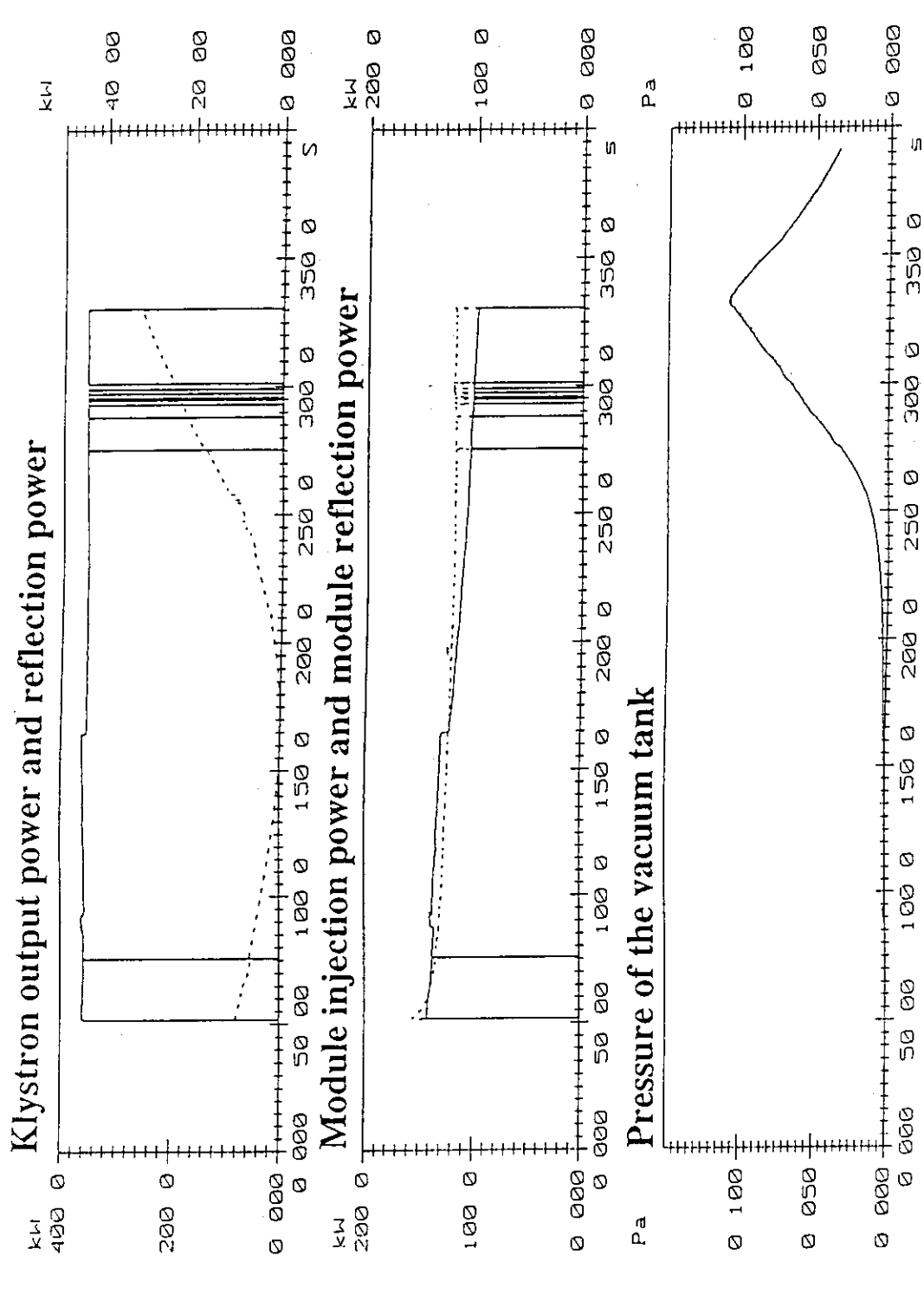

Fig. 50 Time trajectory of klystron output power, module injection power and pressure of the vacuum tank.

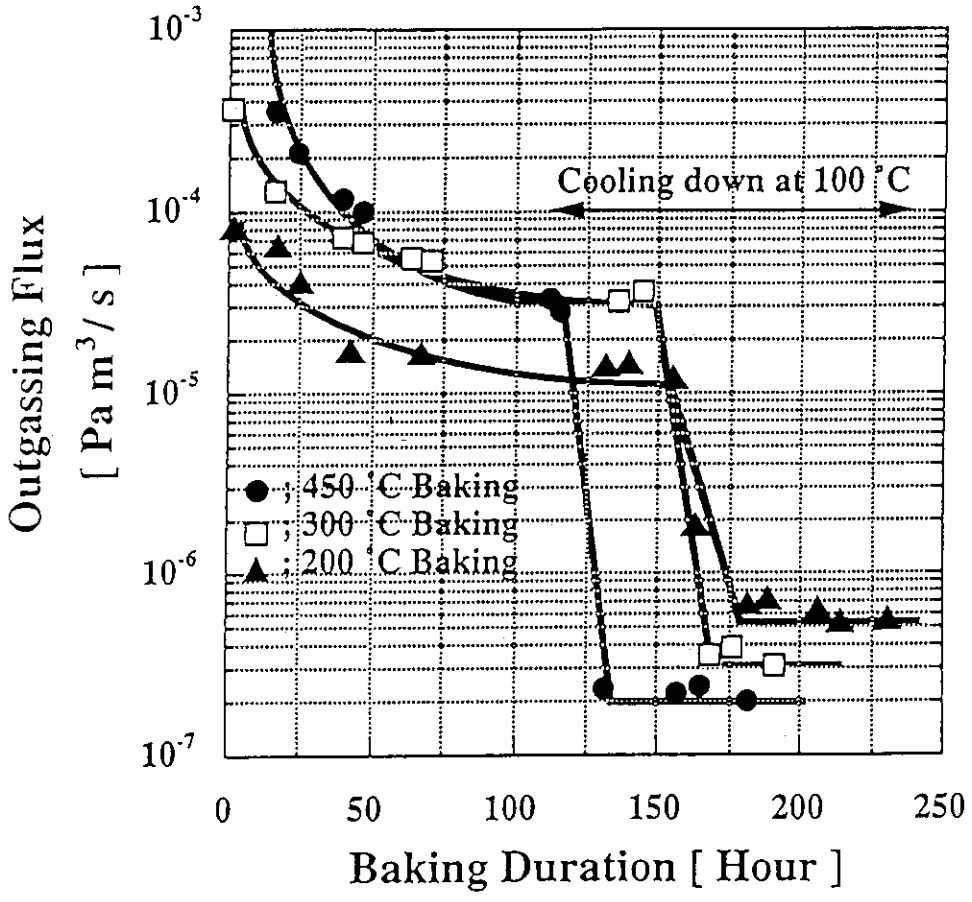

Fig. 51 Dependence of outgassing flux on the baking duration in baking treatment.

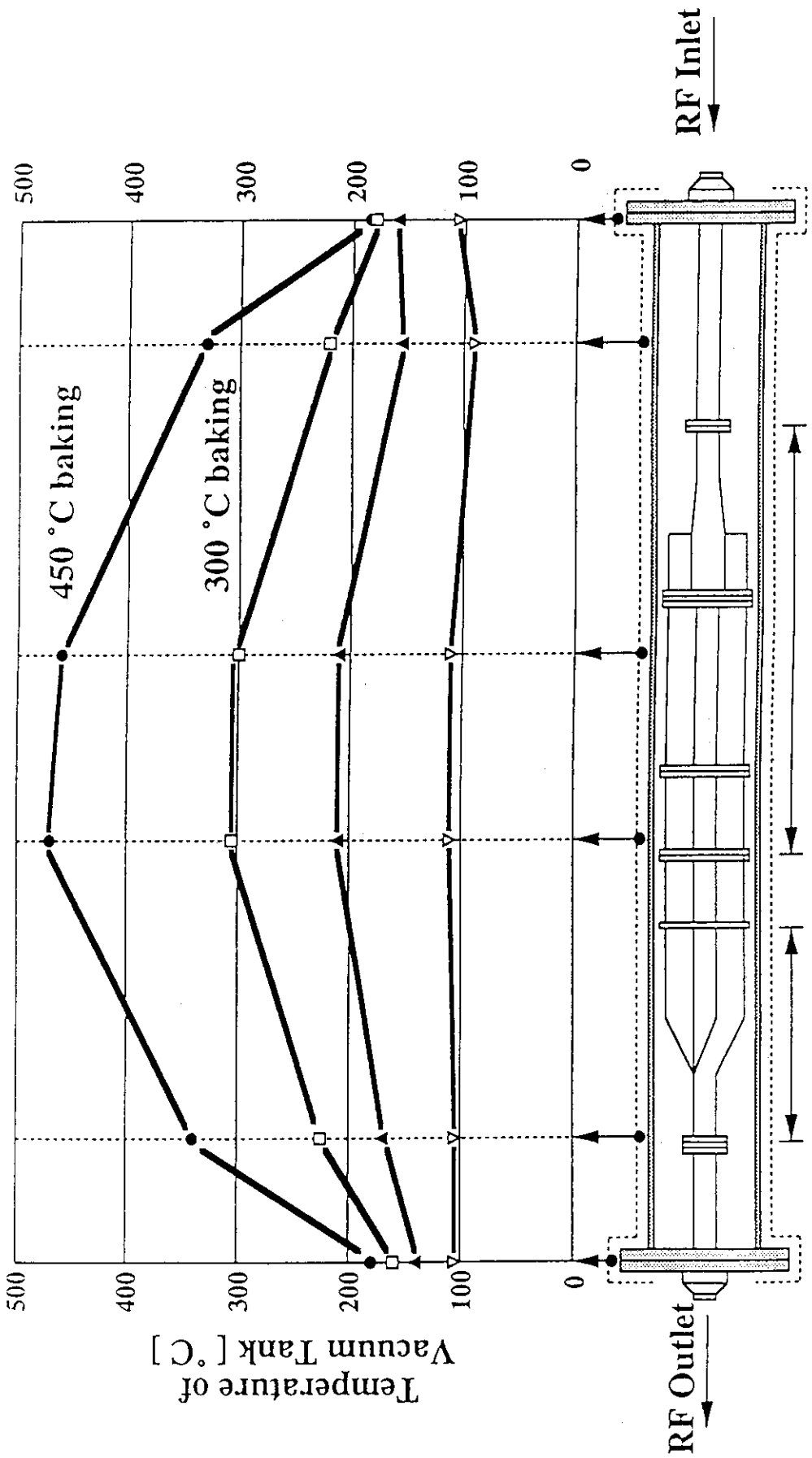

Fig. 52 Temperature distribution of the vacuum tank during each baking treatment.

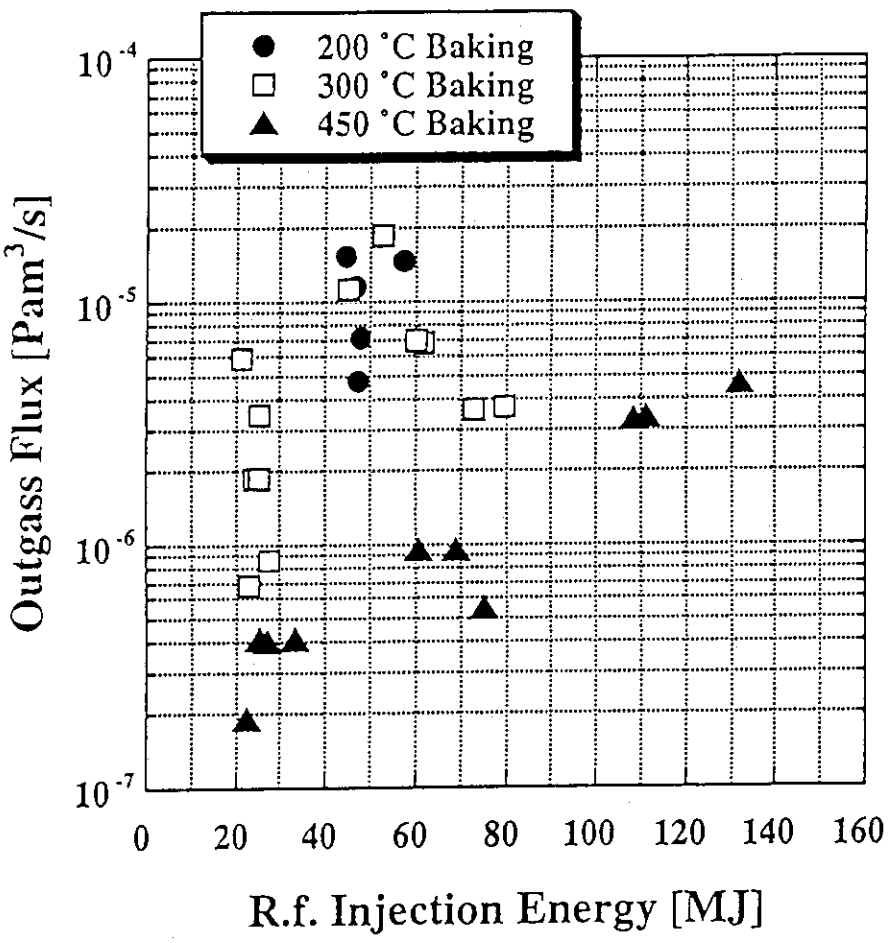

Fig. 53 Dependence of outgassing flux on r.f. injection energy after different baking temperatures.

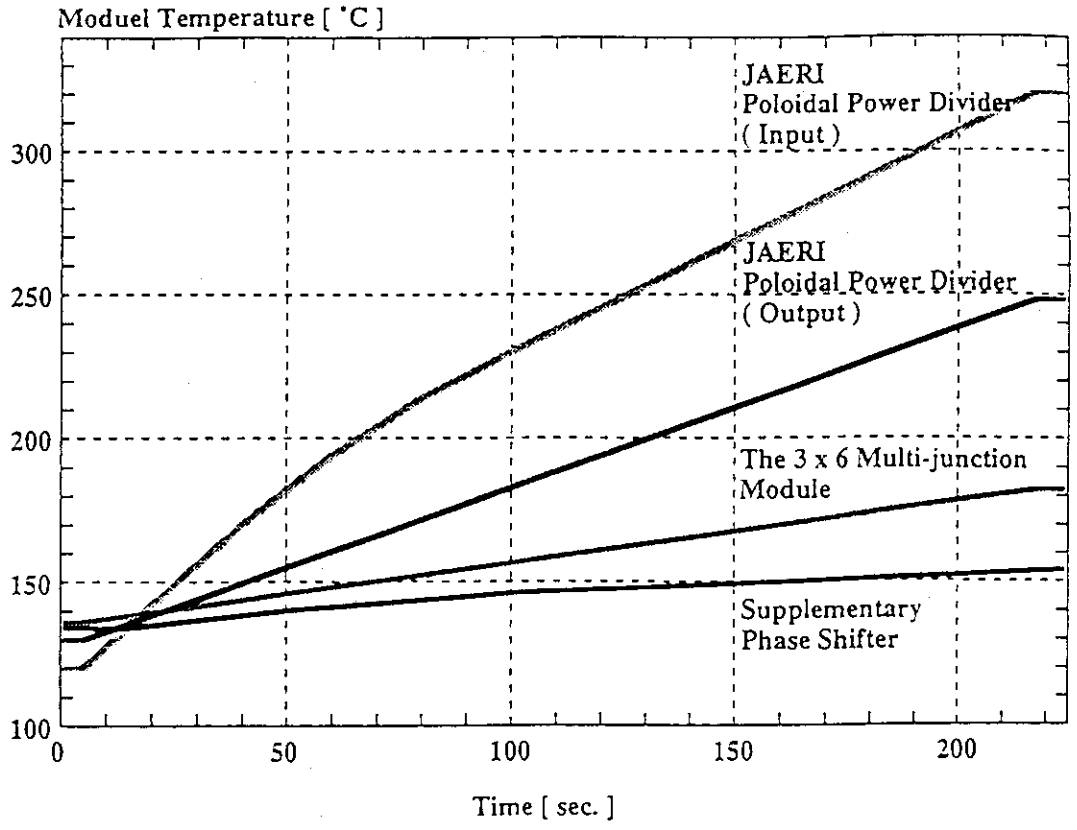

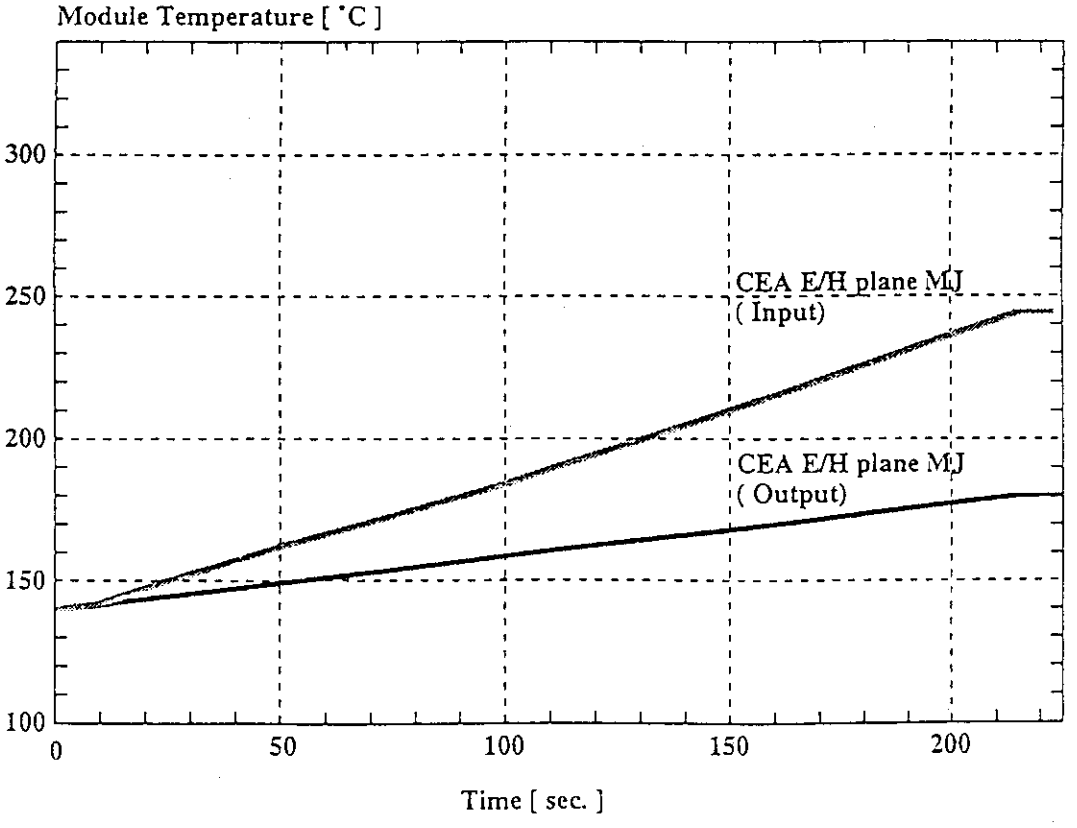

Fig. 54 Temperature rises of each component during a 300 kW r.f. injection.

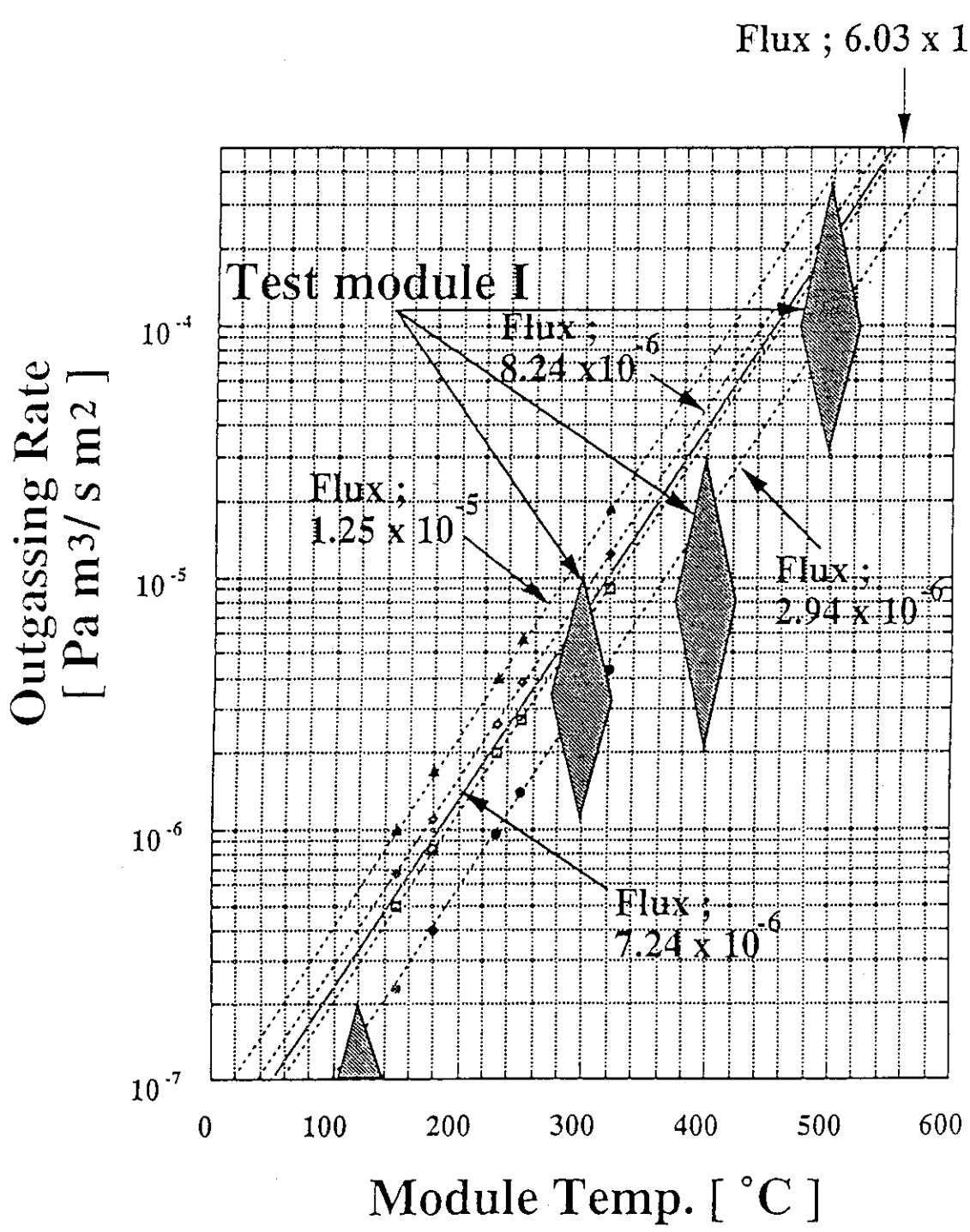

Fig. 55 Outgassing rate of the test module test I and assumed outgassing rates are indicated. When four outgassing rates are assumed, outgassing fluxes in the test module II are obtained using each component temperature and surface areas.

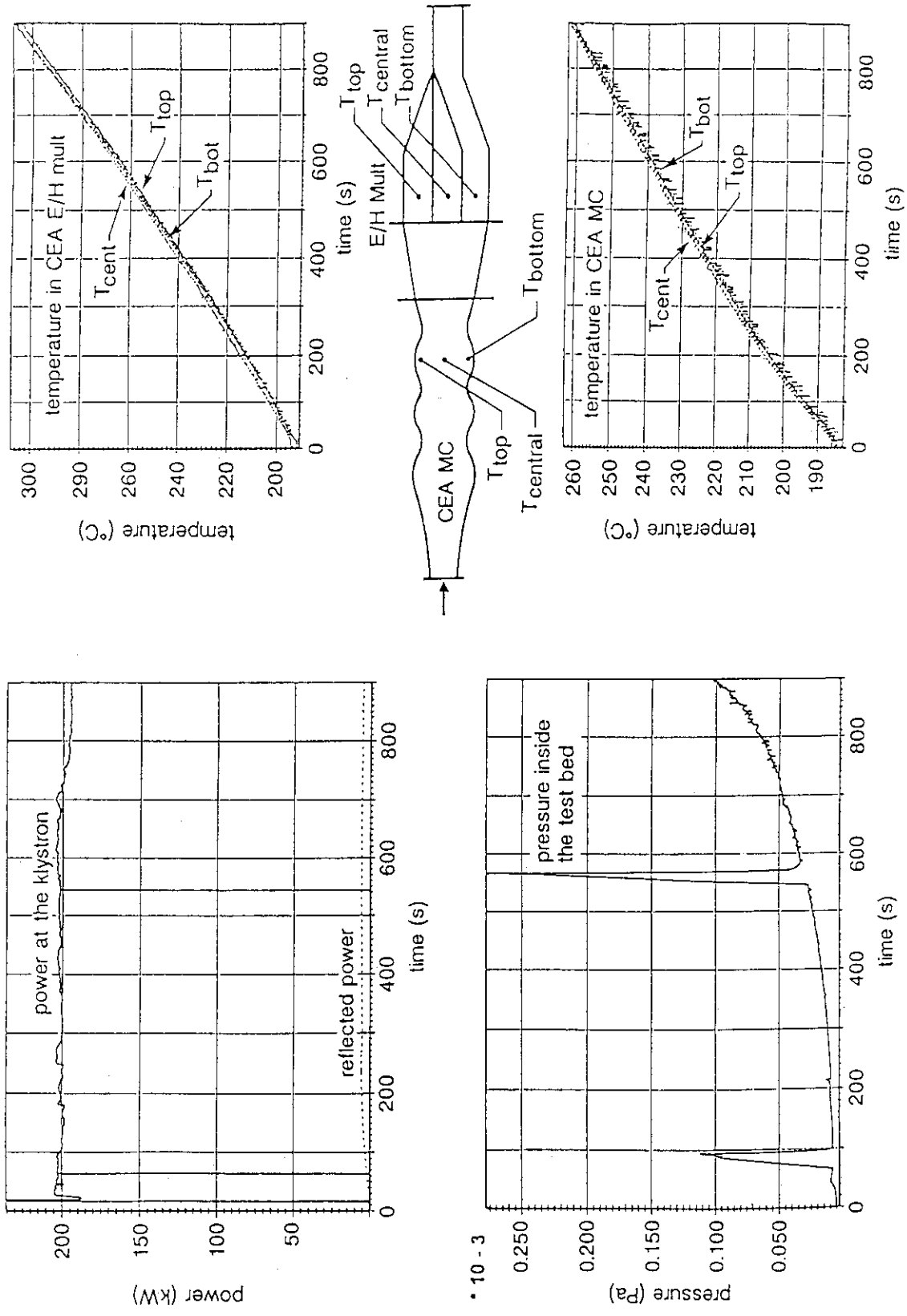

Fig. 56 -incident and reflected power at the klystron vs. time.
-pressure inside the test bed vs. time.
-temperature measurement inside the CEA MC and the E/H plane multi-junction with time during high power r.f. test of CEA MC + PJ + E/H multi-junction. Power at the klystron is 200 kW.

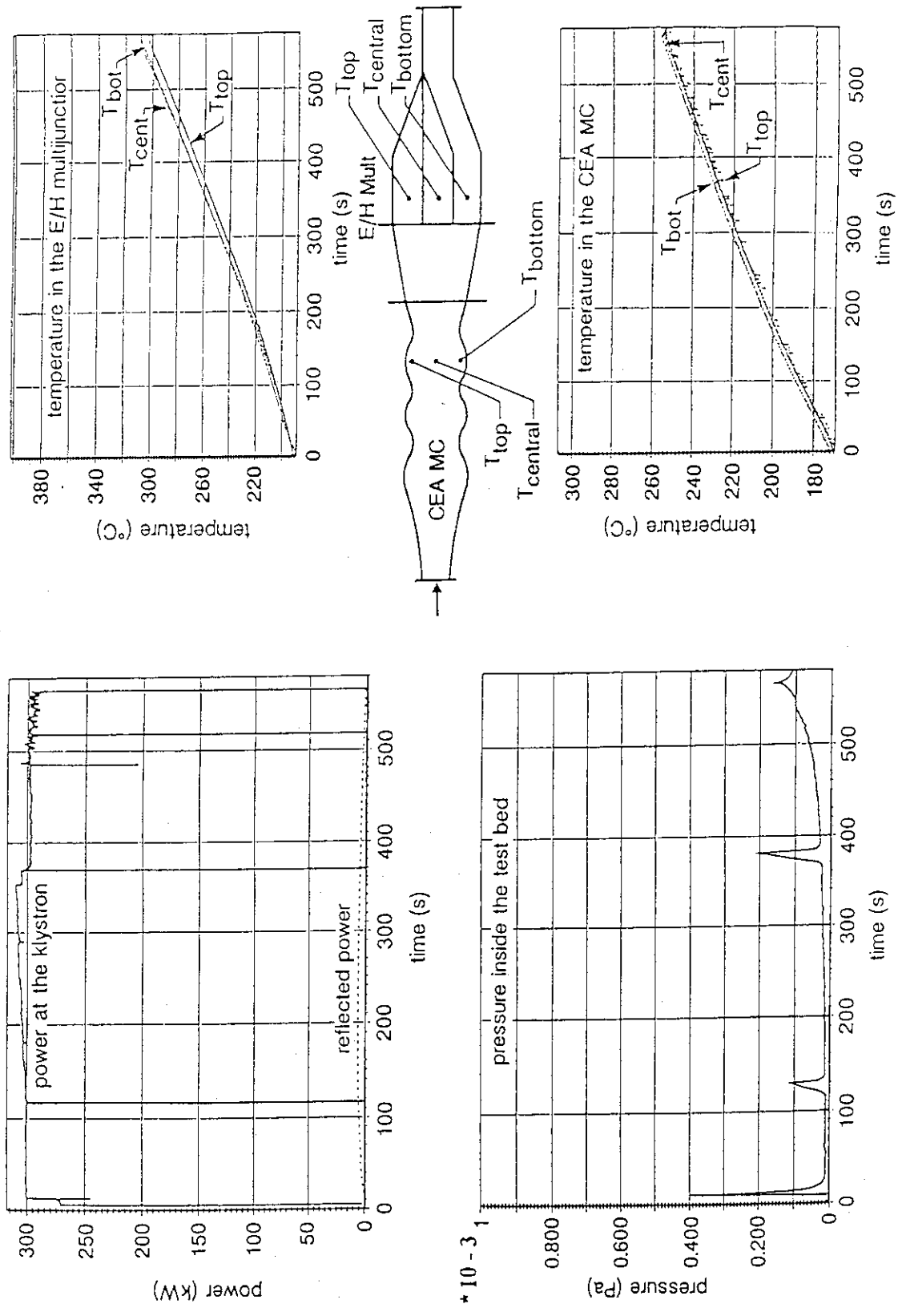

Fig. 57 Variation of the klystron output power, the reflected power, pressure at the vacuum tank, each temperature rise at CEA E/H multi-junction module and CEA mode converter when dividing ratio when an out put power at the klystron is 300 kW.

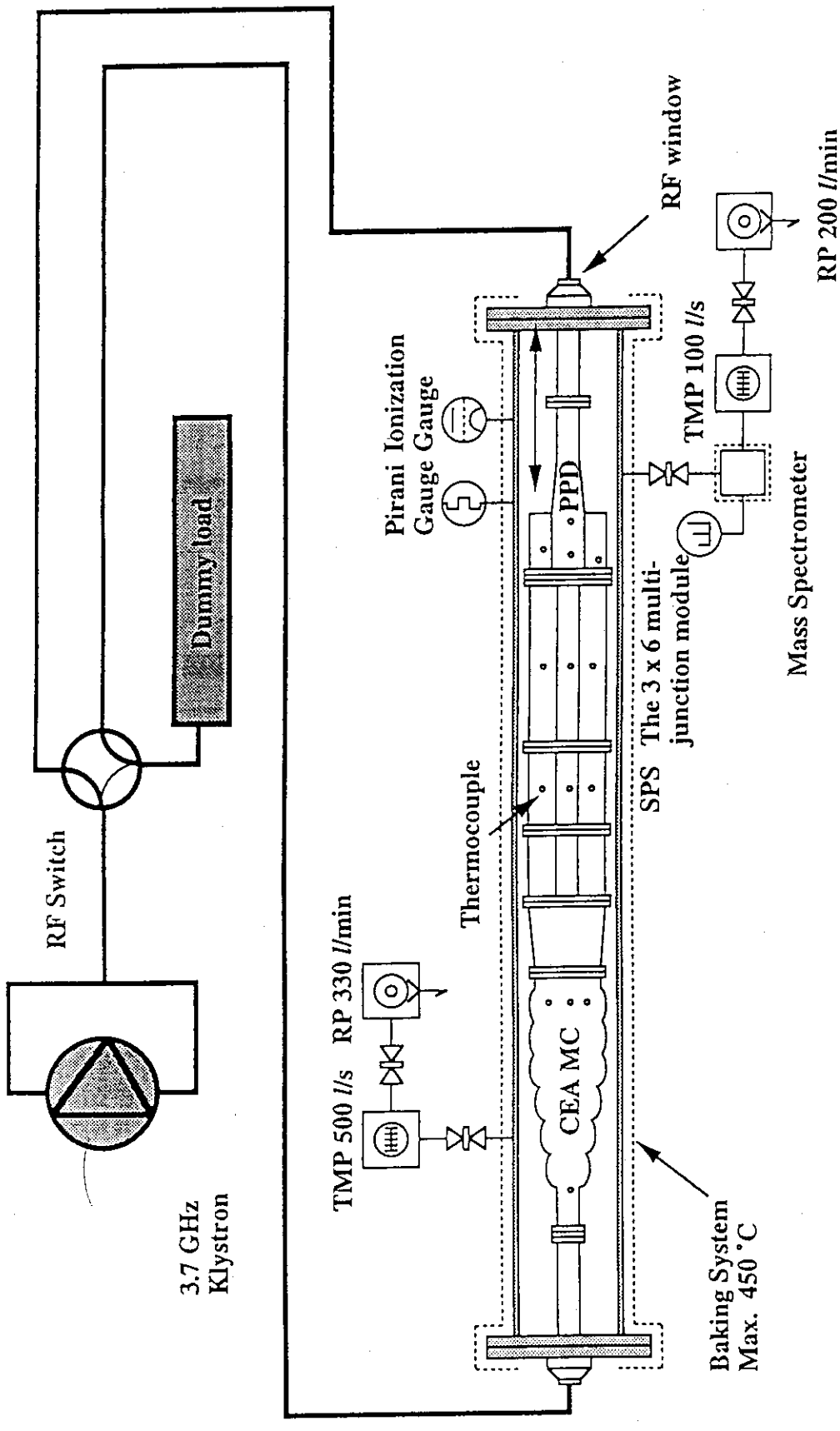

Fig. 58 Schematic drawing of the experimental set-up for the test of JAERI components with the CEA mode converter.

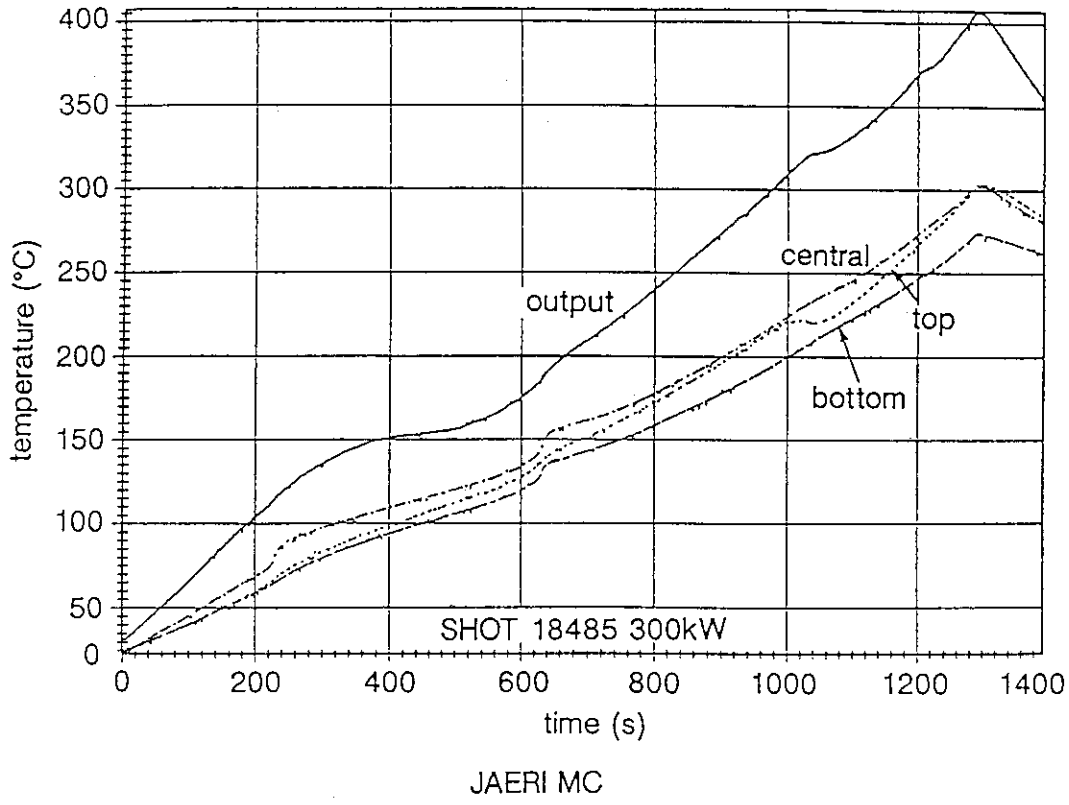

Fig. 59 Time evolution of the temperature of the JAERI PPD at different locations (Shot 18485 - Pinc = 300 kW).

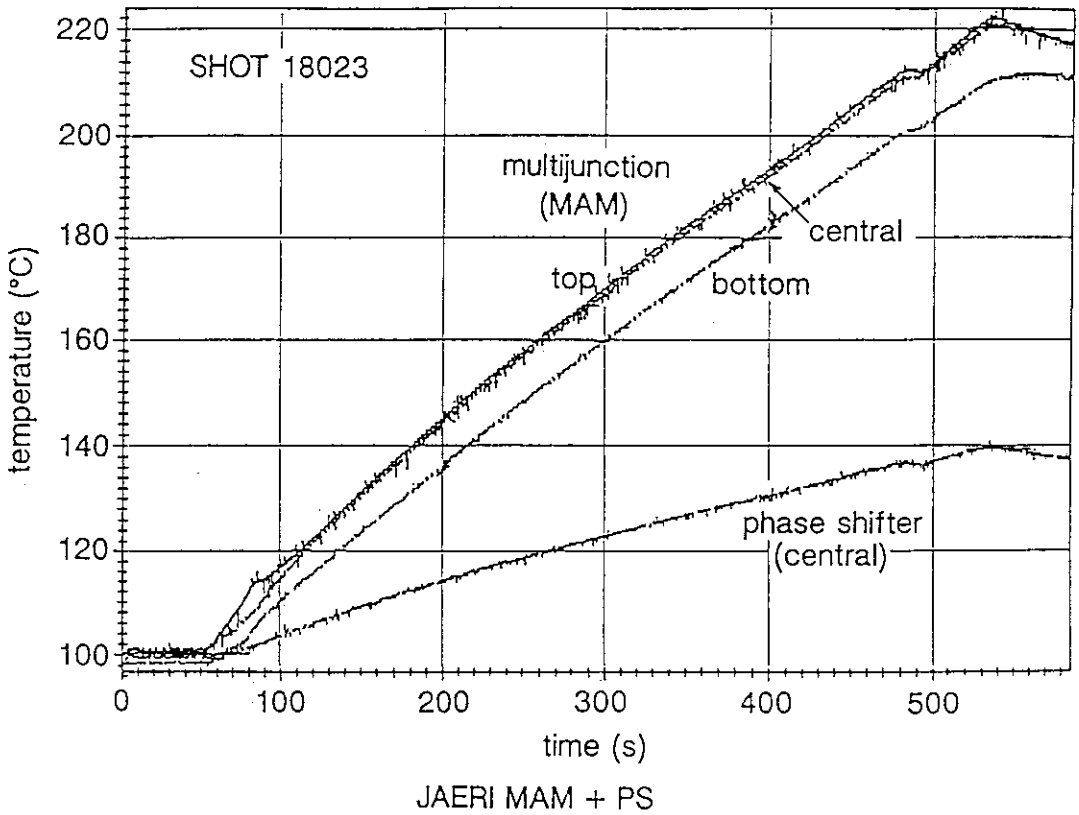

Fig. 60 Time evolution of the temperature of the 3 × 6 MJ and PS at different locations (Shot 18023 - Pinc = 300 kW).

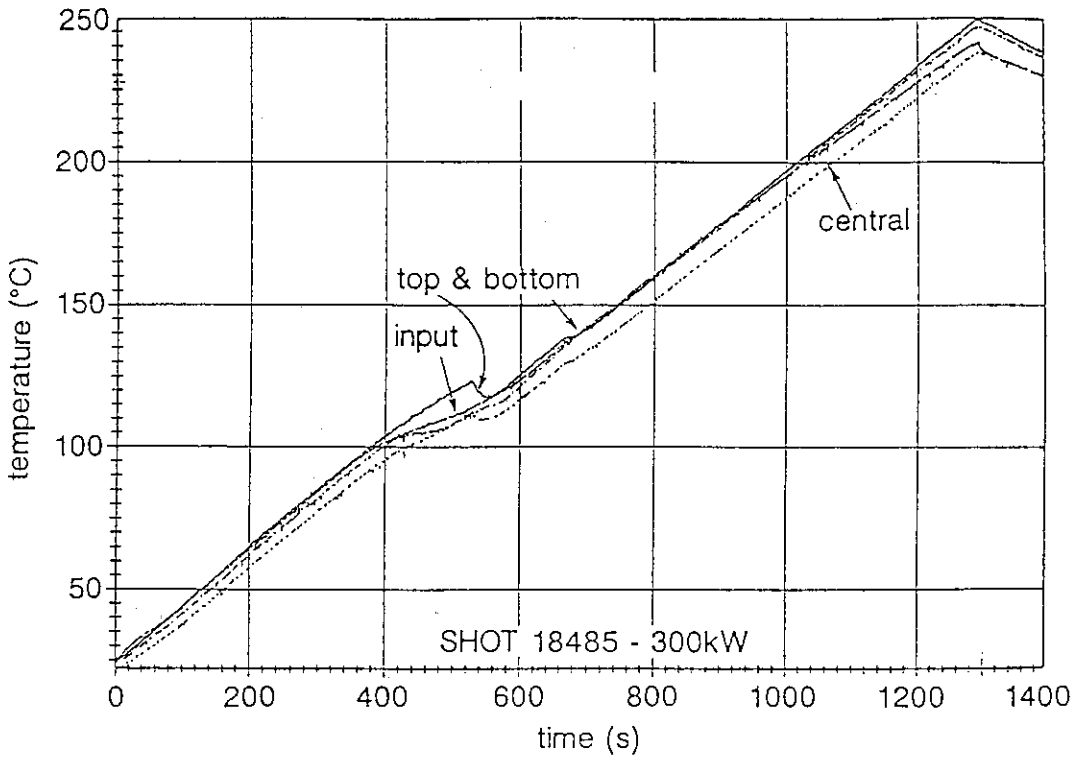

Fig. 61 Time evolution of the temperature of the CEA mode converter at different locations (Shot 18485 - Pinc = 300 kW).

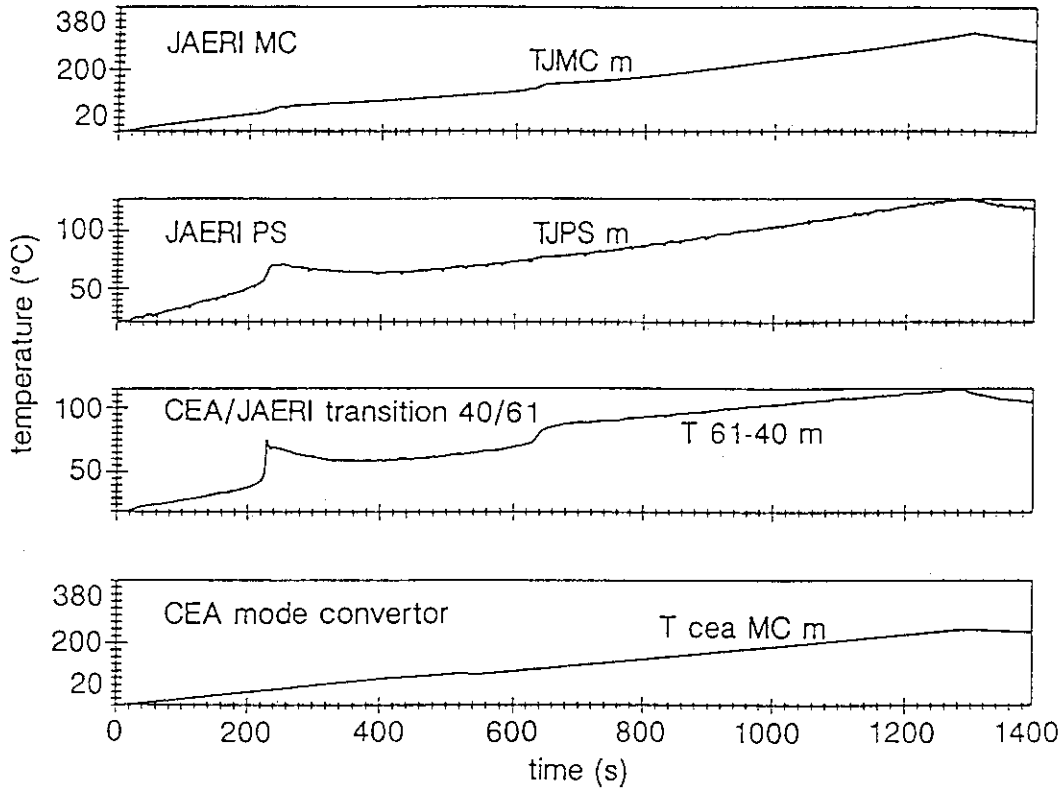

Shot 18485

Fig. 62 Time evolution of the temperature of the PPD, PS, CEA／JAERI transition and MC. The 2 resonance occurrences are shown with an arrow (Shot 18485 - Pinc = 300 kW).

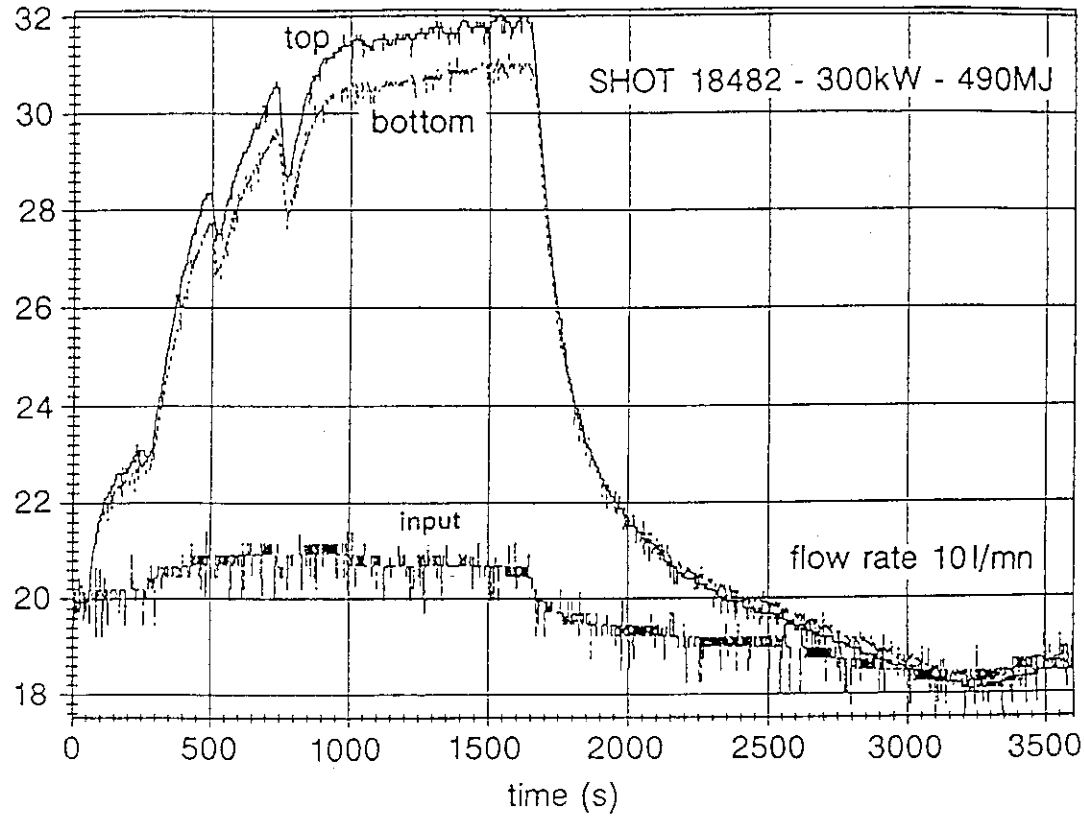

Fig. 63 Inlet and outlets temperature of the water during a water-cooling experiment - (Shot 18482 - Pinc = 300 kW - Einj = 490 MJ).

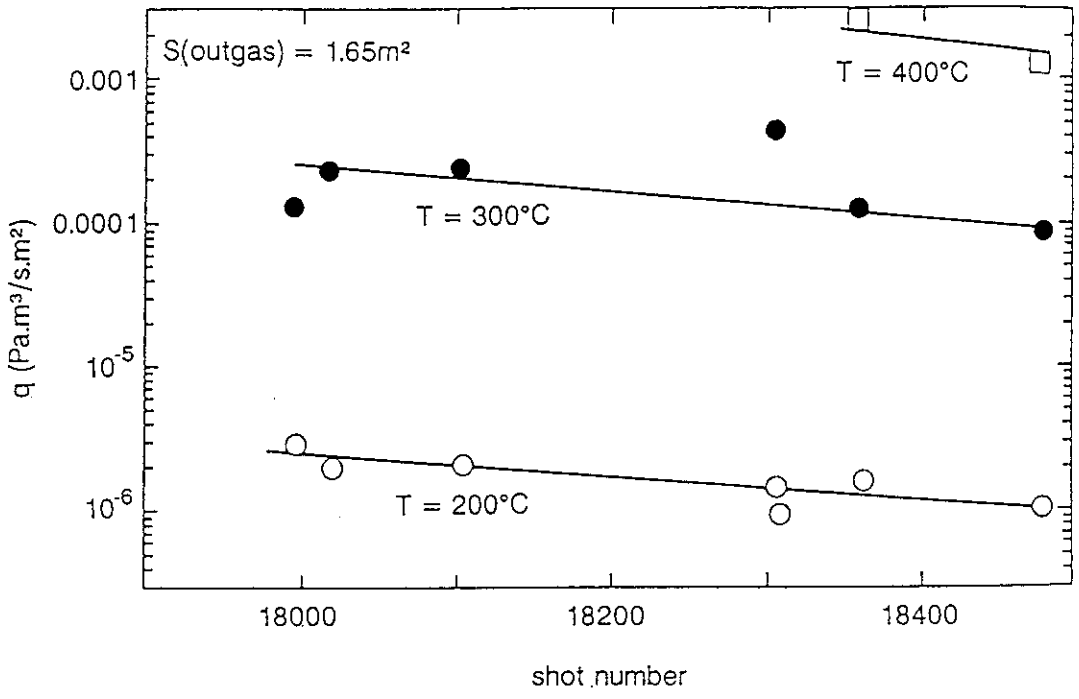

Fig. 64 Outgassing rate of JAERI components with CEA MC. It is assumed that only PPD and multi junction (1.65 m²) are outgassing. PPD input temperature is quoted.

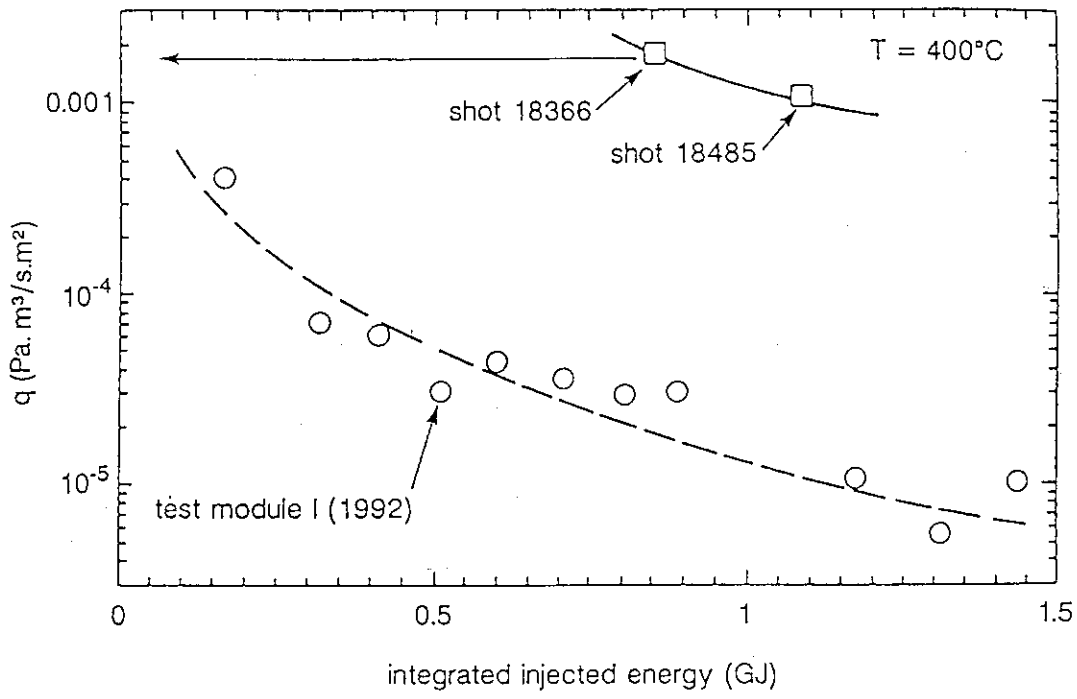

Fig. 65 Comparison of outgassing rates at 400 ℃, for data from Fig. 61, and Test module 1 data.

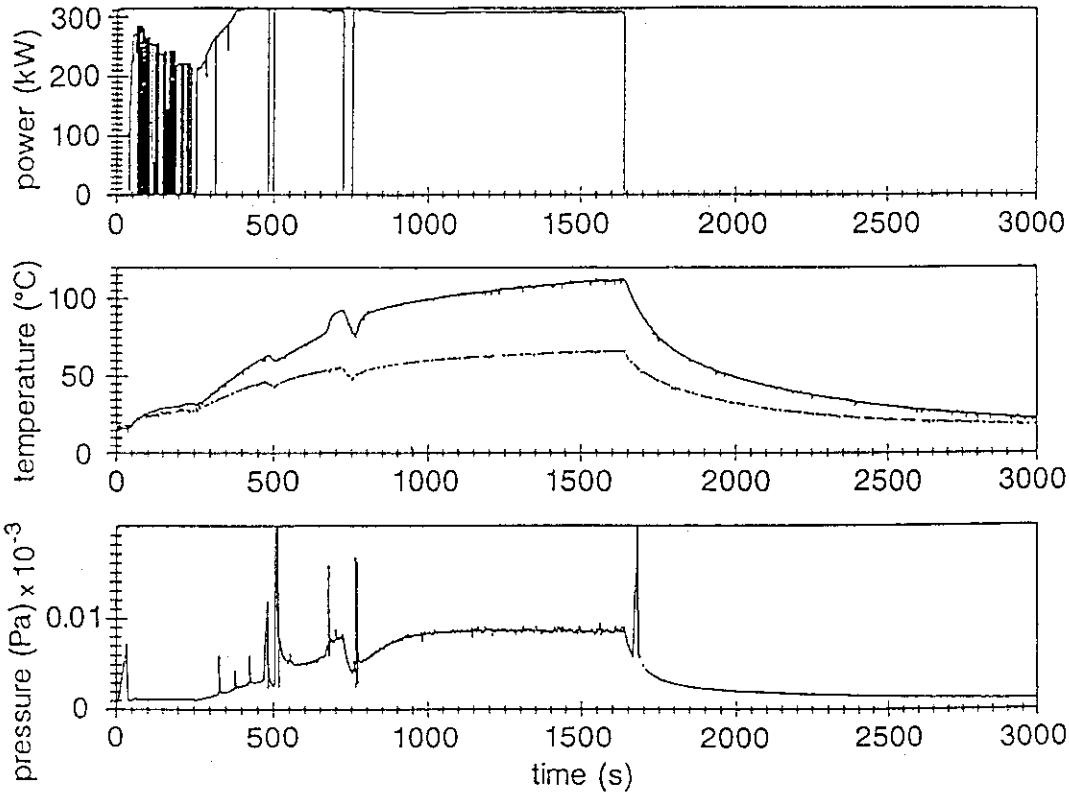

SHOT 18482

Fig. 66 Time evolution of incident power, JAERI PPD and CEA mode converter and pressure during water-cooled experiment (Shot 18482 - Pinc = 300 kW - Einj = 490 MJ).

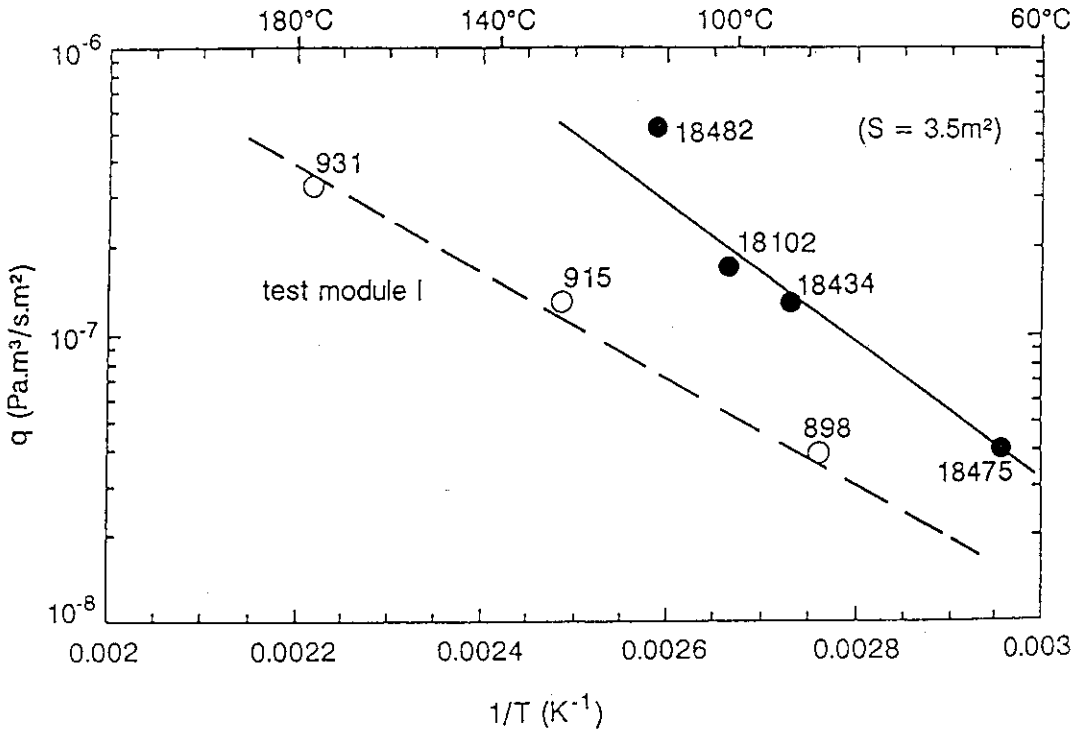

Fig. 67 Steady state outgassing rate versus 1/T for data from JAERI components + CEA MC and Test module 1 data.

APPENDIX 1
CEA CADARACHE RF TEST FACILITY

1. TRANSMITTER

1.1. Klystron

Thomson Tubes Electroniques TH2103
3.7 GHz ± 5 MHz
450/500 kW, 210 s
Duty cycle at full power 1/3
Output power feedback controlled with an accuracy of ±2%
RF pulse shape can be changed :

- constant power with a ramp,
- sequence of short pulse.

(typically 10 ms every 100 ms).

1.2. Transmission line

Standard waveguides WR 284 (loss 0.5 % m^{-1} at 20 °C)
Water cooled (Δ Pmax = 6 bar)
Pressurized with SF_6 (Pmax = 1.3 bar).

1.3. RF load

Thomson Tubes Electroniques
500 kW-CW, water cooled
RF switch to dump the power to the load for klystron testing

1.4. RF measurements

6 power measurements(3xPi + 3xPr)
2 phase measurements.

2. HIGH VACUUM TANK

2.1. Dimensions

L = 3500 mm, Φ_{int} = 343 mm
Volume : 340 *l*
Outgassing surface : 4.2 m^2 .

2.2. Pumping, gas injection and barometry

Turbomolecular pump of 500 $l\ s^{-1}$

Gas injection system for H_2, Ar, N_2

1 capacitive gauge (10^2-10^5 Pa), 1 Pirani gauge, 1 Penning gauge, 1 Bayard-Alpert gauge

1 mass quadruple spectrometer with differential pumping (Balzers QMG 112).

2.3. Baking system

Bakable up to 450 °C

Glow discharge cleaning (600 V - 15 A DC supply)

6 thermocouples installed on the tank

Base pressure at 20 °C : < 10^{-5} Pa after 300 °C / 60 hours

2.4. Cooling system

Feed through for water (P = 6 bar) or air cooling (50 Nm^3 / h) of the part to be tested.

2.5. Flanges

2 NW50 flanges for thermocouples in vacuum

2 NW50 flanges for cooling

3 NW100 flanges with Al_2O_3 window (IR camera)

3 NW100 flanges with glass window

3. CONTROL AND DATA ACQUISITION

3.1. Klystron control

Made by a wired electronics.

3.2. Data acquisition

- desk computer equipped with 2 cards of 64 channels each (fast and slow acquisition rate),
- quadruple data processor (Balzers QDP 101) for partial pressure.

APPENDIX 2
GENERAL DATA FOR JAERI AND CEA COMPONENTS

1. JAERI poloidal power divider

Length (mm) ;	600
Outgassing surface (m^2);	0.374
Material ;	DSC(Cu-Al_2O_3)
Connection ;	
Input W/G (mm) :	76 x 36
Output W/G (mm) :	236 x 61

2. JAERI 3 x 6 multi-junction module

Length (mm) ;	600
Outgassing surface (m^2);	1.273
Material ;	DSC(Cu-Al_2O_3)
Connection ;	
Input W/G (mm) :	236 x 61
Output W/G (mm) :	236 x 61

3. JAERI supplementary phase shifter

Length (mm) ;	314
Outgassing surface (m^2);	0.431
Material ;	Stainless steel
Connection ;	
Input W/G (mm) :	236 x 61
Output W/G (mm) :	236 x 61

4 JAERI / CEA Transition W/G

Length (mm) ;	257
Outgassing surface (m^2);	0.29
Material ;	OFHC
Connection ;	
Input W/G (mm) :	236 x 40
Output W/G (mm) :	236 x 61

5. CEA E/H plane multi-junction module

Length (mm) ;	746
Outgassing surface (m^2);	0.72
Material ;	OFHC
Connection ;	
Input W/G (mm) :	76 x 40
Output W/G (mm) :	236x40

6. CEA 3 WG transition

Length (mm) ;	250
Outgassing surface (m^2);	0.25
Material ;	OFHC
Connection ;	
Input W/G (mm) :	192 x 40
Output W/G (mm) :	236 x 40

7. CEA mode converter

Length (mm) ;	960
Outgassing surface (m^2);	0.76
Material ;	OFHC
Connection ;	
Input W/G (mm) :	76 x 40
Output W/G (mm) :	192 x 40

8. CEA connection waveguides

Length (mm)	290 + 380 or 290 + 570
Outgassing surface (m^2);	0.30 or 0.39
Material ;	OFHC
Connection ;	
Input W/G (mm) :	76 x 40
Output W/G (mm) :	76 x 36